Spring 2010

Quantification of regional pulmonary blood flow parameters via multidetector-row CT: evaluation of vascular-based phenotypes of COPD

Sara Alford
University of Iowa

QUANTIFICATION OF REGIONAL PULMONARY BLOOD FLOW PARAMETERS VIA MULTIDETECTOR-ROW CT: EVALUATION OF VASCULAR-BASED PHENOTYPES OF COPD

by

Sara Alford

An Abstract

Of a thesis submitted in partial fulfillment
of the requirements for the Doctor of
Philosophy degree in Biomedical Engineering
in the Graduate College of
The University of Iowa

May 2010

Thesis Supervisor: Professor Eric Hoffman

ABSTRACT

Emphysema, a subset of COPD, occurs due to an abnormal inflammatory response to noxious gases or particles leading an influx of immunologic cells. Recent studies have demonstrated endothelial dysfunction in COPD subjects and are suggestive of a vascular phenotype present in COPD that is not fully characterized. We hypothesize that processes affecting the pulmonary vasculature lead to early changes important in the pathogenesis of COPD. This work focuses on the use of multidetector-row computed tomography (MDCT)-based measures of pulmonary blood flow (PBF), mean transit time (MTT) and pulmonary vascular volume (TPVV) to gain new insights into vasculature-related changes present in COPD. As a precursor to using perfusion MDCT imaging to phenotype lung disease, we demonstrated good regional correlation of PBF measurements obtained with MDCT imaging and fluorescent microspheres (FMS) at a FMS piece size resolution of 1.9 cm^3 and regional volume level of 8-10 cm^3. Additionally, we developed an *ex vivo* perfusion system, and applied quantitative image analysis techniques to study the lung preparation's stability over 120 minutes. We further validated CT-based PBF and MTT measurements by demonstrating physiologically appropriate responses to a range of flow rates with this new system. Finally, quantitative MDCT-based measurements were used to characterize a novel phenotype of emphysema and test hypotheses regarding vasculature-related changes in smokers and COPD subjects. We demonstrated increased heterogeneity in regional MTT and PBF measurements in smokers with preclinical emphysema compared with smokers with normal lung function and imaging studies and nonsmokers. This data is supportive of the notion that inflammatory-based vascular responses to hypoxia are occurring in smokers susceptible to COPD, but are successfully blocked in smokers without signs of emphysema. A new CT-based measure, TPVV, was studied and we demonstrate its association with total lung volume and body size metrics. TPVV measurements

correlated with measures of COPD severity. A trend linking increased TPVV with increased endothelial dysfunction was observed, suggesting that pathological changes of COPD have an effect on the pulmonary vasculature. This work demonstrates the importance of functional information that can compliment structural, anatomical information to answer questions based on the lung physiology and pathological disease processes.

Abstract Approved: _____
Thesis Supervisor

_____
Title and Department

_____
Date

QUANTIFICATION OF REGIONAL PULMONARY BLOOD FLOW PARAMETERS VIA MULTIDETECTOR-ROW CT: EVALUATION OF VASCULAR-BASED PHENOTYPES OF COPD

by

Sara Alford

A thesis submitted in partial fulfillment
of the requirements for the Doctor of
Philosophy degree in Biomedical Engineering
in the Graduate College of
The University of Iowa

May 2010

Thesis Supervisor: Professor Eric Hoffman

Graduate College
The University of Iowa
Iowa City, Iowa

CERTIFICATE OF APPROVAL

_____

PH.D. THESIS

_____

This is to certify that the Ph.D. thesis of

Sara Alford

has been approved by the Examining Committee
for the thesis requirement for the Doctor of Philosophy
degree in Biomedical Engineering at the May 2010 graduation.

Thesis Committee: _____
Eric Hoffman, Thesis Supervisor

_____
Graham Barr

_____
Edwin Dove

_____
William Lynch

_____
Joseph Reinhardt

_____
Edwin van Beek

ACKNOWLEDGMENTS

The work presented in this thesis could not have been done without the support and assistance of many others. I am very grateful for all the technical and emotional support from the staff and other students in the lab throughout the years. I would like to first thank Dr. Eric Hoffman, my thesis advisor, whose mentorship guided me throughout my time in the lab and with these projects. I would like to thank Drs. Edwin van Beek, William Lynch, Graham Barr, and Tom Robertson for their guidance and direction with our projects. I would like to thank my committee members, Dr. Joe Reinhardt and Dr. Edwin Dove, for their support and useful comments regarding this work and in regards to my biomedical engineering education. For the microsphere project, I would like to thank Wayne Lamm for his help with the microsphere measurements; and Matthew Fuld, Gary Christensen, Paul Song Joo Hyun, and Kunlin Cao for their assistance with image registration. For the *ex vivo* lung perfusion project, I would like to thank Aaron Schmidt and Manish Aggarwal for their assistance with the experiments; Scott Niles who taught me a lot about perfusion circuits; and Ahmed Halaweish for his support and always being ready to help out wherever needed. Human subject recruitment for the BRP projects could not have been done without a strong team at the Physiological Imaging Laboratory. Thanks to Heather Baumhauer, Joanie Wilson, and Angie Delsing for all their hard work recruiting subjects; Jered Sieren, Melissa Hudson, and John Morgan who were responsible for the CT imaging; and Nathan Burnette, Keith Gunderson, and Bryan Walton for all their assistance with data storage on MIFAR, software support, and most importantly, keeping my computer running great. Lastly, for the EMCAP project, I would like thank and acknowledge all the hard work of the team at Columbia University specifically Sonia Mesia-Vela. Lastly, I would like to thank Ann Thompson for her help throughout the years. This work was supported in part by an NIH Bioengineering Research Partnership Grant RO1 HL-064368.

ABSTRACT

Emphysema, a subset of COPD, occurs due to an abnormal inflammatory response to noxious gases or particles leading an influx of immunologic cells. Recent studies have demonstrated endothelial dysfunction in COPD subjects and are suggestive of a vascular phenotype present in COPD that is not fully characterized. We hypothesize that processes affecting the pulmonary vasculature lead to early changes important in the pathogenesis of COPD. This work focuses on the use of multidetector-row computed tomography (MDCT)-based measures of pulmonary blood flow (PBF), mean transit time (MTT) and pulmonary vascular volume (TPVV) to gain new insights into vasculature-related changes present in COPD. As a precursor to using perfusion MDCT imaging to phenotype lung disease, we demonstrated good regional correlation of PBF measurements obtained with MDCT imaging and fluorescent microspheres (FMS) at a FMS piece size resolution of 1.9 cm^3 and regional volume level of 8-10 cm^3. Additionally, we developed an *ex vivo* perfusion system, and applied quantitative image analysis techniques to study the lung preparation's stability over 120 minutes. We further validated CT-based PBF and MTT measurements by demonstrating physiologically appropriate responses to a range of flow rates with this new system. Finally, quantitative MDCT-based measurements were used to characterize a novel phenotype of emphysema and test hypotheses regarding vasculature-related changes in smokers and COPD subjects. We demonstrated increased heterogeneity in regional MTT and PBF measurements in smokers with preclinical emphysema compared with smokers with normal lung function and imaging studies and nonsmokers. This data is supportive of the notion that inflammatory-based vascular responses to hypoxia are occurring in smokers susceptible to COPD, but are successfully blocked in smokers without signs of emphysema. A new CT-based measure, TPVV, was studied and we demonstrate its association with total lung volume and body size metrics. TPVV measurements

correlated with measures of COPD severity. A trend linking increased TPVV with increased endothelial dysfunction was observed, suggesting that pathological changes of COPD have an effect on the pulmonary vasculature. This work demonstrates the importance of functional information that can compliment structural, anatomical information to answer questions based on the lung physiology and pathological disease processes.

TABLE OF CONTENTS

LIST OF TABLES

LIST OF FIGURES

LIST OF ABBREVIATIONS

BDI: Baseline dyspnea index
BMI: Body mass index
BSA: Body surface area
CI: Confidence interval
COPD: Chronic obstructive pulmonary disease
CRP: C-reactive protein
CV: Coefficient of variation
DSR: Dynamic spatial reconstructor
EBCT: Electron beam computed tomography
ECG: Electrocardiogram
EI: Emphysema index
ET: Endotracheal
FEV_1: Forced expiratory volume in 1 second
FMD: Flow-mediated dilation
FMS: Fluorescent microspheres
FOV: Field of view
FRC: Functional residual capacity
FVC: Forced vital capacity
HPV: Hypoxic pulmonary vasoconstriction
HU: Hounsfield unit
LA: Left atrium
LAP: Left atrial pressure
MDCT: Multidetector-row computed tomography
MLD: Mean lung density
MTT: Mean transit time
PA: Pulmonary artery
PAP: Pulmonary artery pressure
PASS: Pulmonary analysis software suite
PBF: Pulmonary blood flow
PEEP: Positive end-expiratory pressure
PH: Pulmonary hypertension
PIP: Peak inspiratory pressure
PVR: Pulmonary vascular resistance
ROI: Region of interest
SD: Standard deviation
TLC: Total lung capacity
TPVV: Total pulmonary vascular volume
TSIA: Time series image analysis
TV: Tidal volume
VEGF: Vascular endothelial growth factor

CHAPTER 1: MOTIVATION AND AIMS

This work focuses on the use of multidetector-row computed tomography (MDCT)-based measures of pulmonary blood flow (PBF) and pulmonary vascular volume to gain new insights into vasculature-related changes and their role in the pathogenesis of chronic obstructive pulmonary disease (COPD). As a precursor to phenotype assessment in COPD, we validated perfusion measurements obtained with MDCT imaging against microsphere perfusion measurements in an *in vivo* swine model (Chapter 3), and also developed an *ex vivo* lung perfusion model for further validation studies (Chapter 4). Quantitative MDCT-based measurements of perfusion and pulmonary vasculature volume were then used to test two hypotheses regarding vasculature-related changes in smokers and COPD subjects (Chapter 5 and 6).

COPD is a heterogeneous lung disease, with cigarette smoke being the most important risk factor. It is known that emphysema occurs due to an abnormal inflammatory response to noxious gases or particles leading an influx of immunologic cells including neutrophils, macrophages and T cells. This leads to irreversible damage in the conducting airways and loss of elastic recoil due to damage of the alveolar structures. Recent studies have demonstrated endothelial dysfunction, assessed by flow-mediated dilation (FMD) of the brachial artery, and increased arterial wall stiffness in COPD subjects. These vascular changes suggest a vascular phenotype present in COPD that is not fully characterized. We hypothesize that these processes affecting the pulmonary vasculature lead to early changes important in the pathogenesis of COPD. A more thorough background on the clinical relevance and current knowledge on the pathophysiology of COPD and more specifically, emphysema, is presented in Chapter 2.

The first aim of this work is to validate the use of dynamic ECG-gated MDCT perfusion imaging for the determination of pulmonary perfusion and perfusion parameters. This was accomplished with regional correlation measurements to

fluorescent microsphere (FMS) blood flow measurements (Chapter 3) and secondly, with studies performed on a newly developed *ex vivo* lung perfusion system (Chapter 4). A series of experiments in a swine model were performed to obtain both FMS and MDCT perfusion measurements and demonstrated good correlation between methods. In order to compare the two techniques, image registration techniques were utilized to match MDCT-based PBF measurements to FMS PBF measurements at the FMS resolution level of 1.9 cm^3. Mean, coefficient of variation, vertical gradients, and correlation were obtained for many normalization methods for each technique, which demonstrate differences which can alter one's interpretation of lung physiology. The need for better models, capable of testing and validating new functional MDCT lung imaging techniques, led to the development of an *ex vivo* lung perfusion system. Lung transplantation techniques were applied to develop a stable system capable of careful control of ventilation and perfusion of the *ex vivo* lung, and the ability to functional assess the lung with MDCT imaging. In chapter 4, the developmental work of this system is presented. Quantitative image analysis of tissue volume from volumetric MDCT images of the *ex vivo* lung and physiological monitoring provided a means to assess the stability of the lungs over time. The model was then used to further validate the MDCT perfusion imaging technique by imaging the *ex vivo* lungs at a range of flow rates, demonstrating appropriate changes in regional PBF and MTT as pulmonary arterial flow was increased from 50 cc/kg/min to 125 cc/kg/min.

In chapters 5 and 6, we present human data collected from MDCT imaging studies performed in two cohorts: the Bioengineering Partnership Lung Atlas (NIH-HL-064368: BRP) and Emphysema and Cancer Action Project (EMCAP). These projects tested hypotheses related to the presence of vascular-related changes with COPD. Chapter 5 focuses on the characterization of perfusion and perfusion heterogeneity in smokers with and without disease, and to test the hypothesis that smokers susceptible to emphysema will have a patchy inflammatory response leading to a patchy distribution of

PBF and MTT throughout the lung parenchyma. We determine normative values of mean and variability of MDCT-based measures of perfusion (regional PBF) and MTT in a subgroup of the BRP cohort including 17 never smokers, 12 smokers with normal spirometry and normal MDCT images, and 12 smokers with preclinical emphysema. Our results demonstrating increased heterogeneity of regional PBF and MTT in smokers with preclinical emphysema compared with smokers without disease and nonsmokers are supportive of our hypothesis that a subset of smokers will be more susceptible to disease due to the inability to block HPV in regions of inflammation.

Finally, in Chapter 6 we explore a new MDCT-based vasculature measure, the total pulmonary vascular volume (TPVV) obtained from non-contrast MDCT lung images. TPVV is defined as the total arterial and venous intravascular volumes plus extralumenal volumes (the volume of arterial and venous vessel walls) in the lungs. TPVV analysis of a subgroup of BRP cohort subjects established a normative range for nonsmokers and smokers. Linear regression between TPVV and possible covariates demonstrated a strong correlation between TPVV and total lung volume, and TPVV and measures of body size such as height and weight. We demonstrated a direct correlation between TPVV and spirometry measures of lung function such as FEV_1. CT images from another cohort (EMCAP study) consisting of 93 former smokers with and without COPD were evaluated to determine if associations exist between TPVV and COPD severity, and endothelial dysfunction. FMD measurements in this cohort have been previously shown to be linearly related to lung function and CT lung density in smokers. TPVV measurements from the EMCAP cohort demonstrate a strong inverse correlation between CT percentage of emphysema and TPVV measurements, indicating a decrease in TPVV with increasing COPD disease severity. Measures of endothelial function from FMD demonstrated a weak correlation of endothelial dysfunction and an increased TPVV. A decreasing pulmonary vasculature volume with increased CT percentage of emphysema and decline in lung function assessed by spirometry suggest that

parenchymal destruction occurring with increasing COPD severity is affecting the capillaries and causing destruction, thereby decreasing the total pulmonary volume. FMD and TPVV analysis demonstrates a trend for endothelial dysfunction to be associated with an increased pulmonary volume. This findings suggests the presence of altered vascular tone in COPD subjects which is not fully characterized. Further study with more sensitive measurements of vascular volume, such as a specific pulmonary arterial volume, will be needed to better characterize these changes in COPD subjects.

This work is important for the characterization of a new vascular phenotype of COPD. Non-invasive CT measures of vascular function are important measures of lung health to be used as endpoint or biomarkers in clinical or pharmaceutical trials, or for studies where phenotyping disease is important. This work validated the perfusion MDCT imaging technique, provided a new model for imaging validation and study of the lung pathology and pathology, and improved our understanding of the pathophysiology and vasculature-related changes present in COPD subjects.

CHAPTER 2: BACKGROUND

Clinical Significance

Lung Physiology

The main function of the lung is to facilitate gas exchange including the uptake of oxygen and removal of carbon dioxide. The pulmonary circulation is a low pressure system (mean arterial pressure: 15 mm Hg) which encompasses the entire right ventricular outflow tract; therefore PBF is equivalent to cardiac output. Blood travels from the right ventricle into the pulmonary artery to pulmonary arterioles to the capillary bed where gas exchange occurs. The capillary bed merges to form pulmonary venules, which then form pulmonary veins, and return blood to the left atrium of the heart. The capillaries lie in the alveolar walls and form a dense network around the alveoli. The capillary-alveolar boundary constitutes the blood-gas barrier in the lung. West describes the capillary-alveolar boundary as extraordinary due to its "extreme thinness, immense strength, and enormous area" (202). This barrier consists of a single layer of alveolar epithelium, capillary endothelium, and an intervening extracellular matrix containing two basement membranes of the two cell layers. This boundary must remain very thin for passive diffusion of the gases to occur, while also maintaining a large area for diffusion (115, 202). Additionally, in order for efficient gas exchange to occur, the lung must have well-matched ventilation and perfusion. Perfusion is a general term describing the delivery of arterial blood to a capillary bed, whereas PBF refers to the rate of delivery of pulmonary arterial blood to the capillary bed in a known mass of tissue (105, 201).

Pulmonary Blood Flow

Early methods for assessment of PBF focused on characterization of perfusion gradients present and explanations for the heterogeneity observed. Nuclear medicine with gamma camera counters were able to demonstrate gradients in the blood flow distribution

and from these studies, John West developed a zonal model of blood flow in the lung (201, 203, 204). Based on his model, the lung is divided into three zones based on the relationship between the alveolar pressure (P_A), pulmonary arterial pressure (P_a), and pulmonary venous pressure (P_v). Regional perfusion to the lung is determined in each zone based on the gravitational effect on the pressures. In an upright human lung, zone 1 is in the apical region, and based on its pressure gradient ($P_A > P_a > P_v$,), capillary beds are collapsed and minimal PBF occurs. In Zone 2, $P_a > P_A > P_v$ resulting in flow proportional to the alveolar-venous gradient. Finally in the basal region of the lung, zone 3 conditions exist. In Zone 3, $P_a > P_v > P_A$,. This means the blood flow through the open capillary beds depends on the typical arterial-venous gradient. A reduction in blood flow in the most dependent region, zone IV, can exist as well in the very most basal region of the lung (81, 82).

In the West model, gravity is the major determinant of regional perfusion and explains a gradient observed from non-dependent to dependent regions of the lung. Many investigators have now shown that pulmonary perfusion exhibits a vast degree of heterogeneity for an iso-gravitational plane or gravity independent region (57, 78, 150). According to the zonal model, a slab of lung at the same vertical level would have equal hydrostatic pressure effects and therefore, the gravitational effects on the distribution of blood flow should be minimal. However, marked heterogeneity in an iso-gravitational plane has been demonstrated, suggesting that factors other than gravity may contribute to blood flow. Glenny et al. have hypothesized that gravity plays a minor role in the spatial distribution of pulmonary blood flow and rather the vascular structure is the major determinant of local blood flow (47, 48, 50). Another possibility is hypoxic pulmonary vasoconstriction (HPV). The lung's normal response to regional alveolar hypoxia is regional HPV, resulting in the shunting of blood towards better-ventilated regions of lung for improved oxygenation. This is an intrinsic response occurring locally in the small pulmonary arteries (64, 127). Microsphere studies in animal models have demonstrated

non-uniform alterations in blood flow in response to hypoxia (67, 102, 180). A diminished HPV response to hypoxia is present in disease states such as pneumonia (120). Imaging has shown that in both sheep (39) and humans (56, 170), HPV is blocked in the presence of inflammation, and this block occurs regionally at sites of inflammation (76).

Chronic Obstructive Pulmonary Disease

Chronic obstructive pulmonary disease (COPD) is a disease that affects the lung's airways, parenchyma and vasculature as well as manifesting systemic effects (7, 148). It is currently the fifth leading cause of death in the United States. According to GOLD standards, COPD is defined as:

> "a preventable and treatable disease with some significant extra-pulmonary effects that may contribute to the severity in individual patients. Its pulmonary component is characterized by airflow limitation that is not fully reversible. The airflow limitation is usually progressive and associated with an abnormal inflammatory response of the lung to noxious particles or gases (148)."

Risk for COPD is related to an interaction of genetic factors and many different environmental exposures (117). The most important risk factor leading to the development of COPD is cigarette smoking. 90% of COPD cases are in smokers, but only a subset of smokers (approximately 20%) will develop clinically symptomatic COPD during their lifetime. Symptomatic individuals present clinically with chronic cough, mucous hypersecretion, and dyspnea on exertion. Diagnosis is based on spirometry measurements demonstrating airflow limitation that is not fully reversible, specifically a post-bronchodilator FEV_1/FVC ratio < 0.70. Further classification shown in Table 1 divides the progression of disease in four stages (I-IV) or mild, moderate, severe and very severe COPD based on post-bronchodilator spirometry (148). Lung function impairment is a strong predictor of mortality, but it does not completely characterize the wide spectrum of disease (117). Despite similarities in altered lung

function, COPD symptoms and signs manifest as different pathological entities including chronic bronchitis and emphysema (188).

Phenotypes of Emphysema

Emphysema is defined anatomically by an abnormal dilation (enlargement) of the air spaces accompanied with destruction of the alveolar walls without obvious fibrosis. The hallmark of the pathogenesis is an abnormal inflammatory response to noxious gases or particles leading to irreversible damage in the conducting airways and loss of elastic recoil due to damage of the alveolar structures (7, 148). Two distinct forms of emphysema have been described. Centrilobular emphysema is commonly seen in smokers. The main region of inflammation and destruction is the respiratory bronchioles, and emphysema is most frequently observed in the upper lobes, especially in the mild form (188). The reason for this localization remains unknown. West et al. analyzed regional stresses in a finite element model of the lung, and found that in the upright position the stress in the lung is maximal at the apex (200, 205). However, the reported intra-pleural pressures (69, 72) while more negative in the apices, are not high enough to explain the predisposition of emphysema destruction to the apices. Panacinar emphysema is the typical presentation for a group of subjects with a rare genetic disease, α_1-antitrypsin deficiency. In this subtype, the respiratory bronchioles, alveolar ducts and sacs are all equally involved in the disease process, and emphysema is localized in the lower lung lobes (188).

Pulmonary Hypertension in COPD

COPD has a systemic inflammatory component (7, 44, 58) and is an independent risk factor for cardiovascular disease (124, 175, 176). C-reactive protein (CRP), a marker of acute inflammation, is increased in COPD subjects specifically during acute exacerbations (4, 32, 116, 186, 191). Higher serum levels of pro-inflammatory markers such as CRP and TNF-α are associated with increases in peak pulmonary artery pressure

in patient with COPD, suggesting a pathogenic role for low-grade system inflammation in the pathogenesis of pulmonary hypertension (PH) in COPD patients (89). PH is a family of disorders characterized by an elevation of arterial pressure and pulmonary vascular resistance (PVR) in the lung (162), and is a well-known clinical feature of advanced COPD and a frequent complication in the natural history of disease (6, 189). PH significantly worsens the prognosis of COPD. In a longitudinal study, Burrows et al. demonstrated that survival was inversely related to PVR and the association was similar to the association of survival to FEV_1 (22). The presence of PH in COPD is also associated with increased hospitalization for acute exacerbations (6).

Evidence for vascular changes with COPD

Recent evidence suggests that endothelial dysfunction and pulmonary vascular-related changes occur early in COPD, which may represent a novel vascular pathway in COPD development. Pulmonary vascular remodeling and endothelial dysfunction have been observed in the pulmonary arteries of smokers and COPD subjects of varying severity. Pathological lesions including thickening of the intimal and muscular layer of the vessel can be identified early on in the pulmonary arteries of smokers with mild COPD and smokers without disease (143, 144, 165, 166). It has been demonstrated that cigarette smoking results in capillary endothelial and alveolar epithelial apoptosis, which can lead to the loss of alveolar septa and reduction in small capillary blood vessels (92, 94). These findings suggest early alterations in the pulmonary vasculature occur and are a direct response to cigarette smoking. As the disease progresses, the structural alterations will ultimately result in a rigid vasculature bed, unable to dilate with increasing pressures (215), accounting for the presence of pulmonary hypertension.

Other work suggests the importance of inflammation as a mechanism for vascular remodeling. Peinado et al. demonstrated that cigarette smoking induced a CD8+ T-lymphocyte infiltrate in the pulmonary arteries and an associated impairment of the

vessel's structure and function (143). Endothelial dysfunction and vasculature changes may be due to an altered balance of vasoactive mediators (216, 217). Animal studies show that blockade of vascular endothelial growth factor (VEGF), a key cytokine in the maintenance of the pulmonary vasculature, causes emphysema (93, 94, 195). This all supports earlier work of Dr. Liebow who in 1959 examined pulmonary arteries and veins of emphysema patients and postulated that changes in the local vascular milieu caused alveolar destruction in COPD (104).

Studies have also demonstrated the diminished ability of the pulmonary arteries to relax in arteries obtained following lung resection in COPD subjects (144). Non-invasive techniques, such as flow-mediated dilation (FMD) of the brachial artery can be used to test endothelial dysfunction according to established guidelines (28). Impairment of endothelial function by the FMD technique has been demonstrated in two COPD cohorts. Barr et al. demonstrated that endothelial dysfunction, assessed by FMD, was associated with a lower post-bronchodilator FEV_1 and higher CT percentage of emphysema in former smokers across a spectrum of disease severity (9). In another study, Moro et al. also demonstrated endothelial function was correlated with FEV_1 (126). Functional data regarding the arterial stiffness can be obtained from the shape of the arterial pressure waveform and can be assessed non-invasively with pulse-wave analysis (137, 209). Chronic cigarette smoking has been associated with increased arterial stiffness (108, 114) with smoking cessation resulting in an improvement in measures over time (87). Two cohort studies show that arterial stiffness is increased in COPD subjects (119, 124, 163) with associations with emphysema severity in one cohort (119), and associations with airflow obstruction, systemic inflammation, and presence of osteoporosis in the another cohort (163).

MDCT Imaging

Technology Advances

CT has emerged as a powerful method for imaging of the lung due to its widespread availability, high spatial resolution, high signal to noise ratio for lung tissue, and fast acquisition speed. MDCT imaging can now provide anatomical and functional information about the lung. CT technology has rapidly evolved from its introduction in the medical field in the early 1970s. An early, experimental scanner, known as the dynamic spatial reconstructor (DSR), built at the Mayo Clinic housed 14 x-ray sources aimed at a hemi-cylindrical fluorescent screen in turn monitored by 14 television cameras. The 20 ton gantry rotated at 15 rpm and provided enough projection data to reconstruct up to 240 slices of the body every 1/60 second (12, 156, 158, 159, 177). Much of the early quantitative imaging analysis tools evolved from the efforts to evaluate data from this scanner. These efforts demonstrated the utility of CT imaging in providing regional lung density measures (71, 75, 157), lung volumes (100) as well as anatomic detail of the airway and vascular trees (18, 109, 110, 219) and regional measures of pulmonary perfusion (218).

Spiral CT was introduced by Willi Kalender and colleagues (90), allowing for volumetric imaging of the lung in a breath hold. While single-slice spiral CT scanners with one x-ray source/detector pair were rapidly adopted to acquire volumetric images of the lung, breath hold times were often too long for patients to sustain and slice thicknesses were large relative to the anatomy of interest. Thin slice, high resolution, step and shoot modes, gathering slices widely spaced from lung apex to base, were introduced and remained the method of choice for assessing peripheral lung anatomy (223, 226) and functional data was not available clinically. Four-slice MDCT systems became available in 1998, followed by 16-slice and 64-slice in 2001 and 2004 respectively. In 2009,

scanners with 320 slices covering approximately 12 cm of the apical-basal lung axis are available.

MDCT scanners use cone-beam x-ray geometry and multiple detector rows to collect more slices per gantry rotation, thereby allowing for increased z-coverage. Its increased speed and ability to image thin slices of isotropic (voxels with the same x,y and x dimensions) resolution provide significant benefits compared to the earlier generation of single-detector or limited multidetector-row scanners. With isotropic voxels and a voxel dimension on the order of 1mm or less, one is able to re-slice the volumetric image according to anatomy of interest. Once 16-slice scanners were developed; full lung volumes in a breath-hold (10-20 seconds compared with the 4 slice scanner requiring 40 seconds) and contrast enhanced images during multiple phases of the cardiac cycle were now feasible. As technology improved, the gantry rotation speed also increased leading to improvements in technical scanner performance. As detector arrays advanced, 64 slices could be acquired in one gantry rotation in as little as 0.33 seconds. With MDCT systems, the scanner can also be used in an axial mode where the detector and x-ray source do not spiral through the patient, but rather remain in the same axial position and provide data for lung in the detector plane. This allows for imaging of a slab of lung slices over time to provide functional imaging such as perfusion.

Volumetric Imaging

Regional lung densities change with lung volume, reflecting regional changes in alveolar expansion. Therefore, it is important to standardize imaging protocols so that all subjects are scanned at similar lung volumes. Imaging of the lung with MDCT should be done under protocols including breath-holds at well controlled lung volumes to minimize artifacts due to respiratory motion. In a clinical setting, x-ray technologists typically coach patients on proper breathing and breath-holding at standardized volumes, typically full inspiration or total lung capacity (TLC). Alternatively, a volume controller system

has been developed in the lab for imaging of human subjects. This controller consisting of a well calibrated pneumotachometer with balloon occlude valve which is linked to a monitoring program (Labview, National Instruments, Austin, TX) to instantaneously measure airflow and hold lung volumes appropriately (73).

Quantitative Image Analysis

CT is a comprehensive tool for studying both the anatomy and function of the lung in normal and disease states. CT measures fit the NIH definition of a biomarker as a "characteristic that is objectively measured and evaluated as an indicator of normal biological processes, pathogenic processes, or pharmacological responses to a therapeutic intervention" (8, 168). Quantitative image analysis of MDCT lung scans provide a new array of potential biomarkers capable of detecting pathologies, tracking disease progression, and tracking therapeutic response.

The structure and integrity of the pulmonary vasculature can be assessed with a non-contrast spiral lung volume scan obtained typically at full inspiration which provide the best contrast between air-filled spaces and the parenchyma, airways and pathological lung processes. Volumetric CT is an accurate method for determining lung volumes and regional lung density. In order to quantitatively evaluate the lung, segmentation of the lung (80, 224), lobes (198, 224), airways (5, 141, 179, 193, 194) and vasculature (171) are completed. CT contrast is based on the attenuation of different tissues, approximately related to tissue densities. Each voxel reflects the tissue density or x-ray attenuation coefficient by its Hounsfield Unit (HU) value. The HU scale is defined as -1000 HU for air, 0 HU for water, and 1000 HU for bone. For a non-contrast volumetric lung scan, if one considers the lung as composed of two materials, air at -1000 HU and “tissue” (including blood volume) at approximately 55 HU, then the density of HU can be convert to the amount of air and “tissue” content per voxel (68). Volumes are determined based on the product of the segmented in-plane cross-sectional area by the slice thickness,

summed over all the slices spanning the segmentation. By combining these two measures, the absolute volumes of air or tissue in the lung can be determined from the region volume multiplied by the fraction of air or tissue (74, 172, 174). 3-D volume rendering images of the lung, lobes airway or vasculature tree segmentations can be used to visualize the anatomy.

With the recognition that many peripheral pulmonary processes either increase or decrease regional lung density, there is a growing focus on quantifying the distribution of lung attenuation values within CT images. Lung parenchyma voxels can be categorized based on their attenuation values (HU value) and according to their place in the lung attenuation histogram. The percentage of emphysema or emphysema index (EI) is defined as the proportion of lung below a designed threshold attenuation value. This has been applied to emphysema with density masks of -950 and -910 HU used to determined percentage of severe and moderate emphysema present in the lung parenchyma (30, 45, 73, 103, 131). Groups have also focused on the development of CT based methods to quantify regional lung expansion with the aim to gain insight into the stress and strain distribution of the lung during normal physiology and pathologic states (152, 154, 173, 174). Airway trees can be segmented and analysis can provide an array of quantitative parameters such as major and minor diameters, areas, perimeters, and wall thickness measurements for each airway branch (29, 153, 193, 194). Pathological changes such as wall thickening have been characterized in subjects with lung disease such asthma and COPD (30, 59, 99, 136, 151).

Being able to compare images performed at different conditions (lung inflation, different time points, merge anatomical and function data) requires methods to match or register the image data sets. Image registration requires a transformation that can be applied to one image to align it with the second image. There are two basic types of registration transformations: rigid body and non-rigid body. Rigid body transformations assume that only translation and/or rotation are necessary. This transformation is

expressed as a matrix that acts on every coordinate in the image data set. A non-rigid transformation may be in the form of an affine transformation (also allowing for shape change via shearing action) or a more complex transformation allowing shape change globally or locally. Common similarity measurements include landmark, surface and edge, and voxel intensity measures (83). In order to quantify the accuracy of registration methods, landmarks are chosen in the two image sets that correspond to the same point, such as an airway branching point. The distance between the true coordinates (determined by the user) and the registered coordinates for a set of landmark points are used to determine the average distance error.

Pulmonary Blood Flow and Imaging

To better understand lung diseases, MDCT imaging and quantitative image analysis can be used to characterize changes in the lung, providing additional insights into lung physiology and pathogenesis of lung disease. By studying perfusion distributions with high resolution MDCT imaging techniques, we can explore physiological and pathophysiological changes present in healthy subjects and those with COPD to improve our overall understanding of the lung. Regional perfusion can quantitatively be assessed with MDCT with a 4-D dynamic imaging method with bolus contrast injection. This method uses indicator dilution theory to determine regional PBF and MTT. Wolfkiel and Rich (212) measured myocardial blood flow by electron beam CT (EBCT), using a single-compartment model of indicator transport. The basic concept of the model is that flow is proportional to maximum enhancement of the tissue region of interest (ROI). It assumes that the height of the curve is a measure of the flow within that tissue ROI (13, 77, 212, 225). For this method to provide valid measurements, the following criteria must be met by the indicator: 1) the indicator should not affect flow through physiologic or volume effects; 2) the indicator should mix with the blood uniformly; 3) the indicator should remain in the intravascular space; and 4) tissue

accumulation of the indicator must be nearly complete before the onset of indicator wash-out. In order to meet these criteria, a sharp, central bolus is needed.

This theory has been applied as a dynamic, ECG-gated axial MDCT technique with bolus contrast injection (19, 77, 212, 213). Perfusion is measured by tracking a central bolus of iodinated contrast over time with sequential CT imaging of a lung volume with the scanner in axial mode (non-spiral mode with the table in a fixed location). The technique employs a central injection of iodinated contrast delivered by power injection, ECG cardiac gating, and is performed during a breath-hold at functional residual capacity (FRC). In order to determine PBF and MTT, time-attenuation curves must be obtained for the pulmonary artery and the lung parenchyma. A gamma-variate function is fit to the data using a Levenberg-Marquardt least-squares minimization routine (25). Indicator dilution theory is applied to the data to determine PBF and MTT on a regional basis. PBF is the ratio of change in HU to the area under the input arterial curve (25, 77). MTT of the residue function is defined as the area under the residue curve divided by the maximum height. The regional residue function refers to the fraction of bolus residing in the local microvascular bed at any given time and is determined by the deconvolution of the regional lung parenchymal time-attenuation curves and the measured pulmonary artery (214).

PBF data can be normalized with various methods including the mean, air content (PBF AIR), non-air content (PBF NON-AIR), and a "per-alveolus" (PBF ALVEOLUS) measurement. To mean normalize, PBF is divided by the mean PBF for the lung. From the baseline image captured just prior to contrast injection, the air content (Fair) and non-air content (Fnonair) of each voxel can be determined for each voxel. The non-air content includes true tissue volume, blood volume and interstitial or alveolar fluid volumes. PBF can be normalized by the air or non-air content of the voxel. For PBF NON-AIR normalization measurements, we also divide by the average tissue density (1.05 g tissue/volume) to get a flow per gram of tissue normalization.

PBF AIR = PBF/(Fair)

PBF NON-AIR = PBF/(Fnonair x 1.05)

Another normalization is a "per-alveolus" normalization which attempts to provide a measure of pulmonary blood flow when the lung is more uniformly expanded at TLC (214). In this calculation, Fmaxair is the maximum value of the parenchymal air fraction present in the segmented lung, calculated from the baseline image data set.

PBF ALVEOLUS = PBF/(Fmaxair/Fair)

MDCT perfusion imaging studies have been performed in animal studies and in human subjects (25, 33, 39, 70, 76, 77, 212, 214, 218). Chon et al demonstrated PBF measurements in dogs and established normative values of normalization methods including vertical gradients and coefficient of variation for supine and prone body postures (25). Won et al. characterized MTT and MTT heterogeneity with an EBCT scanner capable of separating the true microvascular transport function from the small artery contamination (214). Easley et al. used MDCT imaging to assess changes due to hypoxemia in an acute lung injury model demonstrating differences in HPV response in lavage injury versus pneumonia (39). Hoffman et al. demonstrated a regional HPV response with MDCT perfusion imaging. In an animal with an endobronchial valve and pneumonia, HPV was intact in the region of valve placement, but blocked in the region of inflammation corresponding to pneumonia. From this data, Hoffman et al. hypothesized that, in subjects with pulmonary emphysema, one major contributing factor leading to parenchymal destruction is the lack of a regional blunting of HPV when the regional hypoxia is related to regional inflammatory events (alveolar flooding) (76).

Table 1. Global initiative for chronic obstructive lung disease (GOLD) classification for the staging of COPD.

	Stage	Spirometry
Mild COPD	I	$FEV_1/FVC < 70\%$ & $FEV_1 \geq 80\%$
Moderate COPD	II	$FEV_1/FVC < 70\%$ & $50\% \leq FEV_1 < 80\%$
Severe COPD	III	$FEV_1/FVC < 70\%$ & $30\% \leq FEV_1 < 50\%$
Very Severe COPD	IV	$FEV_1/FVC < 70\%$ & $FEV_1 < 30\%$

Note: Spirometry measurements are post-bronchodilator responses.

CHAPTER 3: ANIMAL VALIDATION STUDIES WITH MICROSPHERES

Rationale

In order to validate the ECG-gated MDCT perfusion technique, comparison of CT-based regional PBF measures to a gold standard measurement should be completed. Microspheres have traditionally been employed as a validation method for pulmonary blood flow. The microsphere mapping method to obtain high-resolution measurements involves the *in vivo* administration of intravenously injected radioactive or fluorescent microspheres followed by lung fixation, systematic cutting and piece mapping, and the measurement of radioactive or fluorescent signal from each piece (46, 161). Spatial perfusion maps have been employed in a wide range of studies including work demonstrating flow heterogeneity in the lung (54, 78), the scale-dependent nature or fractal nature of heterogeneity (51, 52, 160), and the relative importance of pulmonary vasculature structure compared to gravitational gradients (47, 48, 50). While measurements of PBF obtained by microspheres correlate well with regional blood flow assessed by erythrocyte flow in the lung vasculature (11), its use is limited to studies on experimental animals due to the destructive nature of the procedure. It has been difficult to cross correlate PBF measurements obtained from MDCT perfusion imaging with FMS measurements because of their differing processing schemes and normalization measures. *In vivo* studies have demonstrated that the choice of normalization parameters can alter one's interpretation of heterogeneity (25). With the development of more sophisticated registration algorithms, it has now become feasible to match lung volumes, allowing for the regional alignment of the microsphere and MDCT perfusion data sets. The purpose of this work is to compare and correlate MDCT and FMS PBF measurements, and to assess different normalization methods to determine the most appropriate normalization approach for method comparison. To accomplish this task, we paired PBF measurements

obtained with *in vivo* perfusion MDCT with measurements obtained by intravenously injected 15-μm FMS in swine. Image registrations techniques were employed to regionally match *in vivo* MDCT measurements with FMS measurements based on cut pieces of air-dried lung specimens.

Methods

Animal Preparation

Seven farm-raised swine with a mean weight of 19.8 ± 1.0 kg (weight range, 18.6 to 21.8 kg) were used for this study. All animal use protocols were approved in advance by the University of Iowa Animal Care and Use Committee and all studies were performed according to the guidelines established by the American Physiological Society and National Institutes of Health. Animals were pre-medicated with an intramuscular injection of ketamine (20 mg/kg) and xylazine (2 mg/kg) and anesthetized with 4% isoflurane by nose cone inhalation. Carotid arterial and external jugular venous lines were placed, and a tracheotomy was performed with an 8.0 mm inner diameter cuffed endotracheal tube. Following surgery, the animal was moved to the MDCT scanner suite and a continuous infusion of thiopental (20 mg/kg bolus followed by 20 mg/kg/hr) sufficient to prevent spontaneous respiratory effort, was used to maintain anesthesia during MDCT scanning and FMS administration. Animals were mechanically ventilated (large animal ventilator, Harvard Apparatus, Holliston, MA) with the following ventilation settings: 15 breaths/min, 7.5-cm H_20 positive end-expiratory pressure (PEEP), tidal volumes 12 cc/kg, with respiratory rate adjusted to maintain pH in 7.45 range. Minute ventilation, end-tidal CO_2, mouth airway pressure, rectal temperature, blood pressure, oxygen saturation levels via pulse oximetry, and ECG signal were monitored throughout the study. A pigtail angiography catheter (7 Fr, Cook Inc, Bloomington, IN) was placed in the right atrium for central contrast injections needed for MDCT perfusion imaging studies.

MDCT and FMS Data Acquisition

MDCT and FMS regional PBF measurements were acquired with animals in both prone and supine positions. All imaging was performed on a Siemens Sensation 64 MDCT scanner (Siemens, Erlangen, Germany). For each body position the following sequence of measurements was taken: spiral non-contrast volumetric MDCT scans obtained at two fixed lung volumes (TLC and FRC), 4-D ECG-gated axial MDCT perfusion scans at two locations, and FMS injection. TLC and FRC volumetric scans were obtained using a continuous PEEP breath-hold at 25 cm H_20 and 7.5 cm H_20 respectively. Volumetric scans were performed with the following settings: mA, 100; kV, 120; pitch, 1mm; rotation time, 0.5 seconds; slice thickness, 0.75mm; slice increment, 0.5mm; matrix, 512 x 512; FOV, 24.0 cm; and reconstruction kernel, B31f. Voxel dimensions were 0.47 x 0.47 x 0.50 mm. Based on the FRC volume scan, two adjacent 2.8-cm transverse sections of lung beginning just distal to the carina and advancing basally were selected for perfusion MDCT imaging. ECG-gated dynamic axial 4-D MDCT perfusion imaging was acquired during a bolus injection of 0.75 cc/kg iodinated contrast medium (Iohexol 350mgI/mL, GE Healthcare, Milwaukee, WI) delivered over 2 seconds into the right ventricle through a high pressure Med Rad contrast injector connected to the intravascular catheter (25, 77). This sequence of 12 images acquired at 20 time points (240 total images per data set) was acquired during a 7.5 cm H_20 continuous airway pressure breath hold. Perfusion imaging parameters were as follows: mA, 150; kV, 80; rotation time, 0.33 seconds; matrix, 512 x 512; FOV, 24 cm; and reconstruction kernel, B30f. Each imaged volume consisted of 12 slices, with a slice thickness of 2.4mm. Voxel dimensions were 0.47 mm x 0.47 mm x 2.4 mm. There was a 5 minute waiting period between scans of the two adjacent regions to allow clearance of contrast. Additionally, regional PBF was labeled utilizing a continuous intravenous injection of 1 $x10^6$ to 2 $x10^6$ 15-µm FMS (FluoSpheres, Molecular Probes, Eugene OR) over a five-minute period. Intravenous FMS color choices for each animal position were

alternated among six color labels. Once MDCT images and FMS injection were completed, the animals were flipped and MDCT imaging and FMS injection was repeated for the other body position.

Following administration of the final pair of FMS labels and MDCT imaging, 5,000 units of heparin, 45 mg of papaverine, and an additional bolus of 25 mg/kg of thiopental were injected intravenously. The deeply anesthetized animals were euthanized by exsanguination. The lungs were flushed clear of blood with a 2% Dextran solution, cut free from the heart, removed from the thorax, and inflated to 25 cm H_2O pressure. Tissue glue was used to fix the lobes as close to their *in vivo* anatomic position, 20-30 punctures of the pleura were made with a 20-gauge needle, and the lungs were air-dried with heated air at 25 cm H_2O pressure for 3 days. The dried lungs were then coated with an approximately 1-cm thick layer of Kwik Foam (DAP Inc. Dayton OH), and encased in a block of rapid setting urethane foam (2 lb. polyol and isocyanate, International Sales Corp., Seattle, WA). Digital photos of the experimental FMS processing steps are shown in Figure 1. Spiral non-contrast volumetric images with the same parameters as outlined for *in vivo* scans were performed on the dried lung specimens encased in foam blocks.

FMS Data Analysis

Beginning at the level of the carina identified from the CT image of the foam block, the lung block was cut into 1.2 cm transverse slices, and the slices were photographed for the confirmation of registration with CT images. The slices were cut into 1.8-cm^3 cubes (1.2 cm x 1.2 cm x 1.2 cm) using a rectilinear grid. The spatial coordinates, weight, and lobe of each cut lung piece were recorded. For any cube encompassing two different lobes, the smaller lobe portion was discarded. Each piece was weighed and soaked in a fixed volume of 2-ethoxyethyl acetate (Cellosolve, Aldrich Chemical, Milwaukee, WI) to extract the fluorescent labels, and fluorescence signals measured with a fluorescence spectrophotometer (Perkin-Elmer LS50B, Boston, MA), as

described previously (46). The fluorescence signals were corrected for spillover from adjacent colors in the emission spectrum using a matrix inversion program (167).

MDCT Imaging Analysis

Lungs were semi-automatically segmented using Pulmonary Analysis Software Suite (PASS). MDCT-based total lung volume, air volume, non-air volume, mean and standard deviation of HU were calculated. ECG-gated perfusion MDCT images were analyzed with the Time Series Image Analysis (TSIA) module within PASS, to determine regional PBF and perfusion parameters (i.e. mean transit time) using indicator dilution theory as previously described (25, 214). PASS and TSIA were developed by the University of Iowa, Division of Physiological Imaging (55, 73). Voxels were binned into 3 x 3 regions of interest (1.4 mm x 1.4 mm x 2.4 mm) resulting in regional data for a 4.7 mm^3 volume of lung parenchyma. Data was filtered to remove major airways and vessels using the following criteria: fractional air content, 0.4-0.9; fractional blood content, 0.02-0.5, blood flow > 0, and chi-squared 0-50,000. Data was excluded if the algorithm could not determine a full-width half maximum value for the curve fit. PBF (ml/min), MTT (seconds), and air and non-air (water) content were determined for each ROI.

Normalization Methods

FMS PBF measurements were normalized by two methods. First, the FMS piece fluorescent is divided by the mean fluorescence to provide mean normalized measurements (FMS PBF MEAN). A second normalization method is used to normalize the regional PBF by the product of the mean and weight of the lung piece, thereby providing weight-normalized PBF measurements (FMS PBF WTNORM). Pieces that predominantly included large conducting airway were excluded.

MDCT PBF measurements were normalized by four different methods: Regional PBF normalized to the mean PBF (MDCT PBF MEAN), PBF normalized to air content (MDCT PBF AIR, ml/min), PBF normalized to non-air tissue (MDCT PBF NON-AIR,

ml/min/g), and PBF normalized per alveolus (MDCT PBF ALVEOLUS, ml/min). The following equations (described in Chapter 2) were used to determine these normalizations:

$$\text{MDCT PBF MEAN} = \text{PBF}/\text{mean(PBF)}$$

$$\text{MDCT PBF AIR} = \text{PBF}/(\text{Fair})$$

$$\text{MDCT PBF NON-AIR} = \text{PBF}/(\text{Fnonair} \times 1.05)$$

$$\text{MDCT PBF ALVEOLUS} = \text{PBF}/(\text{Fmaxair}/\text{Fair})$$

where the fraction of air (Fair) and non-air (Fnonair) content of the parenchyma can be determined from the baseline image obtained prior to contrast injection. Fmaxair is the maximum value of the parenchymal air fraction for the whole lung region sampled. For MDCT PBF NON-AIR, we assume the average tissue density is 1.05 g tissue/volume. The non-air content includes true tissue volume, blood volume and interstitial or alveolar fluid volumes.

MDCT and FMS Data Registration

To compare data sets at the FMS piece size resolution, MDCT and FMS PBF data were registered to obtain a matched data set containing both FMS and MDCT PBF measurements according to the schematic shown in Figure 2. A normalized mutual information based rigid registration algorithm provided by Analyze™ software (Mayo Clinic, Rochester, MN) was used to rigidly (translation and rotation only) match *in vivo* perfusion MDCT PBF data to *in vivo* FRC volumetric MDCT data for the supine and prone positions. The first of the twenty temporal scans from the perfusion data set was extracted as a reference slab to be matched against the FRC volume. During registration, the image intensities were constrained by thresholds for improved contrast in order to narrow the sampling region to the lung boundary. FMS PBF was overlaid on the MDCT images of the *ex vivo* air-dried lungs, obtained prior to FMS processing. The *ex vivo* lung volume was then registered to the *in vivo* FRC volumetric data set for both supine and

prone positions. A multi-modality algorithm that applied information about the shape of the lung and main bronchi airway segmentations after a user-performed rigid alignment of lung volumes at the carina was used to register the lung volumes. This algorithm uses normalized mutual information and small-deformation inverse consistent linear elastic (SICLE) image registration (26). Normalized mutual information image registration method maximizes the mutual information of source and target image intensity histograms and is robust to intensity discrepancies between source and target images. SICLE image registration method jointly estimates forward and reverse transformations between two images while minimizing the inverse consistency error (ICE). ICE is defined as the difference between the starting and ending position of a point that is mapped through the forward transformation followed by the reverse transformation. To quantify registration accuracy, 10-12 landmark points were manually selected at branch points of the airway tree in the *ex vivo* and *in vivo* FRC volumes. For each pair, the *ex vivo* landmark points were mapped to the *in vivo* FRC volume with the registration transformation determined during registration steps. The average registration error was calculated for each registration (prone and supine for each animal) by comparing the registration-predicted positions to the user-determined positions.

Statistical Analysis

All statistical analyses were performed on SPSS (Windows 17.0, SPSS, Inc; Chicago, IL). Mean regional PBF measurements were determined for each method from the matched FMS-MDCT data set at the matched resolution level (volume 1.8 cm^3). The heterogeneity of flow to the region was characterized by the coefficient of variation (CV). CV is defined as the standard deviation (SD) divided by the mean. Vertical y-gradients were assessed for each normalization method in supine and prone positions using simple linear regression methods with regional PBF as a function of height (cm) of the *in vivo* lung from the non-dependent to dependent lung border, with West zone 4 regions

removed (reduced flow in the non-dependent region of lung). Slope and correlation coefficients were calculated. Paired t-tests were performed to determine if significant differences in CV and vertical gradient exist for supine versus prone position. A p-value less than 0.05 was considered significant. Spearman correlation coefficients were calculated between the FMS and MDCT PBF measurements to quantify the similarity between the two methods for piece-by-piece (1.8 cm^3) and larger regional comparisons (8-10 cm^3).

Results

FMS and MDCT PBF measurements were obtained in 6 of the 7 swine, due to loss of catheter line in 1 animal. 1 set of measurements were excluded due to problems with the air drying process that resulted in a small, low-inflation level dried lung. The remaining 5 animals successfully underwent MDCT perfusion imaging and FMS administration and data processing. Images were registered for supine and prone positions; regional PBF measurements were normalized, and compared for ROIs consisting of lung volumes of 1.8 cm^3. This resulted in an average of 437 ± 45 points per data set. PBF measurements obtained with FMS WTNORM, MDCT MEAN at its high resolution level, and MDCT MEAN at the FMS resolution level for supine and prone position for representative slices are demonstrated in Figure 3.

Registration Accuracy

Registrations successfully matched MDCT PBF measurements to FMS PBF measurements in all five animals for prone and supine positions. Visually, lung regions best matched in the central airway region just distal the carina, and degraded in quality as one moved peripherally and basally. Figure 4 shows two axial slices from the *in vivo* volume at PEEP at 7.5 cm H_20 and *ex vivo* volume scan transformed to the *in vivo* coordinate plane. Differences in intensity are present due to density differences in dried versus *in vivo* lung tissue. Registration algorithms utilized segmentation of the left and

right main bronchus to better align the lung. An axial slice just distal to the carina and a coronal slice demonstrating the airway tree for *in vivo* and *ex vivo* matched images is shown in Figure 5 and demonstrates good alignment and overlap between airway trees. Landmark error for each registration is summarized in Table 2. The average landmark error was 2.6 ± 0.8 mm and 3.1 ± 1.0 mm for prone and supine position respectively.

Volumetric Analysis

Results of the total lung volume measurements were obtained for *in vivo* FRC, *in vivo* TLC, and *ex vivo* dried lung data sets are summarized in Table 3. The dried lung volumes were less dense (decreased mean lung density HU) and more homogenous (smaller SD) compared to the *in vivo* lung volumes. Figure 6 shows a 3-D volume rendering of the *in vivo* FRC volume in the prone position that visually demonstrates its similarity to a digital photograph of the *ex vivo* dried lung. The air-dried lung volumes correspond most closely to *in vivo* measurements from the volumetric images obtained at a FRC lung inflation volume and not TLC. *Ex vivo* lung volume were compared to the prone and supine FRC measurements for each animal and are summarized in Table 2. The mean *ex vivo* dried lung volume was 112 ± 8% (range: 102 - 123%) and 107 ± 4% (range: 101 - 112%) of the *in vivo* volume measurement at FRC in the prone and supine position respectively. The *ex vivo* lung volume was greater than the *in vivo* FRC volume measurements in all animals for supine and prone positions. *In vivo* lung volume measurements in 4 out of the 5 lungs in the supine position were greater than volumes in the prone position measurements, and tended to matched more closely with measurements of total lung volume of the *ex vivo* lungs.

MDCT and FMS PBF Measurements

Mean regional PBF and CV measurements for FMS and MDCT methods for all normalization methods are shown in Table 4. CV measurements for supine and prone positions for each animal are shown in Figure 7. While there is marked heterogeneity of

PBF present in the lung parenchyma, PBF was consistently more homogenous when the pigs were in the prone position. CV measurements for FMS PBF MEAN, FMS PBF WTNORM, MDCT PBF MEAN, MDCT PBF AIR, MDCT PBF ALVEOLUS and MDCT PBF NON-AIR were all significantly less in the prone position compared to the supine position (p values: 0.00007, 0.001, 0.006, 0.015, 0.007, 0.012 respectively).

Correlation of MDCT and FMS PBF Measurements

Regional correlation at a FMS piece size (1.8 cm^3) and regional volume (8-10 cm^3), locally grouped, were obtained to compare the associations between FMS and MDCT PBF measurements for the various normalization methods. These results are summarized in Table 5. For the regional volume assessment, data was grouped according to x, y, and z coordinates into volumes of 8-10 cm^3 which corresponded to 80-100 data points per position. Correlations for the 5 animals are shown in Figure 8. Correlations strengthened when the analyzed volume was increased from FMS piece size to the regional volume. MDCT PBF measurements correlated more closely with FMS PBF WTNORM measurements compared to FMS PBF MEAN measurements for all MDCT normalization methods. Strong correlations exist for both resolution levels between FMS PBF WTNORM measurements and MDCT PBF MEAN and MDCT PBF AIR measurements. Moderate correlation exists between FMS PBF WTNORM to MDCT PBF ALVEOLUS. There is essentially no correlation between MDCT PBF NON-AIR and FMS measurements techniques. One of the five animals did not demonstrate good correlations for any normalization method. If one considers it an outlier and removed from analysis, mean correlations improve and standard deviations decrease. Correlations were stronger in the supine position compared with the prone position. Prone positions demonstrated a narrow range of blood flow values, and were more sensitive to outliers and noise.

Comparison of Vertical Gradients

A simple linear regression model was used to determine the vertical gradient (gravitational or y-component) present with each PBF normalization method. The slope was determined in the lung region spanning the non-dependent to maximal flow point. A positive slope indicates a gradient or increase in blood flow from non-dependent to dependent regions of the lung The most dependent region of the lung (zone 4/atelectasis) was excluded for slope and r^2 calculations. An example of FMS and MDCT PBF slope measurements for the supine and prone position is shown in Figure 9. Vertical gradients are summarized in Table 6. Vertical PBF gradients differ from supine versus prone position with higher gradients present in the supine position for PBF measurements with FMS MEAN, FMS WTNORM, MDCT MEAN, MDCT AIR, and MDCT ALVEOLUS, but not for MDCT NON-AIR (Figure 10). FMS PBF MEAN and FMS PBF WTNORM had a vertical slope of 0.19 ± 0.01 and 0.17 ± 0.02 respectively, which based on r^2 values, accounted for 48% and 66% of the variability seen in regional PBF. The vertical gradient accounted for 53%, 55%, 1% and 26% of the variability in the MDCT PBF measurements normalized to the mean, air, non-air and alveolus respectively for the supine position. For the prone position, slope and r^2 values were all decreased except for MDCT PBF NON-AIR measurements where it increased. For the prone position, the vertical gradient accounted for 28%, 25%, 17%, and 22% of the variability for MDCT PBF MEAN, MDCT PBF AIR, MDCT PBF NON-AIR, and MDCT PBF ALVEOLUS measurements respectively. For FMS PBF MEAN and FMS PBF WTNORM measurements, there was no gradient observed (slope: FMS PBF MEAN, -0.003 ± 0.021; FMS PBF WTNORM, 0.03 ± 0.03) in the prone position.

Discussion

FMS and MDCT regional PBF measurements normalized with various methods matched at both a FMS piece size resolution (1.8 cm^3) and regional volume (8-10 cm^3)

resolution demonstrated good regional correlation. Perfusion heterogeneity and vertical gradients are affected by the choice of normalization method. To compare methods or correctly interpret the physiology of the lung, one needs to account for the chosen normalization methods. The strongest correlation observed between FMS PBF WTNORM and MDCT PBF measurements is with the MDCT mean-normalized data, followed closely by the air-normalized data. The FMS PBF WTNORM normalization method demonstrates stronger correlations than the FMS PBF MEAN normalization method to all MDCT-based PBF measurements. FMS PBF WTNORM measurements take in account the weight of the lung piece by a weight normalization which accounts for the piece size, and therefore adjusts for partial volume effects due to the rectilinear cutting grid. Since the edge pieces may only have 15-20% of the total cube volume containing lung parenchyma, the blood flow reported would be dramatically reduced if a partial volume correction were not performed. An edge piece may appear to be a low flow region but the PBF measurement may simply reflect a low piece size, not low flow to the lung tissue. By doing this correction the FMS PBF WTNORM measurements should, and do, match more closely than the FMS PBF MEAN measurements with *in vivo* MDCT PBF measurements, which due to its high resolution, allows for the inclusion of lung parenchyma without much partial volume effect. The sub-millimeter voxel size with MDCT minimizes the impact of edge artifact on the data. Since the MDCT PBF measurement is an average of all blood flow in the FMS-sized ROI, the need for a further normalization for the piece weight is not necessary.

MDCT PBF ALVEOLUS normalization methods demonstrated only moderate correlation to the FMS PBF measurements. This was surprising since this normalization attempts to provide a "flow per alveolus" measurement in order to better match FMS methods. Assuming the maximum air fraction seen in the images corresponds to a fully expanded alveolus, one can correct for differences in expansion level based on HU values or calculated air content with this normalization (25). In this study, MDCT PBF

ALVEOLUS measurements did not provide the strongest match to FMS PBF measurements. FMS literature states that FMS PBF measurements are obtained with alveoli at a uniform size and the number of alveoli for a given piece of lung is proportional to the weight of the piece since the lungs where dried fully expanded at TLC (50, 66). Volumetric measurements of the dried lung compared to FRC and TLC *in vivo* volumes in this study demonstrate the FMS PBF measurements were obtained from air-dried lungs, while thought to be expanded to TLC, once dried where at an inflation level slightly larger than FRC, not TLC. These blood-free, air-dried lungs' volumes have decreased during the drying process and the dried lung parenchymal density is very uniform with decreased density variability compared with the *in vivo* FRC and TLC density measurements. If during the drying process, the lung expansion did not remain at TLC, rather alveolus expansion was at a FRC volume, the alveoli may not have been uniformly expanded. Hoffman et al. demonstrated increasing gradients in regional lung density, with the greatest effect in the dependent lung regions, as lung inflation changed from TLC to FRC (68). If FMS PBF measurements were obtained at FRC, alveoli will not be uniformly expanded, resulting in lung expansion effects on regional PBF FMS measurements. Lung expansion may account for the moderate agreement observed between FMS PBF measurements and MDCT PBF ALVEOLUS measurements. MDCT PBF NON-AIR measurements demonstrated a very weak correlation with FMS PBF measurements. This normalization method accounts for the non-air to "tissue" content of the voxel. This corresponds to the true tissue volume, interstitial fluid volume, and any alveolar fluid. Non-air content increases from the non-dependent to dependent region of the lung. Little to no vertical gradient is observed in the gravitational direction (y-axis) with this normalization.

Both FMS and MDCT PBF techniques demonstrate marked heterogeneity in the lung. Flow was consistently more homogenous when the animal was in the prone position. CV measurements were significantly greater in the supine position compared to

the prone position for all normalization methods. Vertical slope measurements for MDCT PBF demonstrate substantially significant correlation (r^2) in the supine position and less pronounced, but still significant, r^2 values in the prone position, suggesting a vertical gradient component to flow in both supine and prone positions. For mean and air-normalized PBF measurements, vertical gradients in the supine position with the y-direction or height accounting for 53% and 55%, respectively, of the variability existed. These gradients were decreased (though not significantly) in the prone position with the height accounting for only 28% and 25%, respectively, of the variability. FMS PBF measurements demonstrate a significant vertical gradient in the supine position with the height accounting for 66% of the variability. Unlike CT, FMS PBF measurements did not demonstrate a significant height component when lying prone. While it is known that the contrast material used for MDCT imaging is more dense than blood and may lead to a gravitational bias confounding the effects of real gravity on PBF (27), one would expect this effect to be present for all of the MDCT measurements. If this significantly influenced the measurements, one would expect to see larger gravitational components in the MDCT versus FMS PBF measurements for both supine and prone position and not just prone position like what was observed. While alveolus normalized MDCT PBF measurements demonstrated similar heterogeneity compared to other MDCT PBF methods; vertical gradients patterns obtained with this technique differed from mean and air-normalized vertical gradients. Alveolus normalized PBF measurements did not demonstrate significant difference in the vertical gradient or r^2 values obtained for supine or prone positions. Since this normalization is based on a "flow per alveolus", it should not be drastically affected by changes in the lung expansion. Hoffman et al. demonstrated that the lung is more uniformly expanded in the prone versus the supine position (74). We conclude that while lung expansion changes to a more uniform distribution in the prone versus supine position, the flow per alveolus does not drastically change, since similar CV and vertical gradients were observed with this normalization method. MDCT PBF

non-air normalization methods did not match up well with other normalization and FMS methods, demonstrated by a reversal of gradients and poor correlation with FMS PBF WTNORM and FMS PBF MEAN measurements.

While the correlation coefficients demonstrate good agreement between FMS and MDCT PBF measurements, they are not near a perfect correlation value of 1. Several reasons can be given to account for error in our measurements that would diminish the correlation between FMS and MDCT PBF data. First, FMS data acquisition acquired measurements over a 5 minutes period following the CT imaging. All together, this resulted in approximately 10 minutes from the first MDCT imaging scan and the last of the microspheres being deposited in the capillaries. While it has been demonstrated that perfusion patterns are spatially stable over time (49), it is possible that subtle regional changes in blood flow could occur. When the high resolution MDCT data (capable of detecting more subtle changes) was averaged differences in regional PBF measurements could result. Secondly, a narrow physiological range of flows was used to correlate the two methods. PBF measurements made in the supine position demonstrated stronger correlations than measurements obtained in the prone position. This may be due to a more uniform blood flow distribution in the prone position. This data (and correlations from it) would be influenced more by noise or outliers in the data. Stressing the blood flow to include a wider range of blood flow values may be of interest in the future. Lastly, and most importantly, improper alignment of FMS data to MDCT data would result in a mismatch of data and decreased correlation coefficients. Surgical removal and drying of the lung alters the lung shape, density and overall composition (*ex vivo* lung have no blood volume) from the *in vivo* state making accurate registration challenging. Dried lung parenchyma is less dense (lower HU value) and more homogenous (decreased SD) than *in vivo* lung parenchyma. Intensity based similarity measures cannot solely be used to match regions of lung. While an effort was made to match lung shape during air drying, differences in the overall shape, specifically in the apical region occurred. The

lungs were dried without a chest cavity or heart to restrict inflation, and hung vertically from the trachea, causing a slight elongation of the dried lungs compared to *in vivo* lungs. Bleb formation occurred in 3 out of the 5 lungs, distorting the lung shape at the major fissures. Dried lung volumes were inflated to TLC post mortem, but shrank during the drying process. Analysis of MDCT images demonstrated dried lung volumes closer to an FRC lung inflation volume with volumes ranging from 101-123% of the FRC volume. The greater the difference the lung volume, the harder it is for the registration algorithm to match the lung. In order to deal with these challenges, a multi-modality algorithm was used that applied information about density changes, shape of lung, and main bronchi airway segmentations after a user-performed rigid alignment of lung volumes at the carina to match the two lung volumes. Even with this sophisticated algorithm, landmarks demonstrated a mismatch on the order of 2-3 mm, with registration worsening in the peripheral and basal regions. In the future, registration methods may need to include more information such as landmarks (for example beads) placed in the lung to provide a better correspondence between lungs and more accurate matching. Still, with this registration scheme, we were able to demonstrate good correlation on a FMS piece size resolution of 1.8 cm^3 and regional volumes of 8-10 cm^3 between FMS PBF WTNORM measurements and MDCT PBF MEAN and AIR measurements, and moderate correlation between FMS PBF WTNORM and MDCT PBF ALVEOULS measurements.

In conclusion, PBF measurements obtained with MDCT perfusion imaging, correlate well with FMS measurements obtained at a regional level. The strongest correlation exists between the FMS and mean normalized MDCT data. Both measurement techniques demonstrate marked heterogeneity in PBF, with a more homogenous flow distribution in the prone position compared with supine position. Normalization methods affect the interpretation of PBF data and need to be considered when comparing cross-modalities and interpreting the physiology of the lung.

Figure 1. FMS experimental setup and processing. Lungs are air-dried (upper left), coated with an approximately 1-cm thick layer of Kwik Foam (upper right), encased in a block of rapid setting urethane foam (lower left) to secure in a box, and later cut into 1.2 cm^3 transverse slices (lower right). FMS transverse slices are cubed into 1.2 cm x 1.2 cm x 1.2 cm pieces (1.8 cm^3).

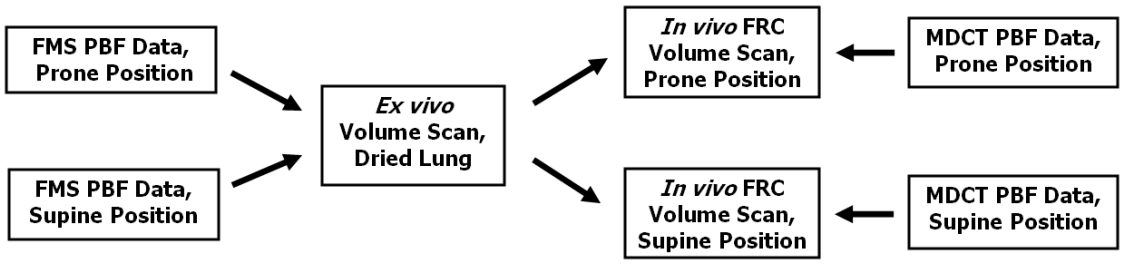

Figure 2. Schematic demonstrating the necessary steps to match the FMS PBF data sets with the MDCT PBF data sets for prone and supine positions. The arrows show the images that were registered.

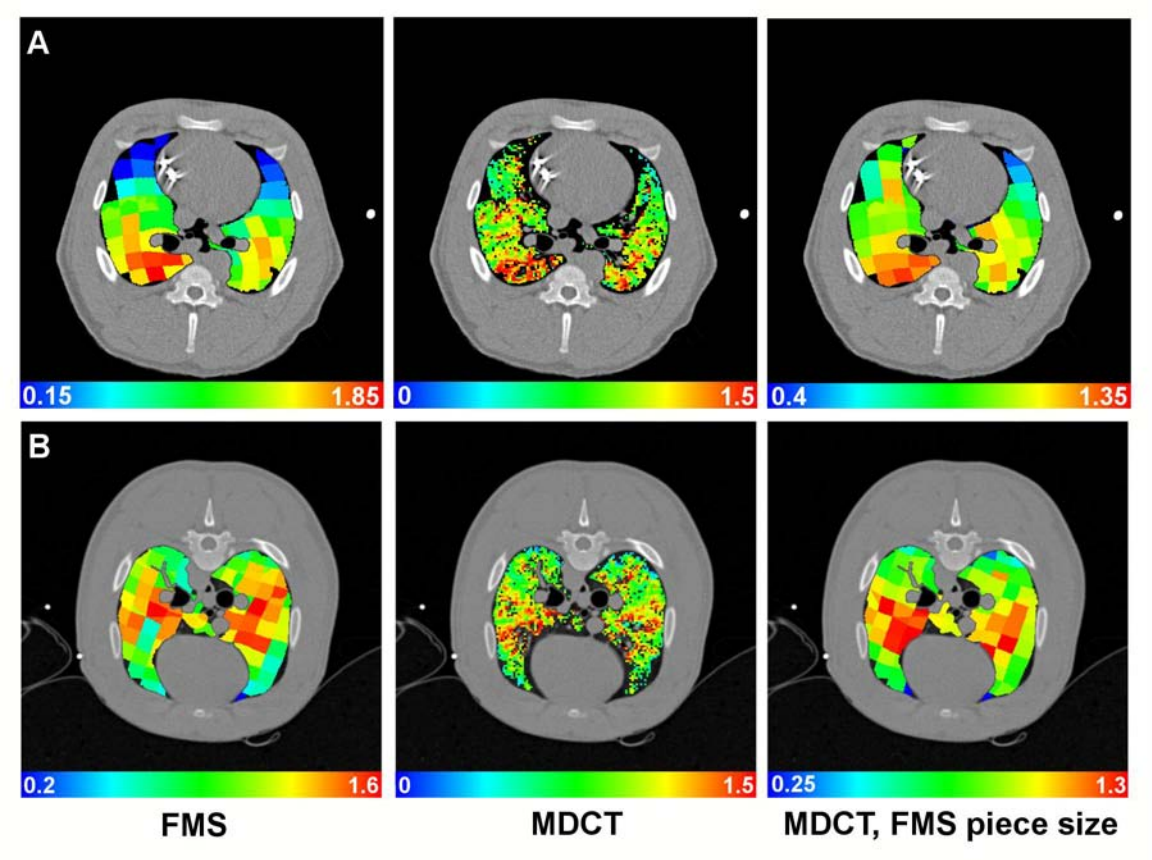

Figure 3. Color-coded maps from a representative slice from an animal in the supine position (top row) and prone position (bottom row), demonstrating the regional PBF measurements obtained by FMS WTNORM measurements (1.2 x 1.2 x 1.2 cm) (Left), MDCT PBF MEAN measurements at original high resolution (voxel: 1.4 x 1.4 x 2.4 mm) (Middle) and MDCT PBF MEAN measurements, averaged to FMS resolution (voxel: 1.2 x 1.2 x 1.2 cm) (Right).

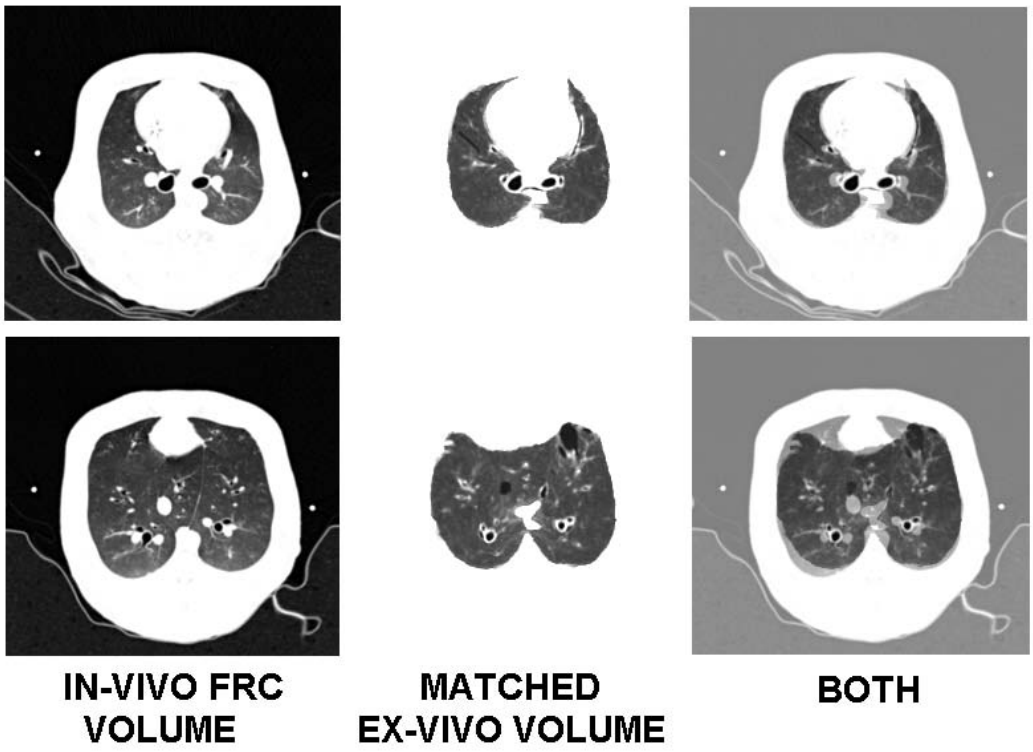

Figure 4. Two axial slices, near the carina (top row) and a basal region (bottom row) of the lung, from a representative animal demonstrating the *in vivo* FRC lung volume (left) and *ex vivo* registered lung volume (middle). On the right is the overlaid merged image demonstrating good overlap in the carina and basal region corresponding to perfusion measurements obtained for both techniques.

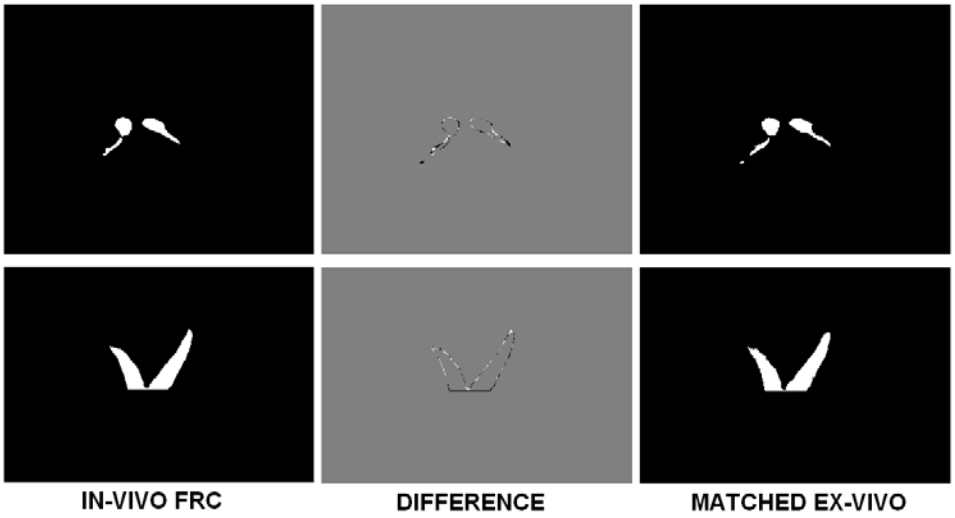

Figure 5. The airway segmentation from the left and right main bronchus was used to improve the registration results. The *ex vivo* airway tree (right) is matched to the *in vivo* FRC airway tree (left). The difference between the matched *ex vivo* and *in vivo* FRC airway tree for an axial (upper) and coronal (lower) slices are demonstrated in the middle region.

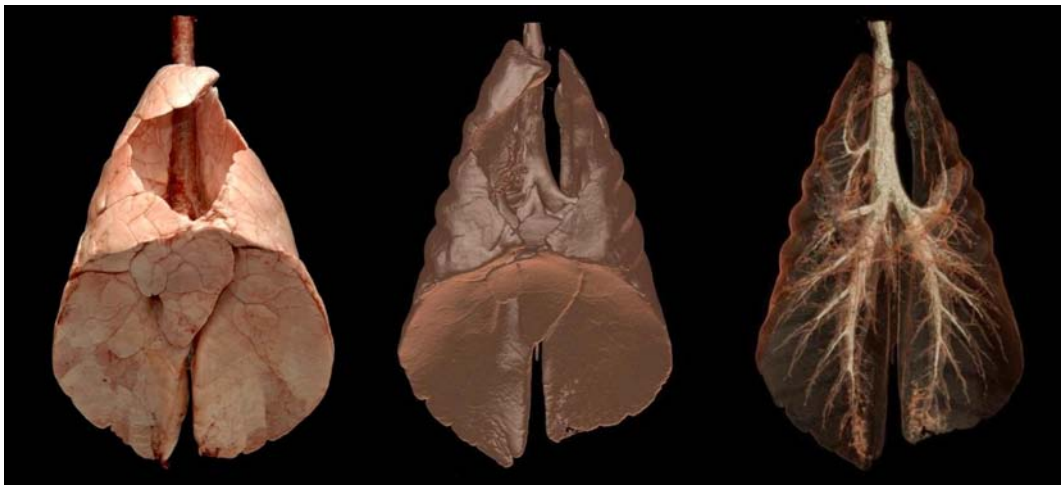

Figure 6. Left) Digital photo of air dried lungs. Middle) 3D volume rendering of the lungs and Right) Vasculature tree and airway tree obtained from the volumetric spiral MDCT *in vivo* image data set at FRC (PEEP of 7.5 cm H_20) in the prone position.

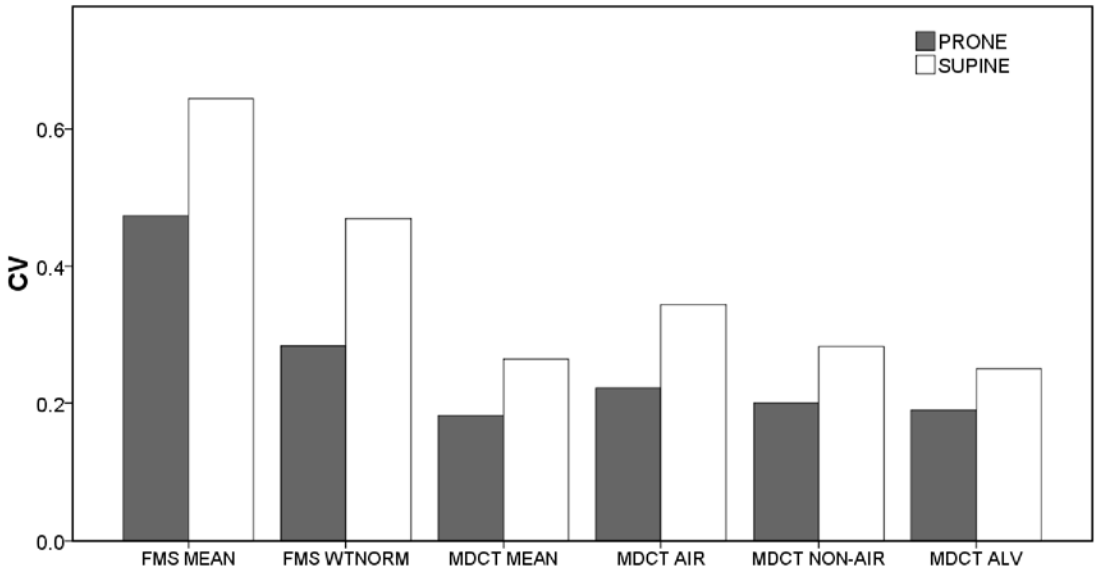

Figure 7. CV measurements for the supine and prone position for the normalization methods. Supine position demonstrated higher CV measurements for all normalization methods. FMS methods, especially FMS mean normalized, had higher CV measurements compared with the 4 MDCT PBF normalization measurements.

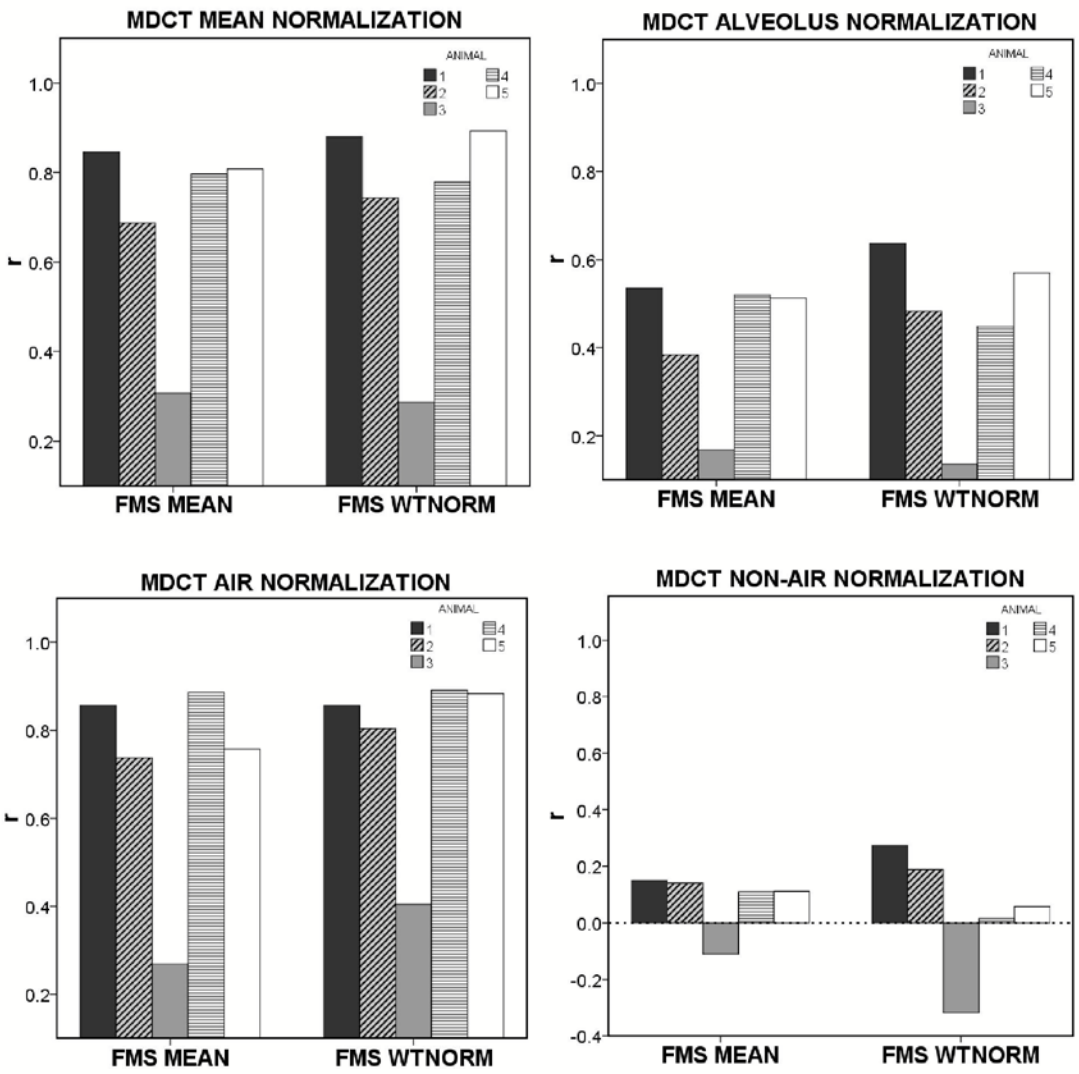

Figure 8. Correlation for FMS MEAN and WTNORM normalization methods and the four MDCT normalization methods: MEAN (upper left), ALVEOLUS (upper right), AIR (lower left) and NON-AIR (lower right) for the 5 animals in a supine position at a regional level.

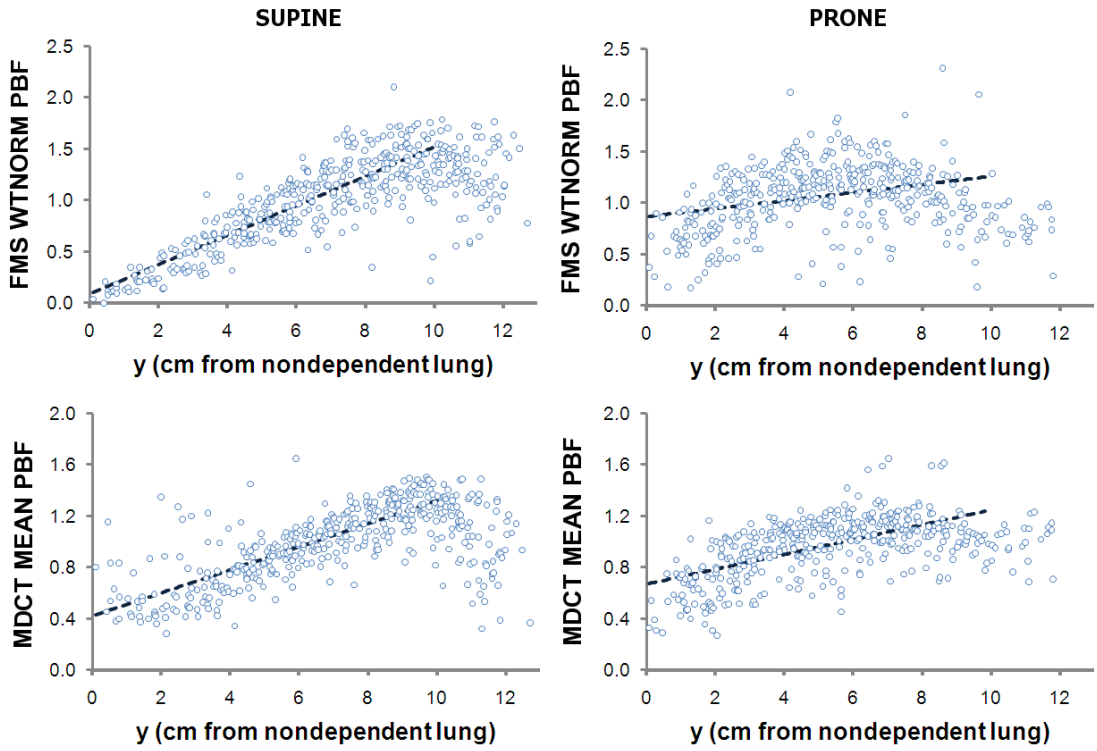

Figure 9. Vertical gradients (y-gradient) from a representative animal for FMS PBF WTNORM (top row) and MDCT PBF MEAN (bottom row) for supine (left) and prone (right) positions. Vertical gradients were higher for FMS WTNORM and MDCT MEAN PBF measurements in the supine versus prone position. Zone IV regions were excluded from the gradient calculation.

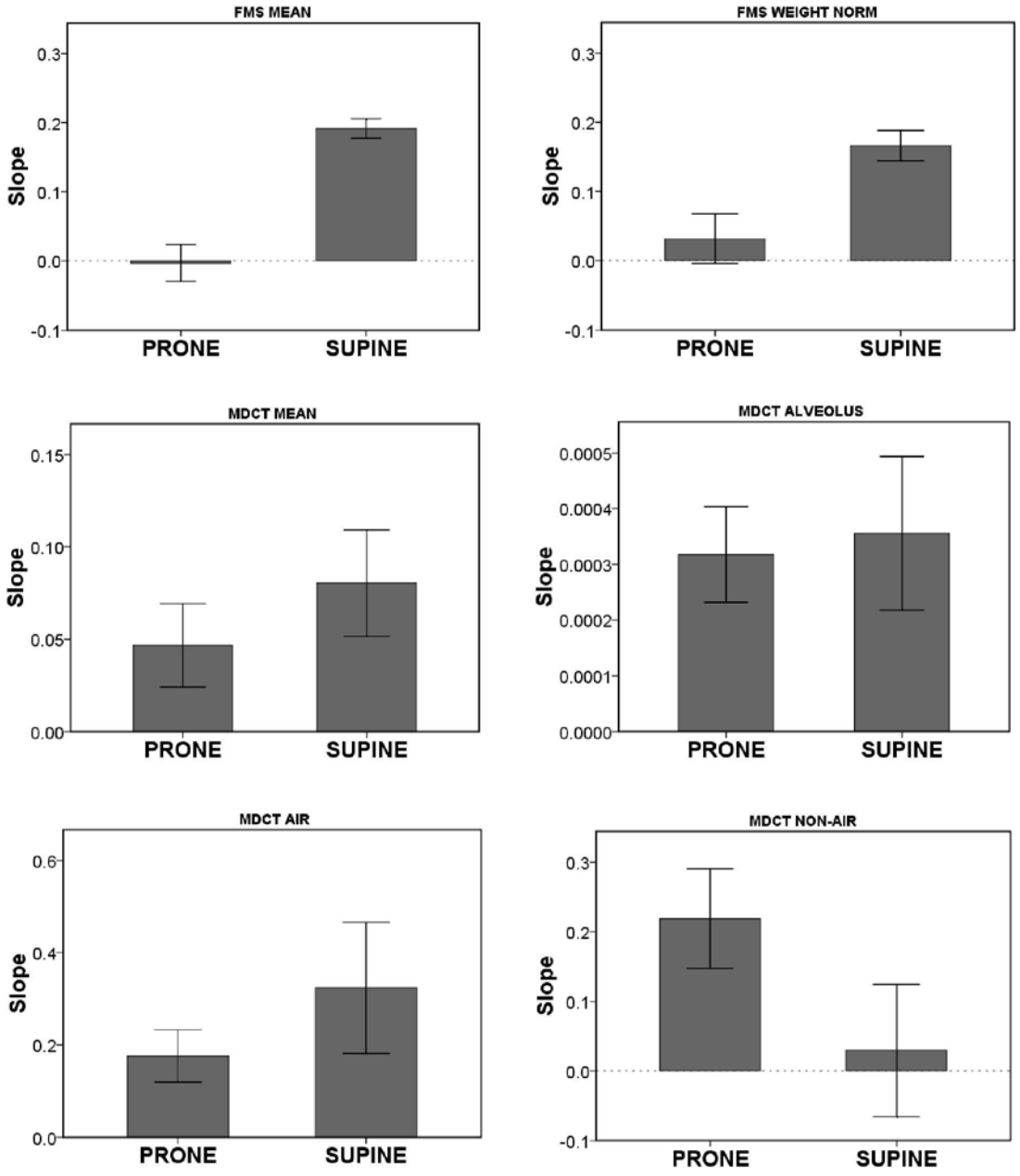

Figure 10. Vertical gradients for supine and prone positions for FMS and MDCT PBF measurements. Error bars represent 95% confidence intervals.

Table 2. Volumetric analysis and quantification of registration accuracy for supine and prone positions.

	Animal					
	1	2	3	4	5	Mean
Ex vivo Lung Volume	1061	1072	1051	1033	943	1032 ± 52
Supine:						
FRC Lung Volume	946	1011	1044	938	876	963 ± 66
Ex vivo: FRC Supine	112%	106%	110%	101%	108%	107 ± 4%
Landmark Error, mm*	1.8 ± 1.3	2.4 ± 1.2	3.0 ± 1.5	3.7 ± 5.2	4.5 ± 6.3	3.1 ± 1.0
Prone:						
FRC Lung Volume	865	1047	933	890	864	920 ± 77
Ex Vivo: FRC Prone	123%	102%	113%	116%	109%	112 ± 8%
Landmark Error, mm*	2.2 ± 2.8	1.8 ± 0.9	2.2 ± 1.1	3.9 ± 3.4	2.7 ± 3.9	2.6 ± 0.8

Note: Lung volume measurements are reported in units of cm^3.

* Error measurements from 10-12 user-determined landmark points are reported as mean ± SD.

Table 3. Volumetric Analysis of *in vivo* prone position and *ex vivo* air dried lung volumes.

	PEEP (cm H_20)	Mean Lung Density, HU	SD Lung Density, HU	Total Volume (cm^3)
In vivo FRC	7.5	-639.6 ± 18.8	148.3 ± 15.0	919.7 ± 76.7
In vivo TLC	25.0	-754.9 ± 21.0	146.0 ± 7.2	1312.7 ± 108.3
Ex vivo Dried Lung	--	-956.6 ± 6.6	46.3 ± 15.3	1032.3 ± 51.9

Note: Results are reported as mean ± SD (n = 5).

Table 4. Mean PBF and CV measurements for FMS and MDCT normalization methods for supine and prone positions in five animals.

	SUPINE		**PRONE**	
	Mean ± SD	CV	Mean ± SD	CV
FMS				
Mean	1.10 ± 0.02	0.64 ± 0.02	1.10 ± 0.01	0.47 ± 0.03
Weight	1.05 ± 0.01	0.46 ± 0.06	1.07 ± 0.02	0.28 ± 0.04
MDCT				
Mean	1.00 ± 0.01	0.26 ± 0.02	0.98 ± 0.03	0.18 ± 0.05
Air	3.16 ± 0.65	0.34 ± 0.03	3.39 ± 0.64	0.22 ± 0.04
Non-Air	6.05 ± 1.29	0.24 ± 0.05	6.26 ± 1.17	0.19 ± 0.04
Alveolus	0.0071 ± 0.0014	0.24 ± 0.04	0.0078 ± 0.0015	0.19 ± 0.04

Note: Results are reported as mean ± SD (n = 5).

Table 5. Correlation coefficients for FMS and MDCT PBF measurements in the supine position for FMS piece volume and regional volume measurements.

	FMS PIECE VOLUME (1.8 cm^3)		**REGIONAL VOLUME** (8-10 cm^3)	
N	874 ± 87		176 ± 15	
	FMS MEAN	FMS WTNORM	FMS MEAN	FMS WTNORM
MDCT MEAN	0.62 ± 0.15	0.65 ± 0.18	0.69 ± 0.22	0.72 ± 0.25
MDCT AIR	0.62 ± 0.16	0.69 ± 0.16	0.70 ± 0.25	0.77 ± 0.21
MDCT ALVEOLUS	0.40 ± 0.11	0.41 ± 0.17	0.42 ± 0.16	0.45 ± 0.19
MDCT NON-AIR	0.10 ± 0.06	0.04 ± 0.19	0.08 ± 0.11	0.04 ± 0.23
Excluding Animal 3 (Outlier)	FMS MEAN	FMS WTNORM	FMS MEAN	FMS WTNORM
MDCT MEAN	0.68 ± 0.03	0.73 ± 0.06	0.78 ± 0.07	0.82 ± 0.07
MDCT AIR	0.69 ± 0.02	0.76 ± 0.04	0.81 ± 0.07	0.86 ± 0.04
MDCT ALVEOLUS	0.44 ± 0.06	0.47 ± 0.11	0.49 ± 0.07	0.53 ± 0.09
MDCT NON-AIR	0.12 ± 0.02	0.10 ± 0.14	0.13 ± 0.02	0.13 ± 0.12

Note: All results are mean ± SD.

Table 6. Vertical gradients of PBF for MDCT and FMS normalization methods.

	SUPINE		PRONE	
	SLOPE	R^2	SLOPE	R^2
FMS				
Mean	0.19 ± 0.01	0.48 ± 0.05	-0.003 ± 0.021	0.006 ± 0.003
Weight	0.17 ± 0.02	0.66 ± 0.12	0.03 ± 0.03	0.08 ± 0.07
MDCT				
Mean	0.08 ± 0.02	0.53 ± 0.23	0.05 ± 0.02	0.28 ± 0.11
Air	0.32 ± 0.11	0.55 ± 0.22	0.18 ± 0.05	0.25 ± 0.12
Non-Air	0.03 ± 0.08	0.01 ± 0.02	0.22 ± 0.06	0.17 ± 0.10
Alveolus	0.00036 ± 0.00011	0.26 ± 0.13	0.00032 ± 0.00007	0.22 ± 0.10

Note: Slope measurements were determined by simple linear regression, with zone IV regions excluded.

CHAPTER 4: DEVELOPMENT OF AN *EX VIVO* LUNG PERFUSION MODEL

Rationale

Lung transplantation is considered an effective treatment for many types of end-stage pulmonary disease, and in some cases, the only treatment option. The main indication for lung transplantation is COPD, accounting for 53% of all single lung transplant cases or 39% of all lung transplants (192). Donor pools are limited resulting in an average wait time of 18 months (3). While criteria exist for lung transplant, the evaluation of donor lungs is subjective, based on very little prospective data, and is made more difficult because decisions must be made quickly (187). The result is 4 out of 5 potential lung donors are rejected. Most transplant surgeons reject lungs with even minor flaws because of the fragile nature of the organs. The main limitations of its application include the limited donor pool, and sub-optimal preservation techniques which have lead to various degrees of ischemia-reperfusion injury (62, 208).

Transplant groups have been developing surgical protocols (36, 62) and special fluids to flush the organs (134, 140, 184, 196, 211) which are focused on the preservation of donor lung function for transplant. Cardiopulmonary bypass systems allow blood to bypass the heart and to continue to flow throughout the body. These systems can be used in *ex vivo* preparations to provide well controlled flow to organs. Steen and colleagues have developed a new method to functionally evaluate lungs in an *ex vivo* system (185). Some transplant groups have then used this *ex vivo* system to assess the lung's function and "recondition" lungs in animal models (85, 182, 185) and for human transplant studies (40, 206). Marginal lungs (not meeting transplant criteria) have been assessed and "reconditioned" in an *ex vivo* perfusion system prior to a successful transplant (183). This method provides an opportunity for transplant surgeons to manipulate the graft *ex vivo* with the hope of enhanced performance post-transplant.

The goal of this project was to develop an *ex vivo* lung perfusion system, stable at physiological flow rates, with the ability to control ventilation and perfusion. Other investigators have attempted to develop lung models capable of simulating pathologic lung conditions with explanted porcine lungs, but only slow flow circulation of 200 ml/min were tolerated (14-16). For the development of our system, we adopted methods from lung transplantation and coupled the system with MDCT imaging to functionally assess the *ex vivo* lungs over time. Having a stable *ex vivo* lung model capable of physiological flow rates will allow for another means of validating new imaging techniques. In order to further validate perfusion MDCT measurements, we obtained perfusion measurements at a range of flow rates and assessed the changes in PBF and MTT as flow rates were increased.

Methods

Surgical Procedure

Eleven sheep with a mean weight of 32 ± 4 kg (range: 28-40 kg) were used for this study. All animal use protocols were approved in advance by the University of Iowa Animal Care and Use Committee and all studies were performed according to the guidelines established by the American Physiological Society and National Institutes of Health. Sheep were administered an intramuscular pre-anesthetic medication (5-15 mg/kg ketamine and 0.1-0.2 mg/kg xylazine), intubated with a size 9.0 cuffed endotracheal tube, and anesthesia maintained via inhalation of isofluorane (2%). The chest cavity was opened via median sternotomy and pericardium was opened longitudinally. The inferior and superior vena cava were tied off and the aorta cross-clamped. The main pulmonary artery was cannulated from the right ventricle and the left atrial appendage was snipped to provide drainage of fluid. Heparin (300 U/kg) was injected directly in the right ventricle at least 5 minutes prior to euthanasia. Animals were euthanized with sodium pentobarbital (Euthasol, 1 ml/10 lb), the lungs underwent a

recruitment maneuver, and then the pulmonary vasculature was flushed with cold (4-8º C) Perfadex (Vitrolife, Gothenburg, Sweden), with 1-2 liters of antegrade flow (PA to LA) followed by 300-600 cc of retrograde (LA to PA) flow. A height of 12-20 inches above the lungs provided continuous flow to the lungs. Perfadex is an extracellular low potassium electrolyte solution developed for the rapid cooling, perfusion and storage of organs in connection with lung transplantation. Each 1,000 ml of Perfadex contains 5% dextran 40, Na^+ 138 mmol, K^+ 6 mmol, Mg^{2+} 0.8 mmol, Cl^- 142 mmol, SO_4^{2-} 0.8 mmol, H_2PO^+ plus HPO_4^{2-} 0.8 mmol and glucose 5 mmol. During the flushing, ventilation was ceased and lungs were clamped in a semi-inflated state. Crushed iced saline was placed around the lungs in the pleural cavity to further cool the lung tissue to minimize ischemia injury.

Once the lungs were removed from the chest cavity, cannulas were secured via purse string sutures in the pulmonary artery (inflow) and left atrium (outflow) to be connected to the perfusion circuit. An ET tube was placed in the cut trachea. Lungs were connected to a primed *ex vivo* perfusion circuit and perfusion was slowly initiated as the lungs were warmed to 37º C, with PA pressure limited to 15-20 mm Hg. Monitoring of PA pressures dictated the speed at which the perfusion rate was adjusted. During warming, temperature, flow rate, and PA and LA pressures were recorded. Careful ventilation with room air (fractional oxygen content, FiO_2: 0.21) commenced at 32º C for the first series of preparations. In the later preparations, the oxygen content was modified to 100% O_2 (FiO_2 of 1.0) to ensure appropriate oxygenation of the lung parenchyma tissue.

Perfusion System

The perfusion system is compatible with MDCT imaging to allow for imaging and physiological monitoring of the lungs (Figure 11). A schematic describing the flow pattern is shown in Figure 12. A perfusate consisting of Steen solution (Vitrolife,

Gothenburg, Sweden) and THAM is used with a volume of 1.5 L of perfusate sufficient for continuous flow. The Steen solution is a buffered extracellular solution that includes human albumin, developed with the intention of providing an optimal colloid osmotic pressure, so that physiologic pressure and flow can be maintained without the development of pulmonary edema (206). THAM, a buffer solution, is used to modulate the pH.

The perfusion system included the following components: centrifugal pump and flow probe, reservoir, heat exchanger and temperature probe, and lung evaluation box. A centrifugal pump provides the user control of non-pulsatile steady flow to the lungs. As the lungs are warmed, the resistance decreases, and the pump adjusts to this by providing more flow for a lower after load. Since the pump is after load dependent, a flow probe is included in the circuit to measure the flow rate accurately. Fluid returns from the lungs to the reservoir, providing storage for perfusate and allows for steady, continuous flow through the circuit. The heat exchanger allows for careful control of fluid temperature and provides a means for gradual, controlled warming of the lung tissue. The temperature probe is placed in the outflow tubing, returning fluid from the left atrium, and the core lung temperature is assessed by measuring the temperature of this fluid. The lung evaluation box houses the lungs during the experiment, and remained covered to minimize the amount of fluid evaporation and keep the lungs from drying.

Physiological Monitoring

We monitored the following physiological parameters over the course of the experiment: left atrium pressure (LAP), pulmonary artery pressure (PAP), pulmonary arterial flow rate (Q), and core lung temperature. Pressure lines for monitoring the PAP and LAP were placed following lung removal. Ventilator settings of PEEP, peak inspiratory pressure (PIP), and tidal volume (TV) were recorded, and minute ventilation

was calculated. PEEP remained at 5 cm H_2O unless lung function declined. Compliance (ml/cm H_2O) and PVR (L/min/mm Hg) were calculated using the following equations:

$$\text{Compliance} = \Delta V / \Delta P = TV / (PIP - PEEP)$$

$$PVR = \text{Flow Rate } (Q) / (PAP - LAP)$$

Imaging Protocol

Images of perfused *ex vivo* lungs were performed on a Siemens Sensation 64 MDCT scanner (Erlangen, Germany). To assess stability of the lung preparation, spiral volumetric non-contrast scans of the lung were obtained at two lung inflation volumes (TLC: 25-30 cm H_20, and FRC: 5 cm H_20) by continuous airway breath hold at a PEEP as noted. Volumetric scans were performed with the following imaging settings: 100 mAs, 120 kV, 1mm pitch, 0.5 second rotation time, 0.75mm slice thickness, 0.5mm slice increment, 512 x 512 matrix, 24 cm FOV and reconstruction kernel of B31f or B35f. Voxel dimensions were 0.47 mm x 0.47 mm x 0.5 mm.

A series of experiments on *ex vivo* sheep lungs in the perfusion system were performed to further validate MDCT-based PBF and MTT measurements. Dynamic ECG-gated perfusion MDCT imaging with bolus contrast injection was performed at flow rates of 50, 75, 100 and 125 cc/kg/min. A contrast injection of 0.5 cc/kg (Visipaque) over 2 seconds was used, with a Medrad power injector system connected to the arterial input flow line just prior to connection to the arterial cannula, thereby still providing a central injection to the lung. Parameters were as follows: axial, ECG triggering mode, FRC breath hold at PEEP of 5 cm H_20, using 80 kV, 150 mAs, 360^o rotations, 0.33 sec scan time, 512 x 512 matrix, and the field of view same as the volume scans. Regional PBF and MTT were determined as outlined earlier in Chapter 2.

Data and Statistical Analysis

Results are reported as mean ± SD. For volumetric images, total, air and tissue volumes were determined with PASS software. The change in tissue volume was quantified for 0 (baseline), 40, 80 and 120 minutes. Mean and coefficient of variation measurements of PBF and MTT were determined for each flow condition.

Results

Eight of the eleven *ex vivo* lung preparations resulted in a stable preparation for the 120 minute monitoring period. 1 sheep died prior to lung removal due to a reaction to anesthesia. Target flow rates ranging from 60 - 100 cc/kg/min for supine position and 25-50 cc/kg/min for prone position were successfully obtained in 8 of the 10 *ex vivo* preparations connected to the perfusion system. Two of the *ex vivo* lungs declined in function to the point that perfusion could not be maintained for the entire 2 hour observation period. The first preparation, declined rapidly over 1 hour at the target flow rate. The second lung declined in function from baseline to 60 minutes. After 60 minutes of perfusion at a rate of 2.8 L/min, the lung retained substantial fluid and required increased PEEP for ventilation. Flow was decreased to 1 L/min and examined for another hour where lung function continued to decline. Alveolar edema resulted and the preparation was terminated early with no blood flow imaging in either of these preparations. One other preparation was physiologically stable and demonstrated stable, but substantial interstitial edema with MDCT volumetric imaging, and therefore no perfusion MDCT imaging was performed. In the remaining 7 sheep lungs studied (5 supine position; 2 prone position). The 5 lung preparations performed in the supine posture were monitored with physiological parameters recorded every 10 minutes and imaging every 40 minutes for 120 minutes. Based on these results, the protocol was modified to prone position, which resulted in visually less edema formation in the lung parenchyma beneath the heart for the 2 preparations. In the supine position, the weight of

the heart on the dependent tissue may have led to increased pressures, thereby increasing the transcapillary gradient, resulting in edema formation.

Physiological Parameters

The following physiological parameters were measured in the *ex vivo* perfusion system: LA and PA pressures (mm Hg), flow rate (Q, L/min), temperature, reservoir fluid level, and ventilator settings: PEEP, PIP, TV, respiratory rate, and FiO2. From these measures, PVR, compliance, and minute ventilation were calculated every 10 minutes for 120 minutes. A summary of the physiological and ventilation parameters during the 120 minutes of observation for the 5 supine *ex vivo* lung preparations is summarized in Table 7. Physiological data from a representative *ex vivo* perfusion preparation is shown in Figure 13. The preparation was physiologically stable with PA and LA pressures within 1 mm Hg of starting values, and no change in PVR or compliance over time.

Assessment of Preparation Stability over Time

Five of the *ex vivo* lung preparations were performed in the supine position and monitored for 120 minutes with imaging. Volumetric non-contrast MDCT images were used to determine if the lungs remained stable over time. Axial slices from one of the MDCT volumetric spiral images after 120 minutes of perfusion from a representative preparation are shown in Figure 14. Regions of fluid accumulation are reflected by an increase in HU value or bright white lung regions. This preparation had minimal edema, or fluid retention, in the dependent region of the lung. Tissue volume for TLC volumetric images obtained at various time points (0, 40, 80 and 120 minutes) were quantified and summarized in Table 8 and graphed for each animal in Figure 15. An increase in tissue volume suggests fluid retention in the interstitial or alveolar spaces. A representative axial slice from one preparation is shown over time (Figure 16) and demonstrates mild fluid retention, specifically in the dependent region of the lung

proximal to the heart. Increases in tissue volume were demonstrated in all preparations. Animal 3 demonstrated an initial decrease in tissue volume at 40 minutes that can be attributed to the recruitment of a lung region previously unopened or atelectatic. From 40 to 120 minutes, the lung did see a small increase in tissue volume. On average, there was a 3%, 6% and 11% increase in tissue volume by 40, 80 and 120 minutes respectively. Lungs demonstrated a greater increase in tissue volume accumulated from 80 to 120 minutes than from 0 to 40 minutes, suggesting a decline in vascular integrity over time.

Regional PBF and MTT at Increasing Flow Rates

Four of the five *ex vivo* lung preparations in the supine position had perfusion MDCT imaging performed at different arterial blood flow rates (Q) to further validate the MDCT perfusion imaging technique. Q, PAP and LAP for each condition per animal are summarized in Table 9. As Q increased, PAP increased. When Q increased above 100 cc/kg/min, PAP typically was above 20 mm Hg. If these flow rates were maintained, hydrostatic edema would most likely occur, but for the short time periods need for perfusion MDCT imaging, the lung preparation tolerated these pressures and flow rates well. Mean and CV measurements for 3 animals at flow rates of 50, 75, 100 and 125 cc/kg/min are summarized in Table 10. Mean PBF were 138 ± 41 ml/min/100ml (CV: 1.15), 187 ± 41 ml/min/100ml (CV: 0.97), 227 ± 40 ml/min/100ml (CV: 0.86), and 262 ± 55 ml/min/100ml (CV: 0.79) for 50 cc/kg/min, 75 cc/kg/min, 100 cc/kg/min, and 125 cc/kg/min flow rates respectively. Mean MTT were 5.4 ± 0.7 sec (CV: 0.62), 4.4 ± 0.3 sec (CV: 0.59), 4.1 ± 0.2 sec (CV: 0.55) and 3.8 ± 0.1 sec (CV: 0.50) for 50 cc/kg/min, 75 cc/kg/min, 100 cc/kg/min, and 125 cc/kg/min flow rates respectively. An example axial slice with color coded maps of PBF and MTT for each of the flow rates and graphs demonstrating the mean and CV measurements are shown in Figure 17. The first preparation (Animal 1) also underwent perfusion imaging, but at different flow rates (2L/min or 60 cc/kg/min; 3 L/min or 90 cc/kg/min, 4 L/min or 120 cc/kg/min, and 5

L/min or 150 cc/kg/min). These Q, PAP and LAP are also summarized in Table 9. Similar trends were observed in this animal with PBF increasing and MTT decreasing as Q was increased. CV decreased with increasing Q demonstrating more homogenous flow patterns for higher flow rates.

Modification of Preparation: Prone Position

The last 2 preparations were performed in the prone position to determine if this would provide a more stable preparation, specifically less fluid accumulation in the lung regions proximal to the heart. The first preparation was monitored for 60 minutes at a flow rate of 25 cc/kg/min (0.8 L/min) before perfusion MDCT imaging was performed. The second preparation was monitored for 120 minutes with a diminished flow rate of 25 cc/kg/min (1 L/min) with CT imaging before a series of perfusion MDCT series were obtained. Difficulties ventilating the lung for prone prep 1 occurred early on during perfusion. A successful warm up period was followed by good ventilation and perfusion of the lung. After 30 minutes of perfusing at our target flow rate, despite good vascular pressures and a good visual assessment of lung tissue, the lungs were declining, and would not expand and contract without high pressures. When removed from the ventilator, the lungs did not collapse at room air, indicative of a non-complaint lung. Air-trapping and increased non-compliant behavior resulted in a decision to terminate early.

Prone preparation 2 was a successful preparation with good ventilation, target perfusion flow rates, and stable pressures over 2 hours. Surgery including flushing the pulmonary vasculature, followed by warming of the lungs proceeded without problem in the preparation. Surgery time for this preparation was approximately 120 minutes. Target flow rate was achieved during an hour warm up period. Despite adequate clear flushing of the lung during the removal surgery, a region of blood and fluid was noted in the very dependent regions of the lung. This has been noted in other preparations and can be appreciated on CT images. Two distinctly bright regions, left and right side, of the lungs

were present throughout the study. This did not resolve over time. Once the target flow rate of 25 cc/kg/min (1 L/min) was achieved, the lungs were monitored with CT volumetric imaging and physiological monitoring for 2 hours. Three axial slices from the TLC volumetric lung data set at baseline and 120 minutes are shown in Figure 18. Lungs were ventilated with mean tidal volumes of 100 ml with a respiratory rate of 6 breaths/minute. Pressures were stable at mean values of 6.2 ± 1.9 mm Hg and -3.1± 2.1 mm Hg for PA and LA respectively. PVR and compliance measurements were stable at mean values of 0.10 L/min/.mm Hg and 6.7 ml/cm H_2O respectively. Quantitative volumetric analysis determined a tissue volume of 855 cm^3 at baseline, which over 120 minutes increased by 3.8% to 888 cm^3. Perfusion measurements at 50, 75 and 100 cc/kg/min were obtained for second prone preparation. Air and non-air content for 4 baseline axial slices of the lung prior to perfusion imaging are shown in Figure 19. They demonstrate good regional air content to the lungs with minimal gradient. Regions near the heart demonstrate lower air content and higher non-air (tissue) content. Color-coded maps of MTT and PBF for a representative axial slice at the 3 flow rates are shown in Figure 20. Mean and CV values are graphed for the flow rates in Figure 21. Mean PBF (ml/min/100 ml) values were 80.2 ± 77.1, 99.9 ± 85.8 and 115.6 ± 96.9 ml/min/100 ml for 50, 75 and 100 cc/kg/min flow rates. CV measurements decreased as flow rate was increased. MTT measurements were 5.8 ± 3.6, 5.3 ± 3.2 and 4.8 ± 2.6 seconds for 50, 75 and 100 cc/kg/min flow rates respectively. CV measurements for MTT also decreased as flow rates increased.

Discussion

We have established an *ex vivo* lung perfusion system that allows for stable, careful monitoring of excised heart-lung blocks in a sheep model. This system was successfully used to monitor physiological, perfusion and ventilation parameters for *ex vivo* perfused and ventilated lungs at normothemic conditions. This preparation is

compatible with CT imaging technique and can be used to assess the anatomy and function of the lung. Short term (1-2 hour) *ex vivo* lung perfusion in an isolated circuit at normothermia has been demonstrated for the assessment of donor lung quality (182, 183, 185), while success with prolonged *ex vivo* lung perfusion systems has been elusive due to deterioration of the lung function (21, 41, 60). We demonstrate moderate stability over a time period of two hours with quantitative imaging analysis of TLC volumetric non-contrast MDCT images. During this time, there was fluid retention in the lung, ranging from a few percent to over 20%. Most of the edema was visually seen in the dependent regions of the lung, specifically in the region of lung resting near or beneath the heart tissue. Preparations that declined in function over time had large transmural pressure gradient (n = 1) or very non-compliant lung tissue (n = 1).

Perfusion imaging PBF and MTT measurements were determined for 4 *ex vivo* lungs in the supine studies for varying flow rates. As pulmonary arterial flow rates were increased from 50 cc/kg/min to 125 cc/kg/min, mean regional PBF increased and MTT decreased as expected. CV measurements demonstrate and visually one can detect a more homogenous flow pattern for PBF and MTT measurements. As flow increases, the capillary are recruited and flow is distributed throughout the lung parenchyma. At high flow levels, flow was divided in newly recruited non-dependent regions and dependent regions of the lung. At low flows, a larger gradient in flow is seen with perfusion mainly in the dependent regions of the lung. These studies demonstrate physiological changes consistent with known lung physiology and blood flow patterns, further validating the perfusion MDCT technique.

In order to best preserve lung function, lung transplantation techniques were adopted. These fluids have been designed to preserve endothelium function, and minimize the formation of edema, and maintain vascular integrity. Perfadex, a solution specifically developed for the rapid cooling, perfusing, and storage of lungs for transplant is used for our preparation. This solution has been formulated to preserve the function

and integrity of lung tissue, specifically the vascular endothelial layer which the fluid has the most direct contact with during flushing. Studies have determined the most favorable conditions including an ideal flushing temperature of 4-8º C (34, 84, 95, 197) and flushing protocols that antegradely and retrogradely flow through the pulmonary vasculature (63, 196, 210, 211). Once connected to the *ex vivo* perfusion system, Steen solution is the perfusate solution. This solution is a buffered extracellular solution provides normal oncotic pressures with the inclusion of human serum albumin. High oncotic pressures of both fluids minimize edema formation during flushing and perfusion. Both Perfadex and Steen solution are extracellular based solutions with dextran 40 and these properties or components are responsible for its preservation effects. The extracellular electrolyte composition (low K^+) minimizes vascular spasm and vasoconstriction of the vasculature bed (97, 98, 129). Dextran 40 protects the vasculature by coating the endothelial layer, inhibiting platelet adhesion (thrombogenesis), leukocyte-endothelial interactions, and reactive oxygen species formation (43, 96, 121, 181).

Warm-up protocols were developed over the course of this study focusing on slowly warming the lungs, as pressures allowed, in a period of one hour. When flow is commenced, it is vital to increase flow slowly and only with knowledge of the PAP. As the lung warms, PVR decreases, PA pressure decreases, and flow can then be increased. There is a risk of reperfusion injury to the endothelial cells with high pressures on a cold, fragile endothelial layer during the first few minutes of flow (101, 178). Profound vascular leak is a central component of ischemic-reperfusion injury. Additionally, a risk of injury also exists during flushing with Perfadex. Injury to the endothelial layer most likely accounts for the rapid decline and formation of interstitial and alveolar edema observed in two of our early preparations. Lung inflammation and blood-alveolar barrier disruptions are common findings in injured lungs. The endothelium controls vascular permeability, vessel tone, coagulation and inflammatory responses. Phenotypic changes of the endothelium in response to hypoxic injury include retraction from one another

promoting edema formation, and become pro-adhesive for circulating leukocytes, leading to microaggregates of leukocytes and platelets (2, 145, 208). Compared to other transplant solutions, Perfadex has been shown to have improved fine structural preservation of the blood-air barrier and less severe intra-alveolar, septal, and peri-bronchovascular edema formation (128). The capillary bed, or blood-air barrier, is a thin, strong interface responsible for gas exchange in the lung (115, 202). Intra-alveolar and interstitial edema increase the thickness of the barrier, resulting in an increased diffusion distance, thereby leading to decreased oxygenation of the lung tissue. New research with using IL-10, an anti-inflammatory cytokine, gene therapy to decrease donor lung inflammation and reperfusion injury present promising results and its addition to the protocol in the future may prove beneficial (35, 118, 222). It is therefore important that an optimized lung preservation method aimed at preserving the capillary endothelial and epithelial cells that make up the blood-air barrier in the lung is used.

In our model, one has control over the LA pressure since it is dependent on the height of the reservoir in relation to the lung preparation. The LAP was negative in a few of our studies, and we have since adjusted the reservoir height to provide a LAP of 0-5 mm Hg in the studies. With lower flows, veins are more apt to collapse. We can see collapsed empty vein in the CT images in the second prone preparations due to the LAP falling below zero during the observation period. The maintenance of a slightly positive LAP will prevent the pulmonary veins from collapsing during the decreases in flow during inspiration (31). More careful monitoring of this parameter in the future may lead to better lung function.

Modification of perfusion flow rates and switching to prone positions were performed in the last two preparations to minimize hydrostatic edema formation over time. For most of the supine position preparations, the region of lung beneath the heart was the first region to accumulate extra fluid. Without the weight of the heart resting on that lung, we hypothesized that less force will be placed on that lung tissue and result in a

less fluid, or a better preparation. The second preparation included an additional modification regarding the maintenance flow rate. We had been performing the last series of preparations at a flow rate of 60 cc/kg/min - 75 cc/kg/min resulting in flow rates between 2-3 L/min. The rationale for this change is based on work done at University of Toronto. Cypel et al. published a "low-flow" strategy which allowed for pig lungs to be perfused for 12 hours without the development of hydrostatic edema, assessed by wet/dry ratios of the lung (31).

To conclude, we developed an *ex vivo* lung perfusion system which can be used to study lung physiology, assess lung function, and validate new imaging technologies. In the future this could include biomechanical imaging techniques examining the local expansion patterns including regional stress and strain (152, 154) or quantification of airway trees such as the one shown in Figure 22. Physiological flow rates and ventilation settings can be carefully controlled during experiments. A lung preservation method focused on the preservation of vascular integrity is key to a working model. MDCT perfusion measures of PBF and MTT obtained at various flow rates demonstrate appropriate physiological responses. As the pulmonary arterial flow rate was increased, regional PBF increased and MTT decreased. CV decreased as flow increased, demonstrating a more homogenous flow pattern as higher flow rates.

Figure 11. Left) *Ex vivo* perfusion system setup for MDCT imaging. The heart-lung block is surgically removed and placed in an evaluation box positioned on the gantry table within the MDCT scanner, and connected to the perfusion circuit. Middle) A close up of the heat exchanger, reservoir, centrifugal pump and flow probe. Right) Lungs are stored in a lung evaluation box during the study. Inflow tubing delivers perfusate to the pulmonary artery while a cannula in the LA collects perfusate from the pulmonary veins and returns it to the reservoir. A close up of the *ex vivo* heart-lung block after two hours of perfusion is shown in the bottom right. Lung parenchyma was visually in good condition and remained healthy and compliant throughout the experiment. The lungs were breath-held with PEEP to obtain volumetric images.

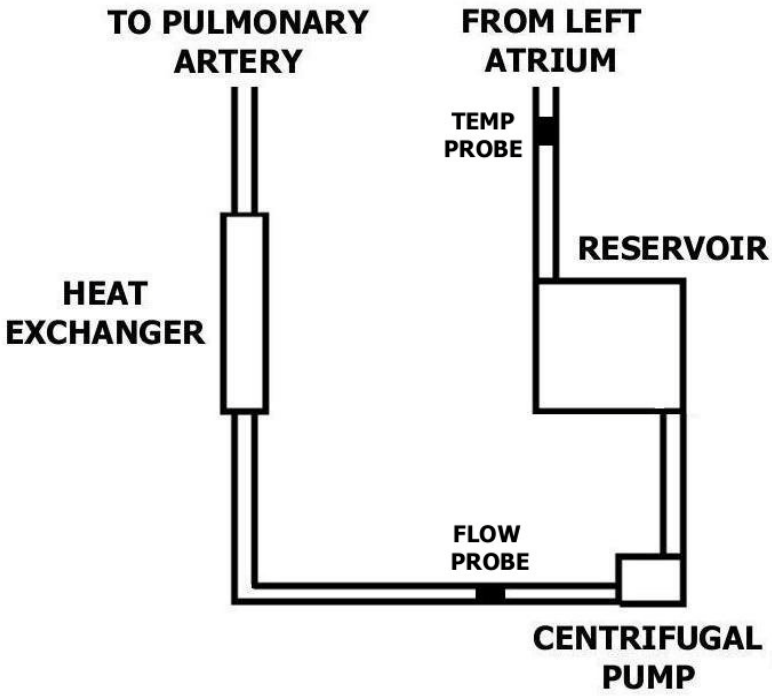

Figure 12. Schematic of the *ex vivo* perfusion system. The perfusion circuit consists of a reservoir, centrifugal pump, and heat exchanger. The perfusate is pumped by a centrifugal pump from the reservoir, through a heat exchanger and into the lung vasculature via a cannula placed in the pulmonary artery. Flow returning from the lungs via pulmonary veins is collected by a cannula placed in the left atrium, and returns to the reservoir. Core lung temperature is assessed by a probe placed on the outflow portion of the circuit.

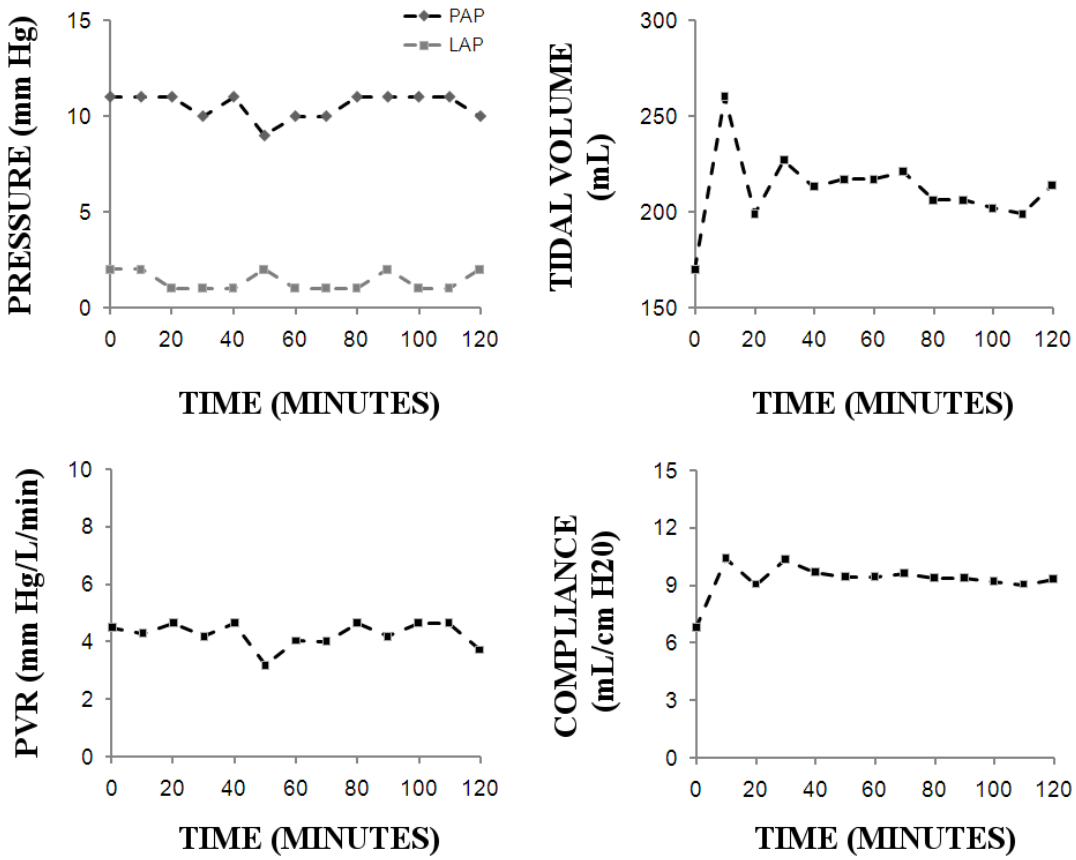

Figure 13. Perfusion and ventilation settings for a representative study (Animal 2) over two hours. This animal was physiologically stable over two hours with not much change in his PA and LA pressure (upper left), tidal volume (upper right), PVR (lower left) or compliance (lower right) measurements. The flow rate averaged 2.2 L/min with a mean minute ventilation of 2.5 L/min for the 120 minutes. The lungs were breathing room air (21% O_2) at a rate of 12 breaths/minute. Other ventilator settings included a PEEP of 5 cm H_20 and a PIP of 25-30 cm H_20, with a mean of 27.8 cm H_20. While physiological parameters were stable over time, the lung had a 20% tissue volume increase over 120 minutes.

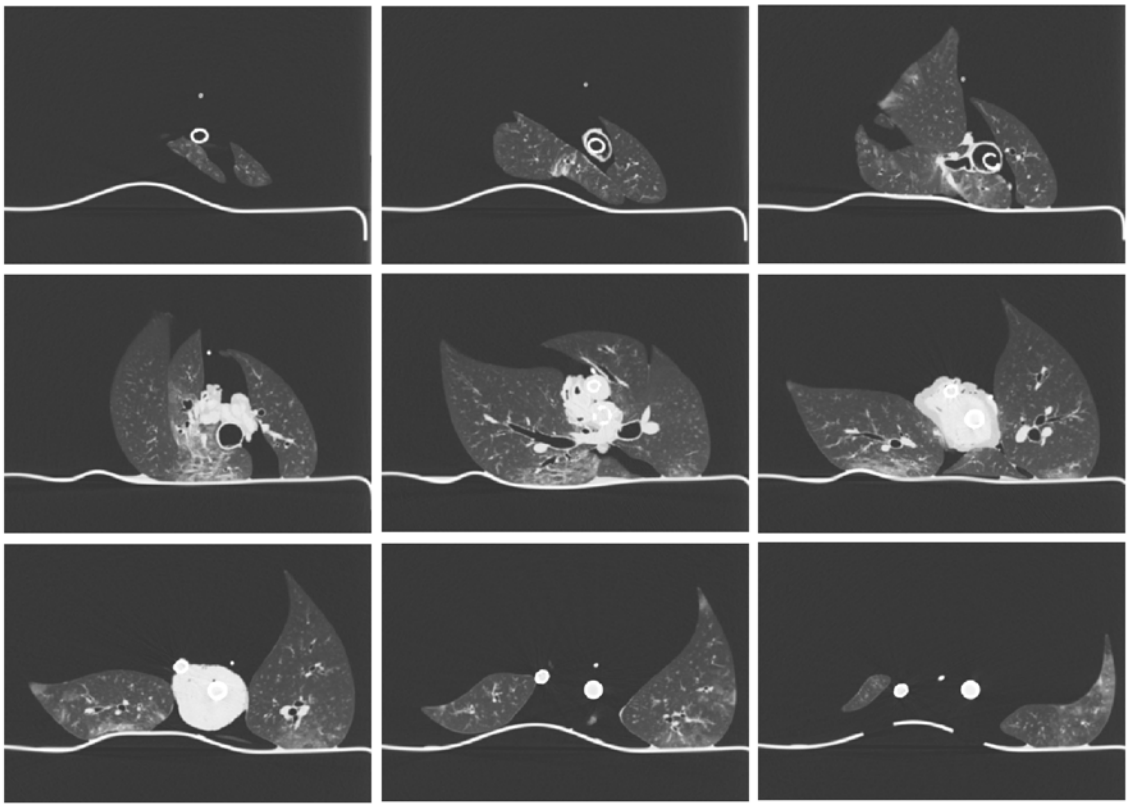

Figure 14. Volumetric MDCT images at a PEEP of 25 cm H_20 (TLC) after *ex vivo* lungs had been warmed up to 37 ºC and perfused for 2 hours at a flow rate of 100 cc/kg/min. This preparation (animal 1) demonstrated minimal edema in the dependent region of the lung. These visual imaging findings match the tissue volume calculations which found a 10% tissue volume increase over 120 minutes.

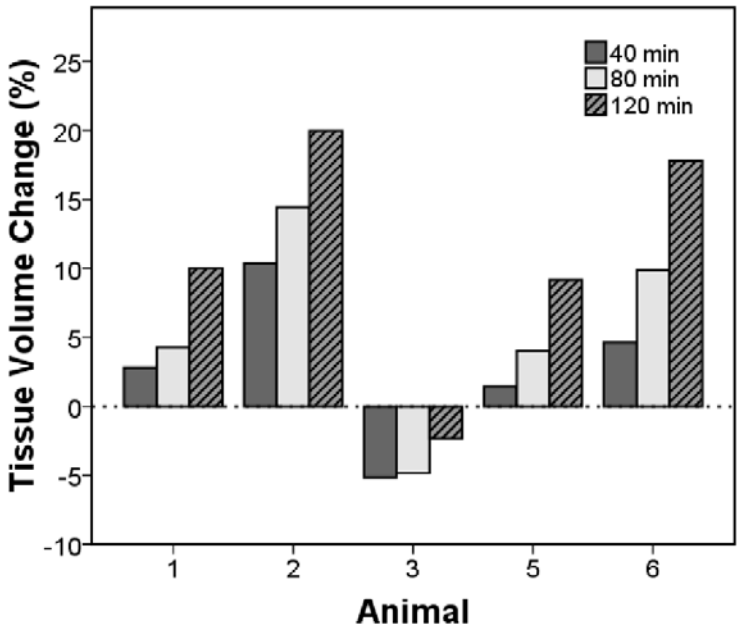

Figure 15. Change in tissue volume from baseline at 40 minutes, 80 minutes and 120 minutes for 5 *ex vivo* preparations. Tissue volume increases over time, suggesting fluid accumulation in the lung. The greatest increase in tissue volume occurred from 80-120 minutes, suggesting the lung function and vascular integrity is declining over time. In animal 3, tissue volume fell at 40 minutes from baseline, and then continue to rise over time. This most likely reflects the recruitment and opening up of an atelectatic lung region from 0 to 40 minutes.

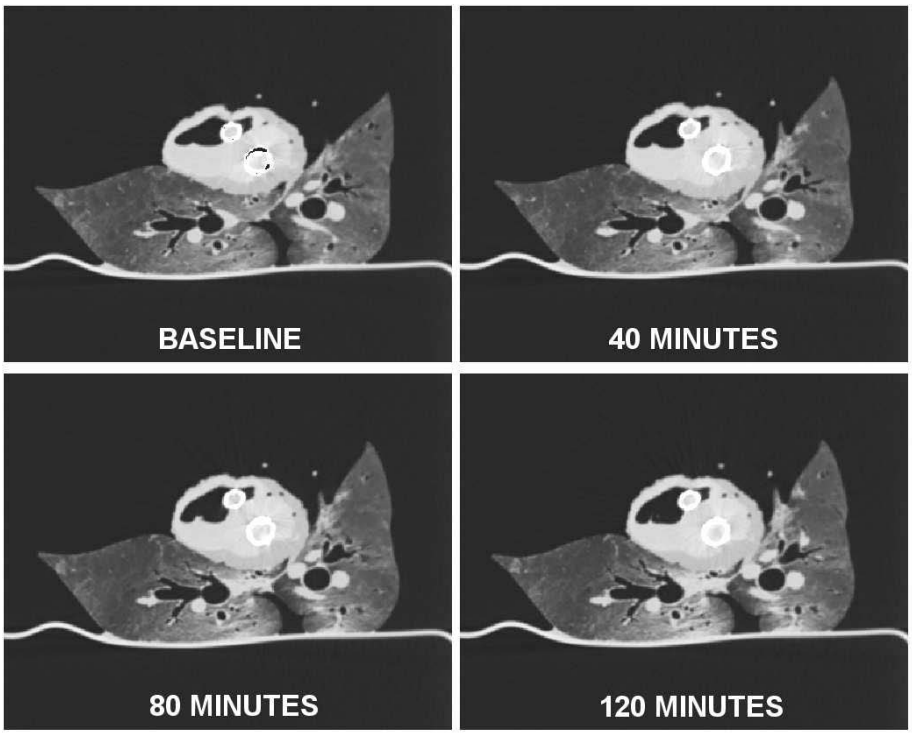

Figure 16. A representative axial slice from animal 5 demonstrating mild fluid retention over time. The dependent region of the lung resting beneath the heart tissue is most susceptible to hydrostatic edema resulting in the most fluid accumulation over the 120 minutes of perfusion.

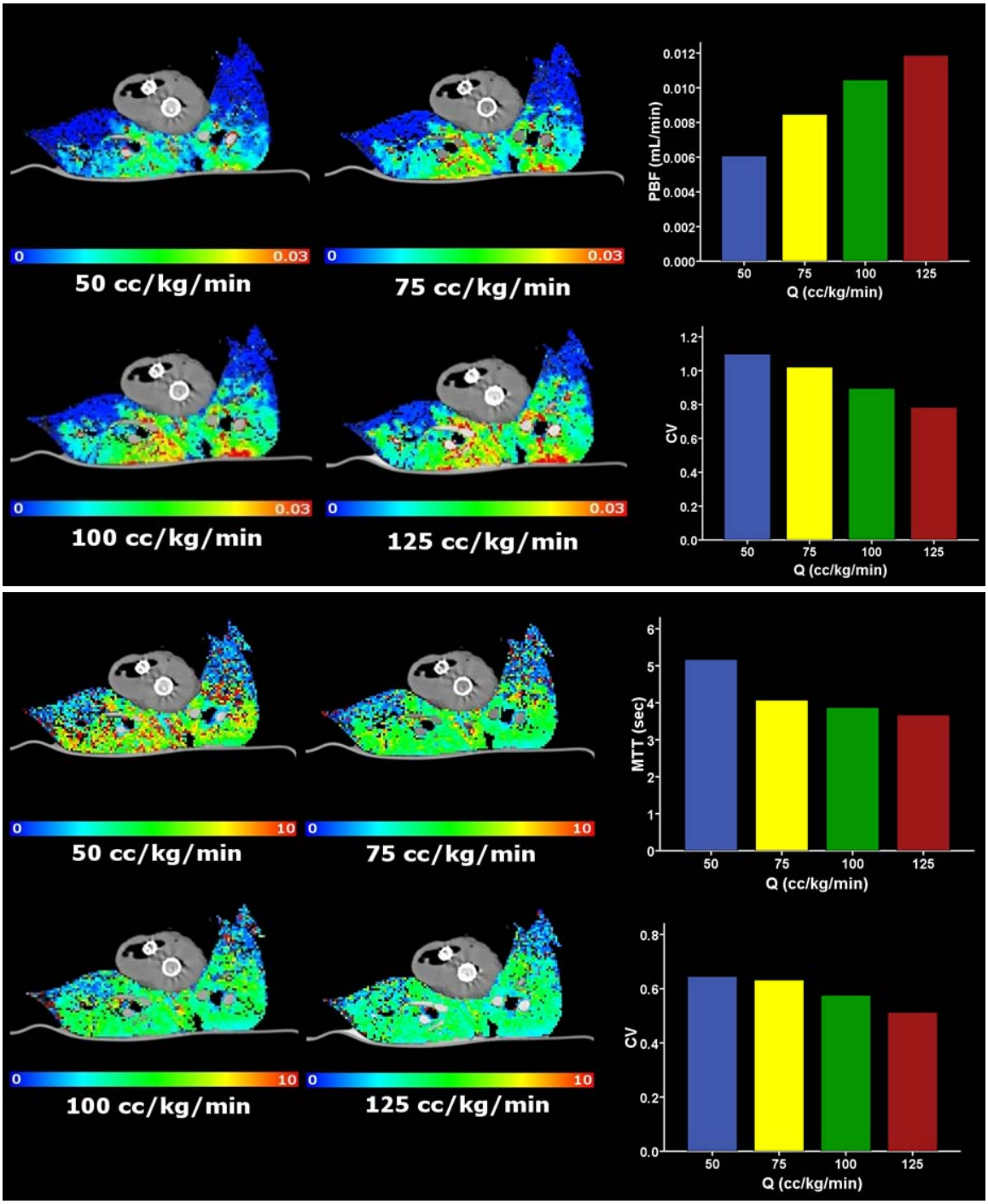

Figure 17. Regional PBF (top) and MTT (bottom) color-coded maps for a representative slice from one animal in the supine position at four flow rates: 50, 75, 100 and 125 cc/kg/min. Bar graphs demonstrates mean (upper) and CV (lower) measurements for each flow rate. Increased flow leads to an increased region PBF (ml/min) and decreased MTT (seconds) as expected. As flow is increased both MTT and PBF distributions become more homogenous (decreased CV).

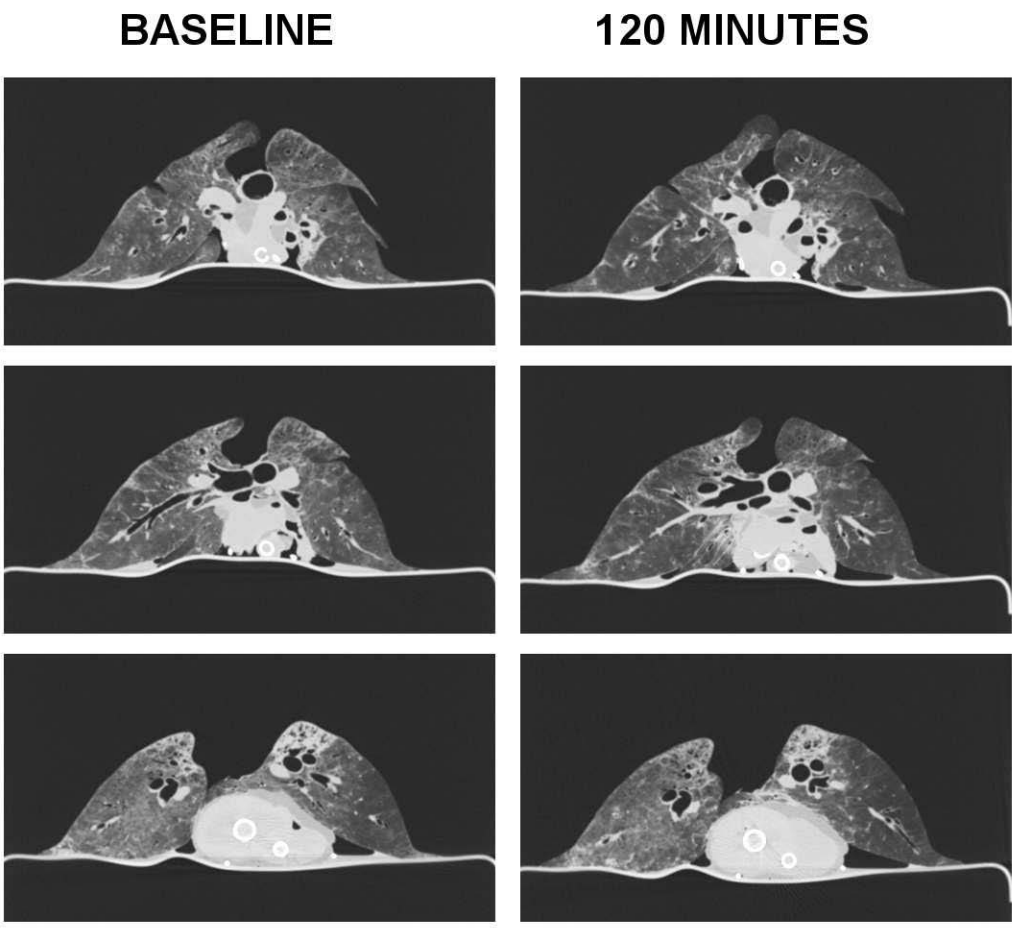

Figure 18. Three axial slices taken from TLC volumetric non-contrast (PEEP of 30 cm H_20) MDCT images obtained at baseline (once lungs are warmed up and target flow rate of 25 cc/kg/min was reached) and 120 minutes later for the prone ex-vivo preparation. Slight lung shifting occurred over the 120 minutes (airways can not be exactly aligned in axial slices). There is minimal visual change occurred in the lung parenchyma. The lack of enhancement suggests minimal interstitial edema accumulation. These findings agree with tissue volume calculations, demonstrating only a 4% increase in tissue volume for the whole lung. A region of enhancement in the upper region of the most basal slice shown here correlated with a hemorrhagic region seen at time of lung removal. This region did not resolve over time, but rather remain unchanged at 120 minutes. Images shown here are 1.5mm slice thickness reconstructions shown using lung windows (WL -500, WW: 1500).

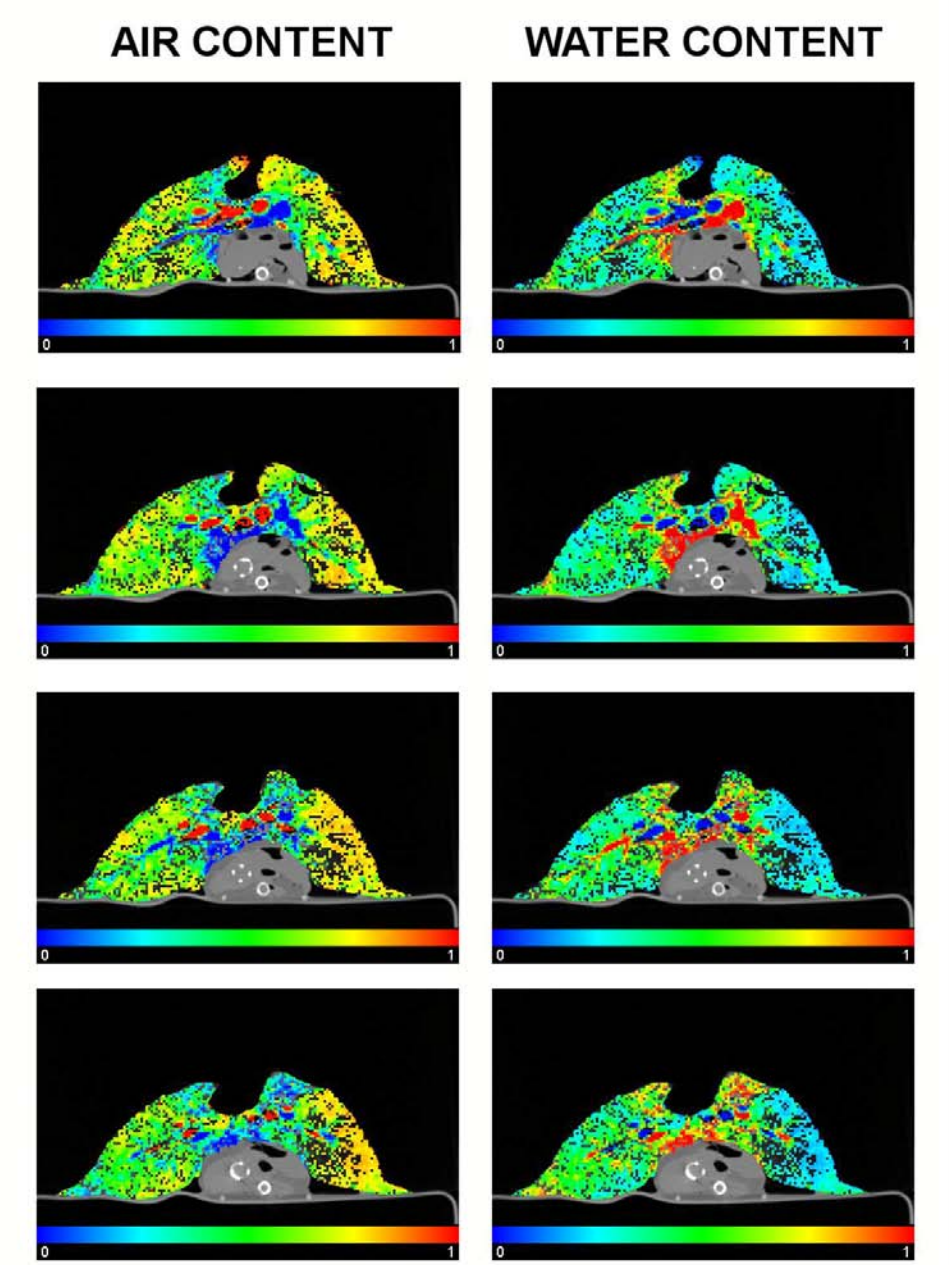

Figure 19. Air and water content (low-high, blue-red) for 4 axial slices, apical (top) to basal (bottom), determined from baseline perfusion images obtained at a FRC lung inflation volume. Regions of high air content (red) and low water content (airways) and no air content and high water content (vessels) will be filtered to analyze blood flow only in the lung parenchyma. The prone ex-vivo lung visually had little air gradient with homogenous airflow to the lung parenchyma.

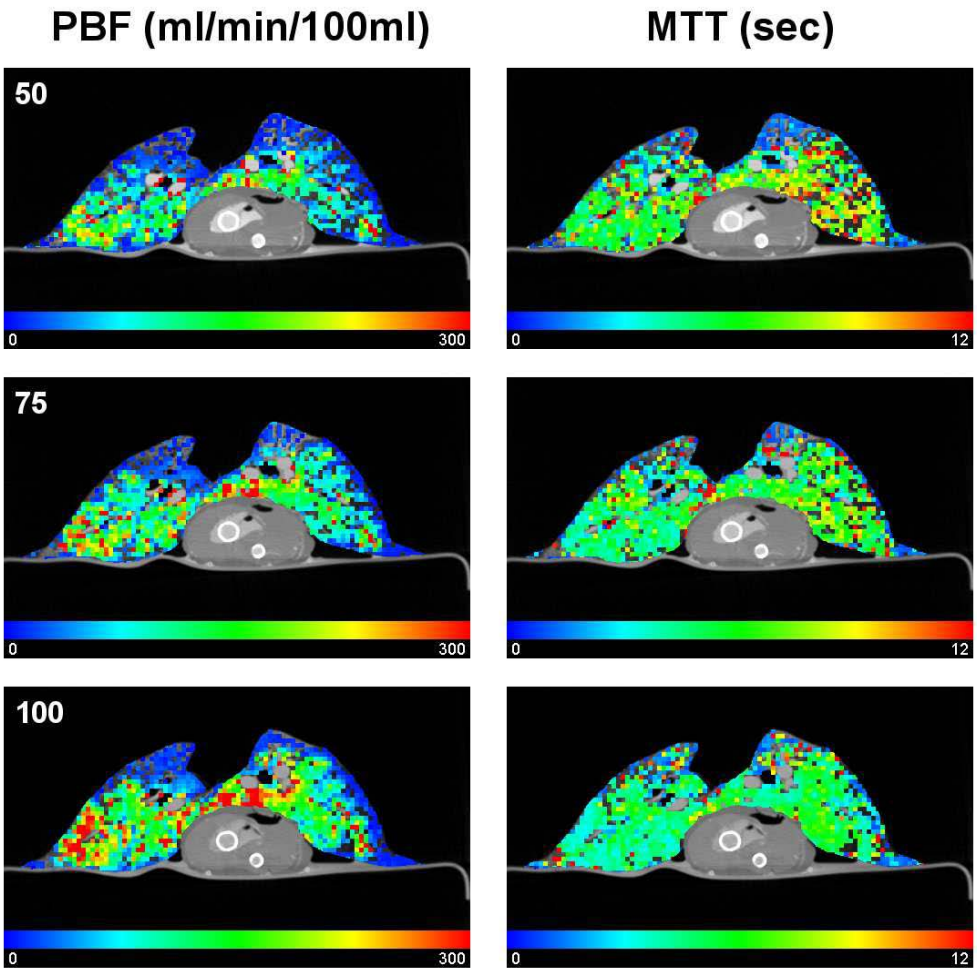

Figure 20. Color coded PBF and MTT maps for a representative slice at 50 cc/kg/min (upper row), 75 cc/kg/min (middle row) and 100 cc/kg/min (lower row) in ex-vivo lungs in the prone position. Regions of interest consisting of a 5 x 5 voxel volume (volume: 2.3mm x 2.3mm x 1.2 mm) were grouped together to calculate regional PBF and MTT. Flow ranged from 0-300 ml/min/100 ml (blue-red). MTT ranged from 0-12 seconds (blue-red).

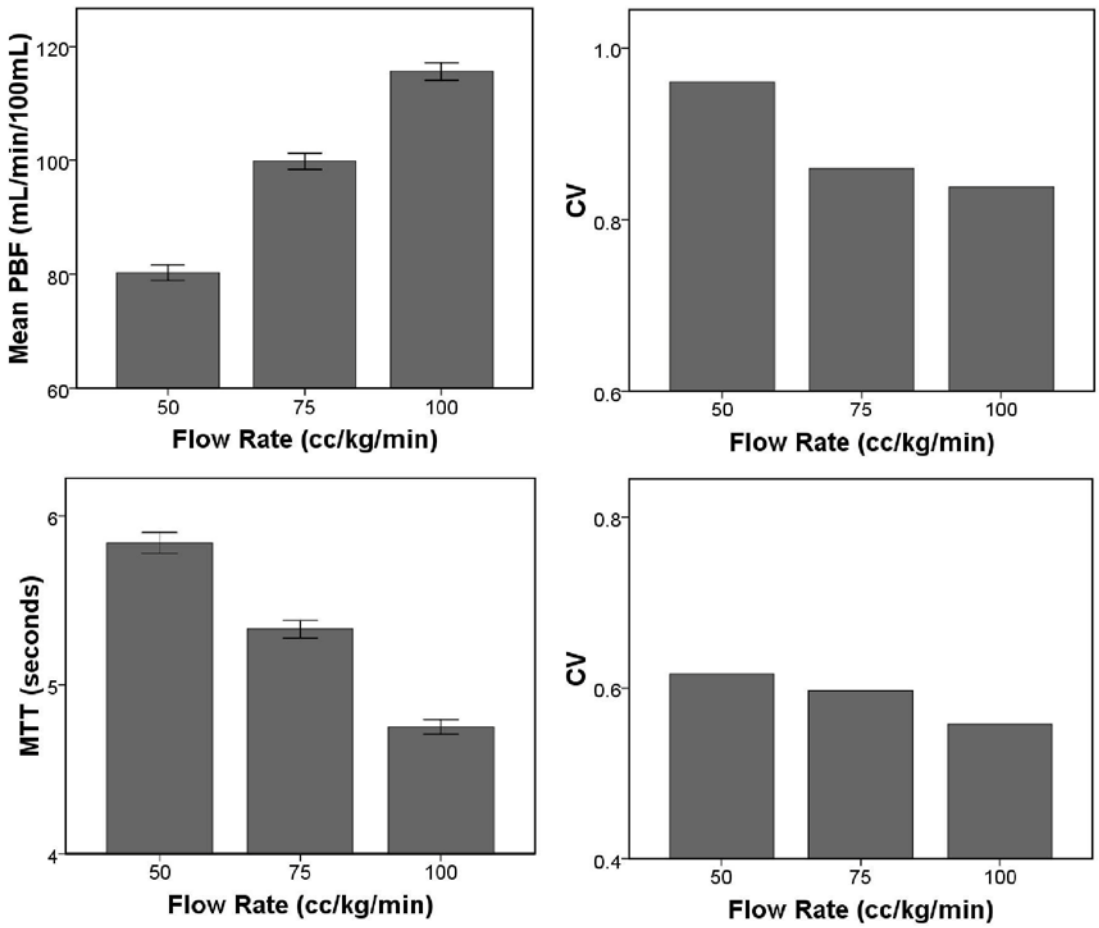

Figure 21. Mean PBF (ml/min/100ml) and MTT (seconds) at 50, 75, 100 cc/kg/min flow rates for *ex vivo* preparation in the prone position. Error bars represent 95% confidence intervals. Perfusion data was filtered to excluded airways and vessels. As flow rate is increased, the mean PBF increases and MTT decreases. CV decrease as flow rates increase from 50 to 75 to 100 cc/kg/min for both PBF (0.96 to 0.86 to 0.84 respectively) and MTT (0.62 to 0.60 to 0.56 respectively) measurements. A region of low to no flow due to fluid around the heart was included in the analysis, resulting in larger CV values reported here for regional PBF than typically observed.

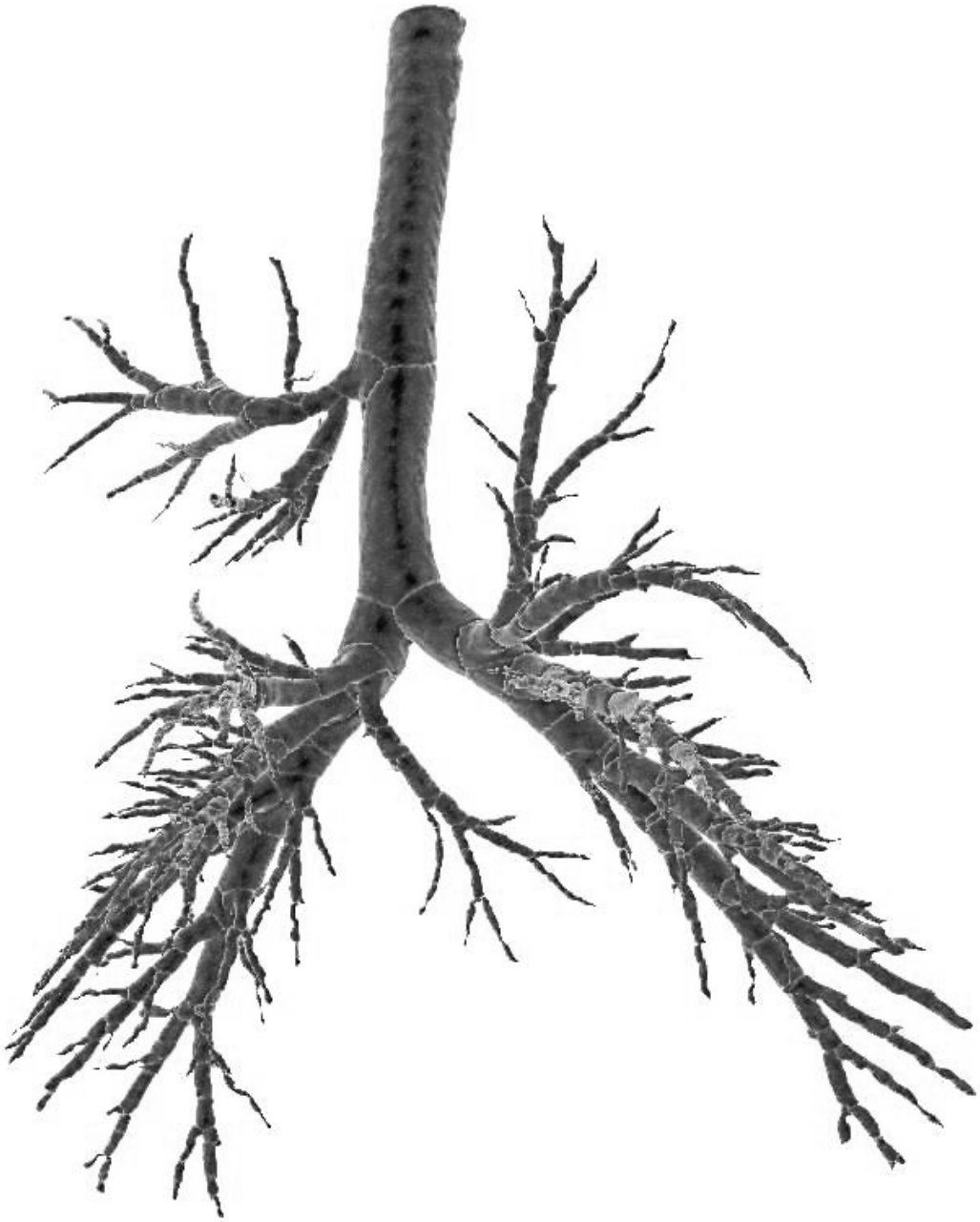

Figure 22. Airway tree of an *ex vivo* sheep lung, obtained from volumetric MDCT images at TLC obtained after 40 minutes of perfusion at 60 cc/kg/min.

Table 7. Perfusion and ventilation settings, pressure measurements, and physiological parameters for the *ex vivo* lung preparation over 120 minutes of observation with MDCT imaging at the target flow rate.

	Animal				
	1	2	3	5	6
Weight, kg	33.6	28.2	31.8	32.3	30.9
Perfusion					
Targeted Rate, cc/kg/min	100	75	75	60	60
Q, L/min	3.2 - 4.8	2.2	2.3	1.9	1.8
Mean Pressure, mm Hg					
PA	10.7 ± 1.5	10.5 ± 0.7	13.4 ± 1.2	13.9 ± 0.6	15.4 ± 1.0
LA	5.8 ± 1.3	1.4 ± 0.5	6.9 ± 0.9	9.5 ± 1.5	-0.7 ± 0.6
PVR, mm Hg/L/min	1.3 ± 0.5	4.3 ± 0.4	2.9 ± 0.6	2.4 ± 1.0	9.0 ± 0.5
Ventilation					
Tidal Volume, ml	338 ± 50	212 ± 20	256 ± 16	119 ± 7	134 ± 8
RR, breaths/ minute	12	12	12	12	8
PIP, cm H_2O	12	28	18	30	35
PEEP, cm H_2O	5	5	5	5	5
FiO2	0.21	0.21	0.21	1.0	1.0
Compliance, ml/cm H_2O	56.7 ± 13.2	9.3 ± 0.9	20.5 ± 3.4	4.8 ± 0.3	4.5 ± 0.2

Note: Mean values were based on measurements taken every 10 minutes over 120 minutes.

Table 8. Lung, air and tissue volumetric measurements of the *ex vivo* lung over time at a target flow rate.

Animal	Baseline			40 min	80 min	120 min
	Total Lung	**Air**	**Tissue**	**Δ Tissue Volume***	**Δ Tissue Volume***	**Δ Tissue Volume***
1	2729	2190	540	+15 (3%)	+23 (4%)	+54 (10%)
2	1886	1224	662	+69 (10%)	+96 (14%)	+132 (20%)
3	1700	1124	576	-30 (-5%)	-28 (-5%)	-13 (-2%)
5	1407	916	491	+7 (1%)	+20 (4%)	+45 (9%)
6	1465	905	560	+26 (5%)	+55 (10%)	+100 (18%)
Mean				+17 (+3%)	+ 33 (+6%)	+64 (11%)

Note: Volumetric MDCT measurements are reported in units of cm^3 and were obtained from images captured with the lungs at a PEEP of 25 cm H_20.

* Tissue volumes at 40, 80 and 120 minutes reflect deviations from baseline with the percent increase from baseline in parentheses.

Table 9. Flow rates with corresponding PA and LA pressures observed during perfusion MDCT imaging in *ex vivo* preparations.

	50 cc/kg/min			**75 cc/kg/min**			**100 cc/kg/min**			**125 cc/kg/min**		
Animal	Q	PAP	LAP	Q	PAP	LAP	Q	PAP	LAP	Q	PAP	LAP
2	1.4	8	-4	2.1	9	0	2.8	8	6	3.5	13	13
3	1.6	14	8	2.4	19	7	3.2	25	10	4.0	28	17
5	1.6	13	8	2.4	20	13	3.2	20	15	4.0	23	20
	60 cc/kg/min			**90 cc/kg/min**			**120 cc/kg/min**			**150 cc/kg/min**		
Animal	Q	PAP	LAP	Q	PAP	LAP	Q	PAP	LAP	Q	PAP	LAP
1	2.0	11	6	3.0	12	6	4.0	17	8	5.0	17	8

Note: Q is reported as L/min, and PAP and LAP are reported in mm Hg.

Table 10. Mean and CV measurements for PBF and MTT at flow rates of 50, 75, 100 and 125 cc/kg/min.

	50 cc/kg/min	75 cc/kg/min	100 cc/kg/min	125 cc/kg/min
PBF (ml/min/100ml)				
Animal 2	98 ± 137	144 ± 159	183 ± 180	205 ± 190
Animal 3	180 ± 164	226 ± 168	262 ± 181	316 ± 199
Animal 5	138 ± 154	191 ± 198	236 ± 213	264 ± 214
Mean ± SD	138 ± 41	187 ± 41	227 ± 40	262 ± 55
MTT (sec)				
Animal 2	4.6 ± 3.4	4.2 ± 2.8	4.0 ± 2.4	3.7 ± 2.1
Animal 3	6.0 ± 3.1	2.7 ± 2.2	4.3 ± 2.0	3.9 ± 1.6
Animal 5	5.6 ± 3.4	4.2 ± 2.7	4.0 ± 2.3	3.8 ± 2.0
Mean ± SD	5.4 ± 0.7	4.4 ± 0.3	4.1 ± 0.2	3.8 ± 0.1
PBF CV				
Animal 2	1.40	1.11	0.98	0.92
Animal 3	0.92	0.75	0.69	0.63
Animal 5	1.12	1.04	0.90	0.81
Mean ± SD	1.15 ± 0.24	0.97 ± 0.19	0.86 ± 0.15	0.79 ± 0.15
MTT CV				
Animal 2	0.74	0.67	0.60	0.57
Animal 3	0.52	0.47	0.47	0.41
Animal 5	0.61	0.64	0.58	0.53
Mean ± SD	0.62 ± 0.11	0.59 ± 0.11	0.55 ± 0.07	0.50 ± 0.08

CHAPTER 5: ASSESSMENT OF REGIONAL PERFUSION AND PERFUSION PARAMETERS IN HUMAN SUBJECTS

Rationale and Hypothesis

Multi-detector row computed tomography (MDCT), along with the development of quantitative image analysis techniques, provides a comprehensive assessment of the lung (70, 73, 76). MDCT has been focused upon the evaluation of extent and distribution of emphysema, a subset of chronic obstructive pulmonary disease (COPD). In this study, we specifically focus on MDCT perfusion imaging in subjects with smoking-associated emphysema. Dynamic 4-D MDCT perfusion sequences quantitatively determine regional PBF and MTT through the detection of temporal changes in the density of the lung parenchyma resulting from a rapid, central intravenous bolus injection of iodinated contrast, followed by the application of indicator dilution theory and first-pass kinetics (25, 33, 77, 214).

While pulmonary hypertension is a well-known clinical feature of advanced COPD (6, 189), less is known about the vasculature response and tone early in COPD pathogenesis. Recent evidence suggests that endothelial dysfunction and alterations in pulmonary vascular response occur early in COPD and may represent a novel vascular pathway in COPD development (9, 91, 119). It has been hypothesized that if there is failure of inherent mechanisms to block the HPV response in the presence of inflammatory processes, the inflammatory response may not be self limited by the normal cascade of events and repair mechanisms, thus leading to chronic inflammation, focal tissue destruction and emphysematous processes (76). We hypothesize that an increased heterogeneity (larger regional variation) of PBF and MTT will exist in smokers with CT-only signs of emphysema. This hypothesis based on the notion that smokers susceptible to emphysema may fail to block HPV in the presence of inflammation leading to increased heterogeneity of MTT, while smokers not susceptible to emphysema would

block HPV in inflaming regions, maintaining a more homogenous MTT. In order to address this question, we formed a cohort of human subjects to determine the normal range of MDCT perfusion parameters for never smokers, and then compared these results to a smoking population, split into two groups, those with and without early CT evidence of centrilobular emphysema.

Methods

Study Population

From November 2004 to April 2008, we recruited 48 subjects from the local community as part of an effort to establish a normative lung atlas. The University of Iowa institutional review board approved this study and written informed consent was obtained prior to entering the study from all subjects. Study inclusion criteria were never smokers with a total smoking history less than 1 pack, and smokers currently smoking a pack a day. Subjects were excluded for known heart disease, kidney disease or diabetes, presence of metal in the lung field, pregnancy, X-ray/CT scan in the past 12 months, contrast allergies, glomerular filtration rate less than 60 ml/min, and body mass index over 32. Never smokers with clinically important pathology detected on CT were excluded along with smokers with significant lung disease other than emphysema (e.g. tumor). A baseline dyspnea index was determined (113). Body mass index was calculated as weight (kg) divided by height squared (m^2). Pre-bronchodilator spirometry was performed on one of two systems: V6200 Body Box (Sensor Medics, Yorba Linda, CA) or the OWL Digital Body Plethysmography (Ferraris Respiratory, Louisville, CO). Before changing from the V6200 to the OWL system, we verified that measures on our subject population were equivalent between systems. Assessment of spirometry quality followed the American Thoracic Society and European Respiratory Society recommendations (123).

MDCT Imaging and Data Analysis

MDCT imaging consisted of two spiral non-contrast lung volumetric scans and a dynamic ECG-gated perfusion scan. Heart rate, ECG, arterial pressure, and pulse oximetry oxygen saturation (SpO_2) were continuously monitored (Philips IntelliVue patient monitoring system, M8010A, Andover, MA). MDCT scanners were upgraded over the course of the study with 12 subjects imaged with a 4-slice MDCT scanner (MX8000, Philips Medical Systems), 4 with a 16-slice MDCT scanner (Sensation 16, Siemens Medical Systems) and the remaining 25 subjects with a 64-slice MDCT scanner (Sensation 64, Siemens Medical Systems).

Two spiral volumetric non-contrast scans of the lung obtained during breath-holds at 2 fixed controlled lung volumes, functional residual capacity (FRC, 20% vital capacity) and total lung capacity (TLC, 100% of vital capacity), with the aid of patient coaching by the imaging technologist and a lab-developed volume controller system. This system consists of a well calibrated pneumotachometer with balloon occlusion valve and is linked to a lab-developed monitoring program (Labview, National Instruments, Austin, TX) to instantaneously measure airflow, airway pressures and hold lung volumes appropriately. Volumetric scans were performed with the following settings for a 64-slice MDCT scanner: mA, 100; kV, 120; pitch, 1mm; rotation time, 0.5 seconds; slice thickness, 0.75mm; slice increment, 0.5mm; matrix, 512 x 512; and reconstruction kernel, B31f. Scan times are under 10 seconds with a z-coverage of 22-30 cm, adjusted in order to capture the whole lung. Voxel dimensions were near isotropic at: 0.47 x 0.47 x 0.50 mm. For the two volume scans, the maximum collective radiation dose (conservatively calculated) delivered to the subject is 10.6 mSv.

4-D ECG-gated axial dynamic MDCT perfusion imaging acquires images over time for a volume of lung. These images are acquired during the administration of a sharp, central bolus (0.5ml/kg, up to a total volume of 40 ml) of iodinated contrast agent (Visipaque 350, GE Healthcare, Princeton, NJ) delivered over 2s by a power injector

system (Mark V ProVis, MedRad, Indianola, PA) through a central line placed in the superior vena cava. An imaging location, based on the FRC volume scan, of lung just distal to the carina is chosen for perfusion MDCT imaging. To ensure a central sharp bolus of contrast, a central venous line (5Fr pigtail catheter) is placed in the proximal superior vena cava, with placement confirmed by contrast injection under fluoroscopic control. Perfusion is assessed in a supine position, during a breath-hold at FRC. Baseline images are obtained followed by the contrast injection and additional imaged time points, one per heartbeat, as the contrast agent flows through the lung fields. Scan protocols for the 4, 16 and 64-slice scanners were selected to maximize the similarity of spatial resolution; and, with increased number of slices, we were able to sample a larger proportion of the lung. Perfusion scanning parameters for the scanners are summarized in Table 11. For the perfusion scan, the maximum radiation dose is 3.2 mSv.

Image Analysis

Mean lung density, and emphysema index (EI, proportion below a threshold attenuation compared to the total volume of the lung) for threshold attenuation of -950 and -910 Hounsfield units (HU) were obtained from TLC volumetric images with the use of PW software (VIDA Diagnostics, Coralville, IA) (131). Since images were obtained with 3 different scanners over the course of four years, base thresholds were modified to correct for interscan variation using the attenuation of air outside the body and blood from the aorta.

Perfusion image data sets were segmented semi-automatically using PASS and analyzed with the Time Series Image Analysis (TSIA) module of PASS (55, 73). This software uses indicator dilution theory assuming a bolus injection, residue detection model (214). Segmented lung parenchymal voxels were binned in 3x3 ROIs (1.4 mm x 1.4 mm x 1.2 mm) resulting in regional data for a 2.4 mm^3 volume of lung parenchyma. Regional PBF and MTT measurements are determined based on time-attenuation curves

for lung parenchyma ROIs. In this model, PBF is defined as the ratio of change in HU to the area under the input time-attenuation arterial curve and MTT is assessed as the area under the residue curve divided by the maximum height. Data was filtered to remove major airways and vessels (ensuring that ROIs were predominately lung parenchyma) using the following selection criteria: fractional air content, 0.4-0.9; fractional blood content, 0.02-0.5; and chi-squared for curve fit, 0-200,000. Absolute PBF (ml/100 ml/min) and MTT (seconds) were determined for each subject and mean and CV values were determined for whole lung, non-dependent, and dependent regions of the lung. Non-dependent and dependent regions of the lung correspond to the upper and lower third of lung respectively when lying supine. To compare regional differences across groups without inter-subject variability from differing cardiac outputs, PBF was normalized to the mean PBF.

Statistical Analysis

Statistical comparisons were performed with SPSS software (Windows 15.0, SPSS, Inc; Chicago, IL). Data are expressed as mean ± SD for the whole lung volume, non-dependent third and dependent third of the lung. Heterogeneity of PBF and MTT is assessed by its CV. One-way analysis of variance, followed by a *post hoc* analysis using the Bonferroni method, is used to determine statistical significance for whole lung MTT and PBF measurements. Paired t-tests assessed differences in dependent vs. non-dependent regions. P-values less than 0.05 were considered significant.

Results

Subject Characteristics

48 subjects underwent perfusion CT imaging, with 7 subjects excluded from the final cohort (2 never smokers with bronchiectasis, 1 never smoker with upper lobe emphysema on MDCT, 1 smoker with large mediastinal mass, 1 smoker with respiratory

alveolitis, and 2 subjects with contrast injection errors). The remaining 41 subjects were categorized based on smoking status (never smoker or smoker), with current smokers further being subdivided into two groups based on the presence (or absence) of emphysema on MDCT determined by a blind-read from an expert chest radiologist with 15 years experience. Baseline demographics and spirometry measurements are summarized for the never smokers (NS), smokers with normal CT imaging studies (SNI) and smokers with CT imaging findings of emphysema (SE) in Table 12. None of the subjects had ground glass present in the region of perfusion MDCT imaging. Out of the 24 smokers imaged, 12 subjects (50%) had radiological findings of emphysema determined visually by an expert chest radiologist. In these 12 subjects, 6 had upper lobe emphysema only, 2 with upper and middle lobe emphysema, and 4 with emphysema present in all lobes. Two subjects had bullous changes present. An example of the extent of emphysema present in SE subjects is shown in Figure 23. SE subjects were collectively older, had greater number of pack years, and their pre-bronchodilator FEV_1/FVC ratios were in the lower range of normal (70-80% of predicted) compared to NS and SNI subjects. However, there was over-lap between the groups. Once smokers were stratified based on presence or absence of emphysema, CV measurements were not significantly correlated with the age or smoking history (pack years).

Volumetric MDCT

CT parameters, mean lung density and EI measurements, obtained from TLC volumetric images are summarized in Table 12. There are no significant differences between groups for EI measurements obtained at a thresholds of -950 HU ($p=0.4$) or -910 HU ($p= 0.3$) from whole lung measurements. In order to determine extent of emphysema in the lung region imaged for perfusion, the lung was divided into thirds based on the apex to costophrenic angle distance. EI analyses were performed on the middle third of the lung (covering the lung volume distal to the carina and ending near the diaphragm)

which corresponded to the region of perfusion imaging in all subjects. These EI measurements for the 3 groups did not demonstrate differences in percent emphysema-like lung with thresholds of -950 HU (p=0.3) or -910 HU (p= 0.2). The mean percentage of volume for the middle third below -950 HU were 6.7%, 4.1% and 4.0% and below -910 HU were 37.2%, 29.6% and 26.5% for NS, SNI and SE subjects respectively.

Pulmonary Perfusion Parameters

An example of perfusion data obtained from a SNI subject demonstrates time-attenuation curves obtained for the input arterial ROI and larger ROIs (11 x 11 voxels) placed in the non-dependent and dependent region of the lung parenchyma (Figure 24). PBF and MTT measurements for NS, SNI, and SE subjects were determined for the whole imaged slab and are summarized in Table 13. An example of perfusion images obtained in a SE subject is shown in Figure 25.

Absolute mean PBF (ml/100 ml/min) and MTT (seconds) were determined for each group and no statistical significant differences existed between the 3 groups for either PBF (p = 0.8) or MTT measurements (p = 0.2). The one-way ANOVA demonstrated significant differences in CV measurements for MTT between the groups (p = 0.0005). The ANOVA was followed with *post hoc* analysis demonstrating significant differences in MTT CV measurements between the SE group compared with SNI and NS groups, but no significant difference between the SNI and NS groups. Similarly, for PBF CV measurements, the one-way ANOVA demonstrated significant differences in CV measurements between the groups (p = 0.0007) with *post hoc* analysis demonstrating a significant increase in CV in the SE group compared with SNI and NS groups, but no significant difference between the SNI and NS groups. A representative PBF and MTT color map from a subject from each group in Figure 26 demonstrates this difference in heterogeneity. Differences in CV measurements for PBF (p = 0.02) and MTT (p = 0.02) were significant after accounting for the effects of age. Accounting for

both age and smoking pack years in the two smoking groups, MTT CV measurements were significant different ($p = 0.015$) but differences in PBF CV measurements did not reach significant levels ($p = 0.11$). P-values from the models analyzed are summarized in Table 14. With the concern that the different models of MDCT scanners may play a significant role in the observed differences in CV measurements, a subgroup of 10 NS and 10 SE subjects' perfusion images, both performed on the 64-slice scanner, were compared and significant CV differences for PBF and MTT were observed, similar to our larger population.

Non-dependent and Dependent Comparison

Regional data are also summarized in Table 13 and displayed graphically in Figure 27. MTT measurements did not significantly vary through the lung volume sampled. No significant differences were observed in mean MTT in non-dependent, dependent and whole lung MTT measurements. PBF measurements demonstrate an increasing flow gradient from non-dependent to dependent regions of the lung in all three groups. CV measurements of PBF and MTT exhibit significantly increased CV in the non-dependent region compared to the dependent region for NS (PBF: $p = 0.0001$, MTT: $p = 0.00001$), SNI (PBF: $p = 0.003$, MTT: $p = 0.001$) and SE (PBF: $p = 0.001$, MTT: $p = 0.007$) subjects. These differences in CV did not differ among the groups of never smokers and smokers.

Comparison of ROI Size

Perfusion image analysis was performed for four different resolutions of lung parenchyma: 3x3,5x5,8x8, and 11x11 voxels per ROI. As the ROI size increased from 3 to 11, more lung volume was included in each voxel analyzed. PBF (ml/min) measurements per voxel correspond to the blood flow for that voxel and as expected, regional PBF measurements increased as ROI size increased. No significant differences in MTT exist between ROI sizes, though mean MTT slowly trended upward as ROI size

increased for all groups. The relationship between the 3 groups for CV measurements remained consistent over these ROI sizes. CV for MTT and PBF increased as the ROI volume decreased from ROI sizes of 11 to 3, as expected. The SE group had a significant increase in CV compared to NS and SNI groups for all ROI sizes for MTT and PBF measurements.

Discussion

In this study, we evaluated the use of a dynamic 4-D ECG-gated MDCT perfusion technique to determine regional PBF and MTT in human subjects. We demonstrated an increased heterogeneity, as assessed by CV measurements; in regional PBF and MTT distributions in SE subjects compared with SNI and NS subjects. The data from this study suggest that heterogeneity of flow may serve as a functional "phenotype" of smoking related centrilobular emphysema. We hypothesized that these changes in perfusion patterns reflect changes in pulmonary vascular tone resulting from patchy inflammatory processes in the lung in smokers where regionally, the lung is unable to block HPV in the face of inflammation. These findings do support our initial hypothesis that failure to block HPV with local inflammation may serve as a precursor to destruction in a smoking population susceptible to emphysema. Pulmonary vascular changes, characterized by a thickening of the vessel wall, have been characterized early in the history of COPD disease (142, 215). More recently it has been observed that, in the presence of inflammation, there is an enhanced delivery of progenitor cells to the lung (220, 221). Remy-Jardin et al. observed an increased propensity for the lung to develop emphysema in regions of suspected inflammatory processes as defined by ill-defined ground glass opacities and micro nodules (155). There are also suggestions in the literature that, in response to inflammatory processes, the HPV response to shunt blood towards a better-ventilated region is normally blocked (56, 170). In a sheep model, Easley et al. (39) used MDCT to demonstrate the regional failure of HPV in a lung region

flooded with endotoxin but not with saline, and Hoffman et al (76) showed the co-existence of an intact HPV to normal lung regions and a failure of HPV in inflamed lung regions. If HPV shuts down blood flow in an emphysema-susceptible smoking population, this would tend to shut down the cascade of events serving to resolve an inflammatory event, including the blockade of progenitor cells which would serve to repair the damage caused by the inflammatory response. Furthermore, if the increased vascular tone in an inflamed region serving to block blood flow to the region is a critical event in the etiology of emphysema, this would have greater consequences in the lung apex where blood flow is further compromised (relative to the lung base in the upright body posture due to gravitational effects), explaining the predominance of apical pathology in smoking related emphysema.

Another possibility explaining this study's findings is that the increased PBF and MTT heterogeneity is a result of micro-vascular destruction caused by micro-emphysema (including very peripheral destruction of vascular and airway structures) undetectable with the resolution of MDCT. Loss of peripheral pulmonary capillary bed due to parenchymal destruction is a known feature of advanced disease (142) but has not been demonstrated in transformational regions. If our findings were due to very peripheral disease undetectable by purely anatomic-based metrics on the CT image, the present study's findings would indicate that functional imaging provides for a differentiating phenotype where anatomical imaging with CT provides no differences including quantitative measures of emphysema-like lung at a threshold of either -950 or -910 HU.

Regardless of the underlying mechanism (failure to block HPV in the presence of inflammation, or micro-destruction with loss of peripheral vascular and airway structures), the increased CV of MTT and PBF measurements in this population offers a new phenotype differentiating our NS and SNI subjects from our SE subjects. Currently, both density and airways changes are considered to be the primary imaging-based phenotypes serving to differentiate COPD groups (29, 30, 133). We describe a new

functional-based image derived phenotype (CV of PBF and MTT) within regions of lung with no density-based changes, and this phenotype may link more closely to specific disease etiology.

In this study, a cohort of human subjects including NS, SNI and SE subjects was formed, and normative regional PBF and MTT values were established. Our cohort consists of individuals with normal spirometry and no clear differences in CT densitometry emphysema measurements between groups, indicating a population of smokers with preclinical emphysema. The presence of centrilobular emphysema, mainly in the apical lobes, did not typically correspond to the region of lung sampled for perfusion imaging. Therefore, the increased heterogeneity demonstrated in smokers susceptible to emphysema is not due to gross parenchymal destruction. We also explored the relationship of perfusion in the non-dependent and dependent regions of the lung, demonstrating an increasing blood flow gradient in the supine position consistent with gravitational forces fighting perfusion, most likely in zones 2 and 3 West conditions (201). This gradient is present in all groups, and therefore did not relate to smoking status. The gradient is consistent with reports in the literature from CT (33), MR (79, 107, 138, 146) and PET (132, 169) imaging modalities. The high spatial resolution perfusion maps obtained with CT perfusion imaging demonstrated regional heterogeneity in the lung parenchyma. When quantified by CV measurements, an increased heterogeneity is demonstrated in the non-dependent region compared to the dependent region for both MTT and PBF measurements in all three groups. Smoking status did not change this regional difference in heterogeneity when imaged supine.

The CT perfusion technique assesses a region of lung corresponding to the z-axis coverage of the multi-detector scanner array. A new generation of scanner, the dual energy CT (Siemens Somatome Definition, Erlangen, Germany) has been recently introduced and can provide a map of the enhanced blood volume by the visualization of the distribution of iodine following contrast administration. While initial studies have

demonstrated the application of perfused blood volume maps to pulmonary diseases such as pulmonary emboli or COPD (20, 42, 190), these measurements are not dynamic measures of perfusion and thus do not quantitatively provide for regional MTT and PBF measurements described here that were obtained with first pass kinetics. Faster scanners such as the Siemens Definition Flash which can image the whole lung in 0.75 seconds along with Toshiba's Aquilion One which covers 16 cm of the z-axis in one rotation may, in the future provide the ability to assess true perfusion parameters over the whole lung. However, the partial lung coverage we present here is adequate for phenotypic differentiation amongst smoking populations. Contrast enhanced MR imaging can also provide quantitative measurements of PBF and MTT, although the signal to noise ratio is more dependent on factors that are more difficult to control, such as contrast concentration and injection rate and RF coil sensitivity (61, 138, 139, 147). Recent studies using this MR perfusion technique have been used to explore perfusion in COPD subjects (86, 106, 138). These cohorts included severe COPD (stage III of IV) subjects, and therefore, represent a much more severely diseased population than studied here.

This study is limited by its cross-sectional study design. A subpopulation of the SNI subjects could be susceptible to emphysema and may develop signs of the disease later in life. This group tended to be younger than our SE subjects. While there was a significant difference in our SE population vs the NS and SNI groups, there was overlap between the populations in regards to our MTT and PBF measures. Further studies to determine if SNI subjects with higher CV measurements represent a group of emphysema-susceptible individuals would be of great interest.

In summary, perfusion MDCT imaging provides a minimally-invasive means of obtaining functional information regarding the pulmonary vasculature, and provides valuable information as we continue to characterize a vascular phenotype of emphysema. Our data show a blood flow pattern of significantly increased heterogeneity, indicative of increased regional variability of PBF and MTT in a subset of smokers with very minimal

MDCT-based evidence of disease and normal spirometry. These findings do not prove but are consistent with our hypothesis that inflammation-based vascular responses to hypoxia (HPV) are occurring in smokers susceptible to COPD but are successfully blocked in smokers without signs of emphysema. An alternative explanation is that there is micro-destruction occurring in the region of lung in which blood flow measures were made, undetectable by other quantitative CT measures. In either case, our functional CT measures provide a new phenotype which may be of importance as imaging gains importance in the search for genotypes associated with COPD and other potentially genetic-based lung disease.

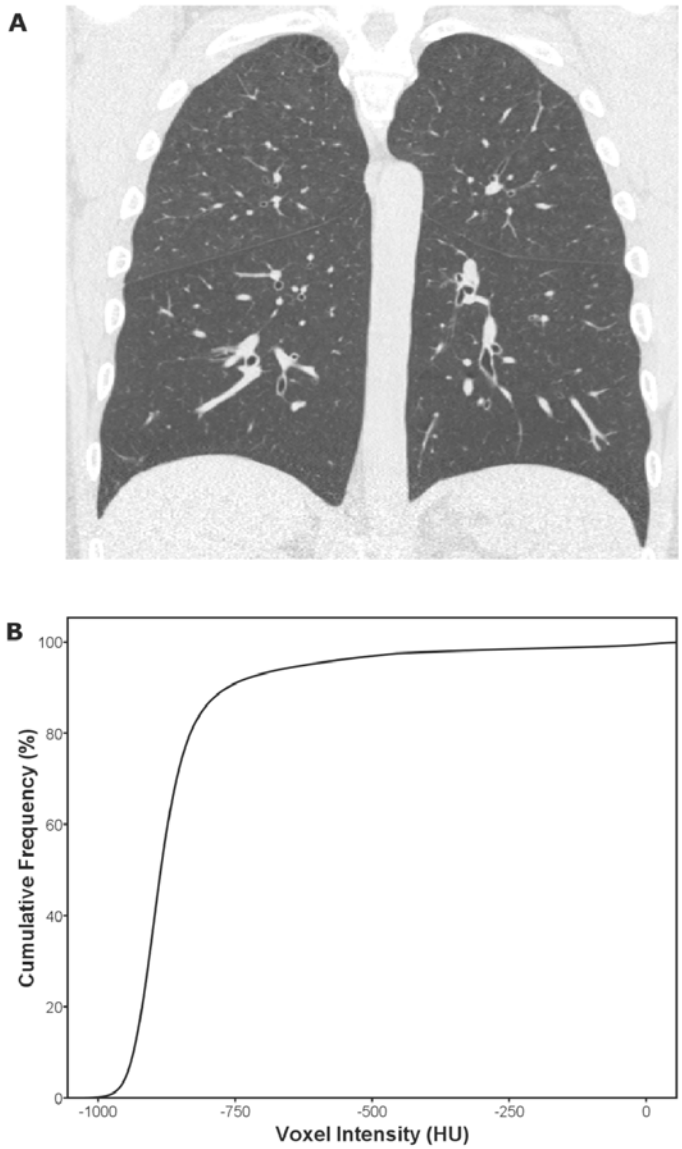

Figure 23. An example of a SE subject. This subject is a 41 year old male smoker with a 45 pack year history. A) A representative coronal image from the volumetric spiral MDCT scan performed at a breath-hold of TLC. This subject demonstrated mild centrilobular emphysema with emphysematous changes present in the upper lobes. Lung window leveling of -500 / 1500 HU was used. B) A cumulative histogram for the whole lung demonstrates the distribution of voxel intensity of the lung parenchyma. EI measurements for -950 HU and -910 HU were 5.1% and 28.9% respectively.

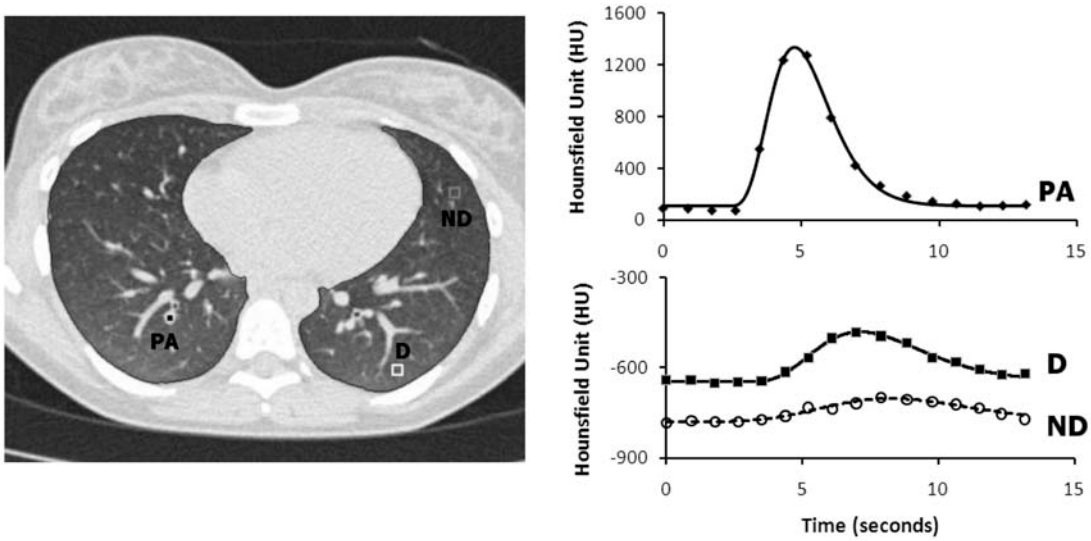

Figure 24. Left: MDCT perfusion baseline image obtained in a SNI subject. The pulmonary artery (PA) and two regions of lung parenchyma in the dependent (D) and non-dependent (ND) region are shown. Right: Corresponding time-intensity curves demonstrate the dynamic change in Hounsfield units (HU) as the bolus of contrast passes through the PA (upper) and in the dependent and non-dependent regions of the lung parenchyma (lower). Regional PBF and MTT are obtained through the application of indicator dilution theory to the data.

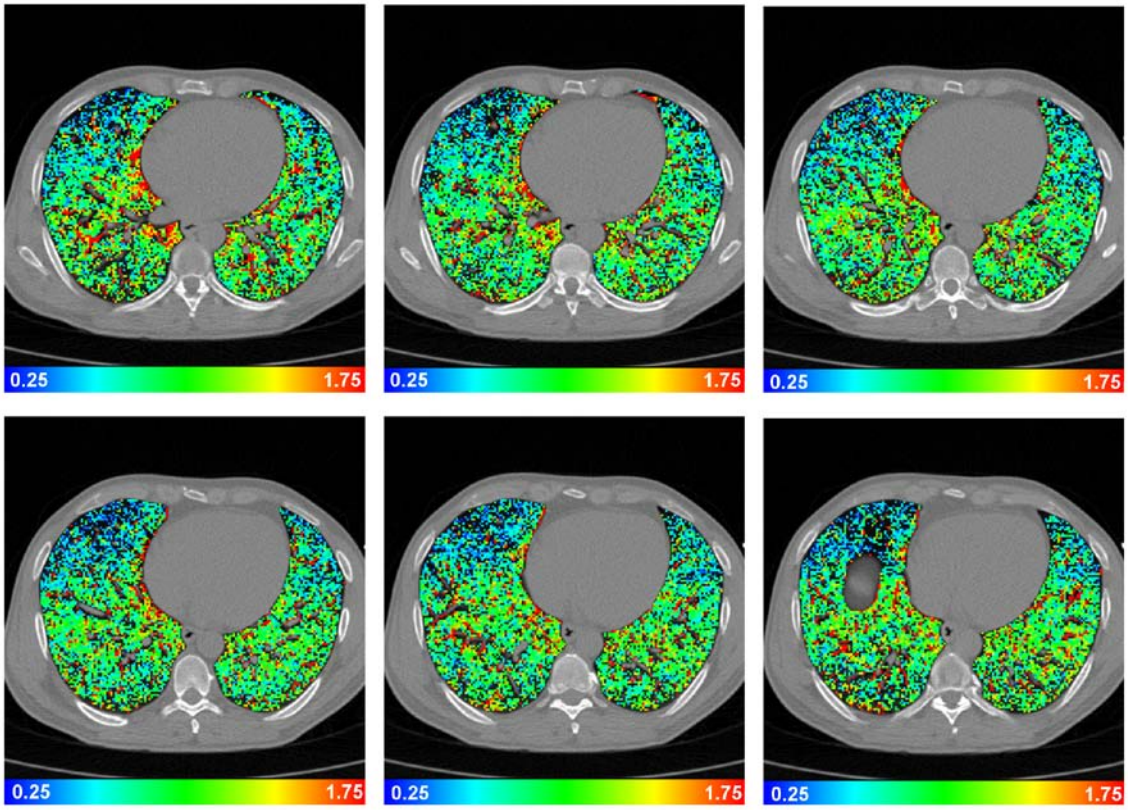

Figure 25. Perfusion maps demonstrate regional PBF measurements obtained from dynamic, ECG-gated CT imaging in a SE subject. Images are obtained during a breath-hold at FRC with 2.4 cm axial coverage (64-slice MDCT scanner). Baseline images (just prior to bolus contrast injection) for six of the twenty slices are shown here with the perfusion map overlaid. Regional PBF, mean normalized, is demonstrated with low to high flow corresponding to blue and red coloring respectively (range: 0.25-1.75). Perfusion measurements have an in-plane resolution of 1.875 mm x 1.875 mm and slice thickness of 1.2 mm. There is marked heterogeneity of PBF present in the lung parenchyma. There is a flow gradient visually apparent with regions of lower flow present in the non-dependent regions and greater flow in the dependent regions of the lung.

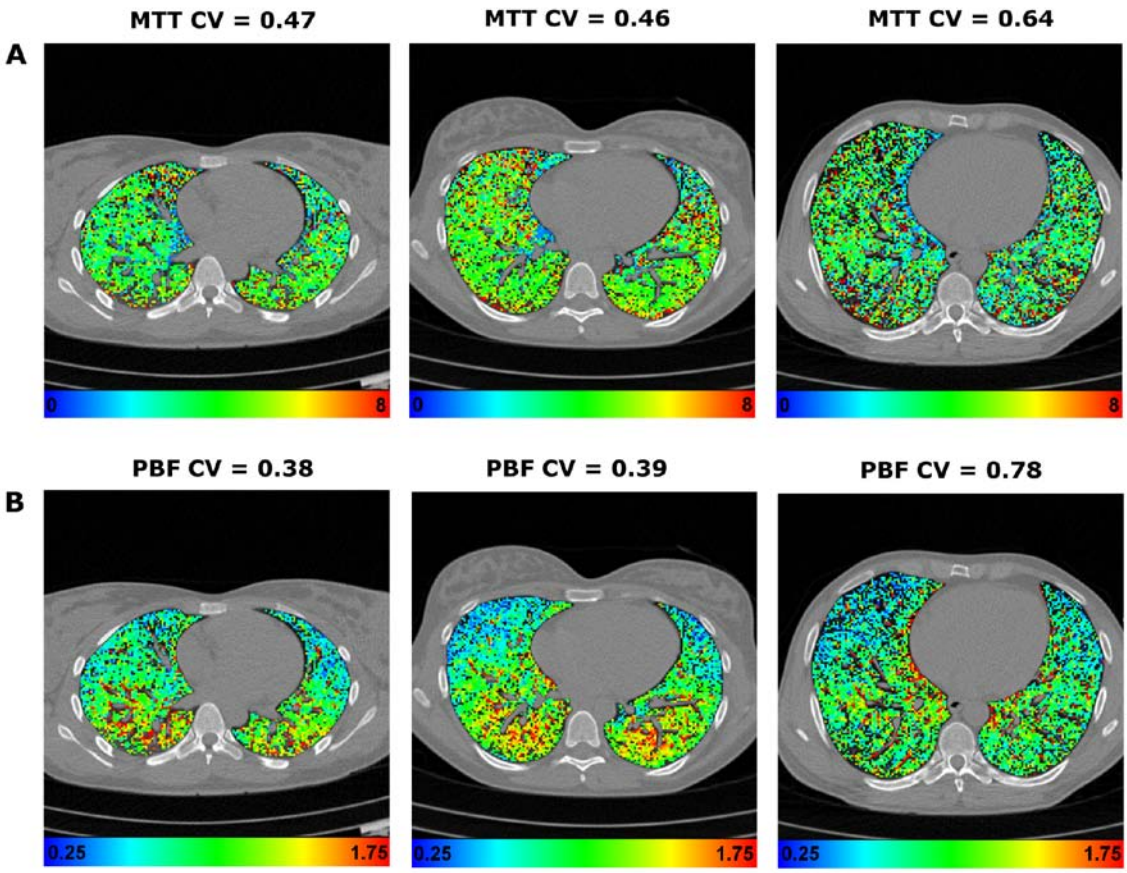

Figure 26. Color coded maps of perfusion parameters overlaid on imaging slice for subjects in each group. A) MTT maps for NS (left), SNI (middle), and SE (right) subject. Maps demonstrate significantly increased regional heterogeneity of MTT measurements in SE subjects as compared to NS and SNI subjects. Range: 0-8 seconds. B) PBF normalized to the mean PBF for NS (left), SNI (middle), and SE (right) subject. Similar to MTT findings, there is increased regional heterogeneity in mean normalized PBF measurements in SE subjects compared to NS and SNI subjects. Range: 0.25-1.75.

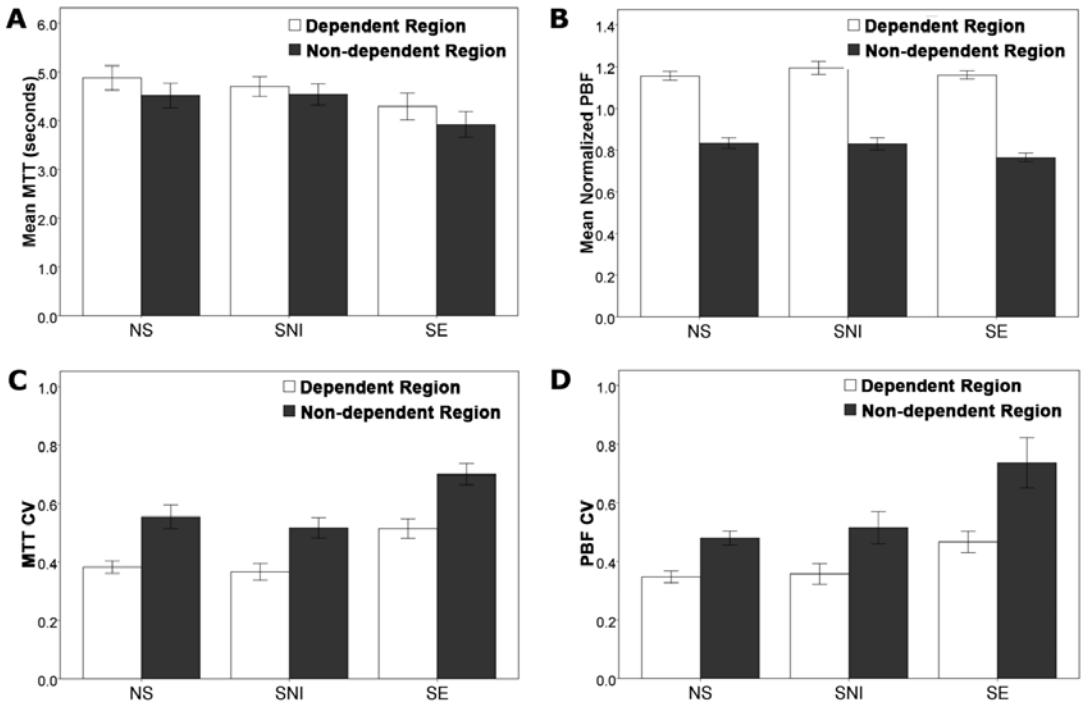

Figure 27. MTT and PBF measurements for dependent and non-dependent regions of the lung. Error bars represent ± SEM. A) Mean MTT did not differ between the non-dependent and dependent region for any of the groups. B) In all groups, mean normalized PBF measurements demonstrate increased flow in the dependent region and decreased flow in the non-dependent region of the lung. C) The CV of MTT is significantly increased in the non-dependent region compared with the dependent region in all three groups (NS: $p = 0.00001$, SNI: $p = 0.001$, and SE: $p = 0.007$). D) CV of mean normalized PBF is significantly increased in the non-dependent region compared to the dependent region in all three groups (NS: $p = 0.0001$, SNI: $p = 0.003$, and SE: $p = 0.001$).

Table 11. CT Perfusion Scan Parameters.

	Philips MX8000	Siemens Sensation 16	Siemens Sensation 64
Total number of studies	12	4	25
Detector rows	4	16	64
Scan type	Axial	Axial	Axial
mAs	150	150	150
KV	80	80	80
Collimation	4 x 2.5 mm	12 x 1.2 mm	24 x 1.2 mm
Detector width (z-axis coverage)	10 mm	14.4 mm	28.8 mm
Slice thickness (mm)	2.5 mm	1.2 mm	1.2 mm
Rotation time (sec)	0.5	0.375	0.33
Filter (kernel)	B	B30	B30
Matrix	512 x 512	512 x 512	512 x 512
Gating	ECG	ECG	ECG
# of triggers	1	1	1
Lung volume	FRC	FRC	FRC

Table 12. Characteristics of Subjects.

Characteristics	NS	SNI	SE
N	17	12	12
Gender - male, %	35	58	58
Age, years	31 ± 10	32 ± 14	46± 11
BMI, kg/m^2	24 ± 3	25 ± 3	25 ± 4
Heart rate, bpm	68 ± 10	72 ± 11	70 ± 13
Blood pressure, mm Hg			
Systolic	116 ± 13	119 ± 15	128 ± 13
Diastolic	66 ± 11	65 ± 12	74± 7
Creatinine, mg/dL	0.8 ± 0.1	0.8 ± 0.1	1.0 ± 0.2
Packyears	---	15 ± 14	31 ± 15
Age started smoking, years	---	17 ± 3	16 ± 4
BDI	11.9 ± .2	11.3 ± 1.2	11.2 ± 1.3
Daily cough in past 2 weeks, %	6	33	50
Pre-bronchodilator FEV_1, %	98.3 ± 8.9	84.9 ± 16.7	98.2 ± 23.5
Pre-bronchodilator FVC, %	100.7 ± 10.5	91.7 ± 11.5	103.9 ± 15.6
Pre-bronchodilator FEV_1/FVC, %	81.4 ± 7.0	77.2 ± 11.6	74.5 ± 4.9
MLD, HU	-849 ± 36	-848 ± 18	-846 ± 21
EI, -950 HU, %	6.3 ± 5.9	4.1 ± 4.3	4.3 ± 3.8
EI, -910 HU, %	34.8 ± 16.9	28.3 ± 14.9	26.0 ± 12.5

Note: Results are expressed as mean ± SD unless noted. Spirometry is reported as percent predicted.

Definition of Abbreviations: NS: never smokers; SNI: smokers with normal CT imaging studies; SE: smokers with emphysema present on CT; BMI: body mass index; BDI: baseline dyspnea index; FEV_1: forced expiratory volume in 1 second; FVC: forced vital capacity; MLD: mean lung density; EI: emphysema index.

Table 13. MDCT-based Perfusion Parameters.

	NS	SNI	SE
WHOLE LUNG			
PBF (ml/100 ml/min)			
Mean ± SD	221.5 ± 55.6	226.0 ± 47.5	210.3 ± 83.7
Range	132.9 - 323.6	152.0 - 307.2	140.1 - 420.2
PBF mean normalized			
Mean	1.00 ± 0.00	1.00 ± 0.00	1.00 ± 0.00
CV	0.43 ± 0.07	0.45 ± 0.11	0.58 ± 0.12
MTT, seconds			
Mean ± SD	4.68 ± 1.01	4.54 ± 0.70	4.08 ± 0.88
Range	3.34 - 6.36	3.21 - 5.47	2.02 - 5.21
CV	0.45 ± 0.09	0.44 ± 0.08	0.58 ± 0.10
Fractional Air Content (%)	74 ± 3	74 ± 2	75 ± 4
NON-DEPENDENT REGION			
PBF mean normalized			
Mean ± SD	0.83 ± 0.10	0.83 ± 0.10	0.76 ± 0.07
CV	0.48 ± 0.10	0.52 ± 0.19	0.74 ± 0.30
MTT, seconds			
Mean ± SD	4.52 ± 1.05	4.54 ± 0.77	3.92 ± 0.91
CV	0.55 ± 0.17	0.52 ± 0.12	0.70 ± 0.13
Fractional Air Content (%)	80 ± 4	79 ± 3	82 ± 2
DEPENDENT REGION			
PBF mean normalized			
Mean ± SD	1.15 ± 0.09	1.19 ± 0.11	1.16 ± 0.07
CV	0.35 ± 0.08	0.36 ± 0.12	0.47 ± 0.13
MTT, seconds			
Mean ± SD	4.88 ± 1.03	4.70 ± 0.71	4.29 ± 0.96
CV	0.38 ± 0.09	0.37 ± 0.10	0.51 ± 0.12
Fractional Air Content (%)	68 ± 5	67 ± 5	69 ± 5

Note: Results are expressed as mean ± SD unless noted. Range: low- high value.

Definition of Abbreviations: NS: never smokers; SNI: smokers with normal CT imaging studies; SE: smokers with emphysema present on CT; PBF: pulmonary blood flow (mean normalized); MTT: mean transit time (sec); CV: coefficient of variation.

Table 14. P-values measuring the significance of group status (NS, SNI, SE) on CV measurements of regional PBF and MTT for models accounting for age and/or pack years.

	Covariates	CV of PBF	CV of MTT
Model 1	---	0.0007 *	0.0005 *
Model 2	Age	0.022 *	0.020 *
Model 3[#]	Age, Pack years	0.11	0.015 *

* denotes significant with a p value < 0.05.

[#] Nonsmokers were excluded from this model and p-values reported relate only to the two smoking groups.

CHAPTER 6: TOTAL PULMONARY VASCULAR VOLUME MEASUREMENTS

TPVV Measurement

As we characterize vasculature alterations in COPD and other lung diseases, having non-invasive measures of vascular parameters such as pulmonary blood volume will be important. In the past, pulmonary vascular volume determined by a dye injection method (149) were used to measure characteristics of the entire pulmonary bed including cardiac output, mean transit times from the pulmonary artery to left atrium, and pulmonary blood volume in human subjects (37, 125). In this chapter, we present a new CT-based measure of blood volume for the pulmonary circulation, total pulmonary vascular volume (TPVV). TPVV is defined as the total arterial and venous intravascular volumes plus extralumenal volumes (the volume of arterial and venous vessel walls) in the lungs. TPVV can be determined from analysis of vascular segmentations obtained from volumetric MDCT lung images.

TPVV measurements were made in two human subject cohorts. The first group, obtained from the BRP cohort, focused on the establishment of normative TPVV values for nonsmokers and smokers without lung disease. TPVV measurements were reported for 40 subjects (20 nonsmokers, 20 smokers). Pulmonary vascular volume was reported on a whole lung, left and right lung, and lobar level for 10 nonsmokers at two lung inflation volumes: TLC and FRC. Linear analysis was used to determine possible covariates and confounders of TPVV that would need to be accounted if TPVV is used as an endpoint or biomarker for follow up or clinical studies. The second cohort, the EMCAP study, focused on determining if an association between TPVV and the following parameters: COPD severity, spirometry, and FMD measures indicative of endothelial dysfunction exist.

Normative TPVV Measurements

Methodology for the BRP Cohort

Study Design

From September 2004 to October 2008, 40 subjects from the local community were recruited as part of an effort to establish a normative lung atlas. The University of Iowa institutional review board approved this study and written informed consent was obtained prior to entering the study from all subjects. Study inclusion criteria were never smokers with a total smoking history less than 1 pack, and smokers currently smoking a pack a day. Subjects were excluded for known heart disease, kidney disease, diabetes, presence of metal in the lung field, pregnancy, X-ray/CT scan in the past 12 months, contrast allergies, glomerular filtration rate less than 60 ml/min, and body mass index over 32. Never smokers with clinically important pathology detected on CT were excluded along with smokers with significant lung disease other than emphysema. Height and weight were determined and body mass index (BMI) calculated as weight (kg) divided by height squared (m^2), and body surface area (BSA) were calculated (38). Pre-bronchodilator spirometry was performed on one of two systems: V6200 Body Box (Sensor Medics, Yorba Linda, CA) or the OWL Digital Body Plethysmography (Ferraris Respiratory, Louisville, CO). Before changing from the V6200 to the OWL system, we verified that measures on our subject population were equivalent between systems. Assessment of spirometry quality followed the American Thoracic Society and European Respiratory Society recommendations (123).

MDCT Imaging and Data Analysis

Spiral non-contrast volumetric MDCT imaging was performed in the supine position with a 16-slice (Sensation 16, Siemens Medical Systems, Erlangen, Germany) or 64-slice MDCT scanner (Sensation 64, Siemens Medical Systems, Erlangen, Germany) at

two fixed breath-hold controlled lung volumes: total lung capacity (TLC, 100% of vital capacity) and functional residual capacity (FRC, 20% vital capacity). A well calibrated pneumotachometer with balloon occlusion valve, linked to a lab-developed monitoring program (Labview, National Instruments, Austin, TX), instantaneously measured the airflow and airway pressures and was used to breath-hold lung volumes appropriately. Heart rate, ECG, arterial pressure, and pulse oximetry oxygen saturation (SpO_2) were continuously monitored while the subject was in the scanner (Philips IntelliVue patient monitoring system, M8010A, Andover, MA). Scan protocol for the 64-slice MDCT scanner for volumetric scans were as follows: mA, 100; kV, 120; pitch, 1mm; rotation time, 0.5 seconds; slice thickness, 0.75mm; slice increment, 0.5mm; matrix, 512 x 512; and reconstruction kernel, B31f or B35f. Voxel dimensions were near isotropic at 0.47 mm x 0.47 mm x 0.50 mm. Scan times are under 10 seconds with a z-coverage of 22-30 cm, adjusted in order to capture the whole lung. A subgroup of 28 subjects (9 nonsmokers, 19 smokers) also underwent perfusion MDCT imaging and was included in the cohort described in Chapter 5.

Volumetric images were analyzed with PW 2.0 (VIDA Diagnostics, Coralville, IA) for the segmentation of lung, lobes and vessels. Lung and lobar volumes were determined. Manual editing of the lung segmentation was necessary to include the vascular tree to the main branch pulmonary arteries. Vascular segmentations were obtained in PW using a previously described algorithm (171), and volumes were obtained for the whole lung (TPVV), left and right lung, and lobes using PASS software (55, 73).

Statistical Analysis

Statistical comparisons were performed with SPSS software (Windows 17.0, SPSS, Inc; Chicago, IL). Normality of TPVV was assessed by Shapiro-Wilk statistic. Mean ± SD for TPVV measurements were determined for the whole group, and for the subgroups of nonsmokers and smokers. Vascular volumes were compared to lung volume

on a whole, left and right, and lobar scale. Associations of TPVV and potential confounders, such as BMI, were estimated with simple linear regression models. Pearson correlations were obtained for possible confounding factors. The association between TPVV and the following factors, accounting for total lung volume and body size, were obtained: spirometry measures including FVC, FEV_1, and FEV_1/FVC; and perfusion parameters including PBF, MTT, CV of PBF, and CV of MTT. Partial correlation coefficients were obtained. P-values less than 0.05 were considered significant.

Results for the BRP Cohort

Normative TPVV Measurements

Forty subjects (20 non-smoker and 20 smokers) completed pulmonary function testing and MDCT imaging. Baseline demographics are summarized in Table 15. All smokers were without clinical symptoms or signs of disease based on initial assessment. Pre-bronchodilator spirometry results were within normal range and percent predicted values of FVC and FEV_1 and FEV_1/FVC ratio are summarized in Table 15.

Volumetric scans were read by a chest radiologist with 15 years experience. Nonsmoking subjects had normal chest reads (n=18) or minor, nonvascular-based pulmonary disease (n =2 mild bronchiectasis). In the smokers, 12 out of 20 subjects demonstrated mild emphysema on CT, identified by the chest radiologist. Volumetric MDCT images obtained at full lung volume (TLC) had a mean total lung volume of 6339 cm^3 and a range from 4154 to 8539 cm^3. Some variation in lung volume is expected since we imaged a range of body sizes and types. In the 40 subjects, the total lung volume is strongly correlated with the subject's height ($r = 0.76$) and BSA ($r = 0.52$), mildly correlated with weight ($r = 0.30$, $p = 0.06$), but not BMI ($r = -0.18$, $p = 0.26$) or age ($r = 0.01$, $p = 0.94$).

Figure 28 shows a vascular segmentation obtained from a TLC MDCT lung scan, demonstrating the vascular volume for a nonsmoking subject. Histograms of TPVV and

TPVV normalized to lung volume are shown in Figure 29. TPVV was strongly correlated with total lung volume measurements (Figure 30) and therefore TPVV normalized to lung volume measurements were also determined and reported. TPVV measurements ranged from 114.6 cm^3 to 255.2 cm^3, with a mean TPVV value of 172.2 ± 35.5 cm^3 (95% CI: 160.9 - 183.6 cm^3). TPVV and TPVV normalized to lung volume measurements are normally distributed (Shapiro-Wilk statistic, $p = 0.44$ and $p = 0.74$ respectively). When divided based on smoking status, mean TPVV were 169.0 ± 32.2 cm^3 and 175.5 ± 39.1 cm^3 for nonsmokers and smokers respectively. TPVV and TPVV normalized to lung volume are graphed based on gender in Figure 31. Table 16 summarizes TPVV and TPVV normalized to total lung volume for the subjects and divided based on smoking status and gender. TPVV measurements in males were larger, but so were total lung volumes. Once normalized to total lung volume, the vascular volume did not differ between males and females, and nonsmokers and smokers.

TPVV for TLC and FRC Lung Volumes

TPVV measurements were divided to determine the vascular volumes for lung and lobar regions at TLC (Table 17). In all subjects, the right lung (80.6 cm^3, 53%) demonstrated slightly higher pulmonary vasculature volume than the left lung (91.6 cm^3, 47%). Vascular volumes in the lobes were 37.3 ± 9.3 cm^3 (22%) and 43.3 ± 10.5 cm^3 (25%) for LUL and LLL, respectively, and 31.4 ± 6.4 cm^3 (18%), 12.8 ± 3.6 cm^3 (7%), and 47.4 ± 10.2 cm^3 (28%), for RUL, RML and RLL, respectively. The distribution of vascular volume matched the lobar volume distribution within a percent. Therefore, pulmonary vasculature volume per lung volume was consistent, and the vascular and lung volume maintain the same relationship across lungs and lobes.

A subset of 10 nonsmokers had TLC and FRC pulmonary vascular volume measurements determined for the lung, left and right lung, and lobes. Results are summarized in Table 18. An example of vascular segmentations obtained at TLC and

FRC for one subject are shown in Figure 32. Visually, the FRC segmentation compared to the TLC segmentation did not contain as many generations of vasculature and seemed to be missing some of the small vessels. Mean FRC TPVV measurements for the 10 nonsmoking subjects was 101.4 ± 26.4 cm^3 compared to 163.0 ± 30.0 cm^3 for the mean TLC TPVV measurement. This represents a 38% decrease in blood volume from TLC to FRC. In all FRC scans, the right lung (56.6 ± 13.4 cm^3, 56%) also demonstrated slightly higher blood volume than the left lung (45.1 ± 14.0 cm^3, 44%) The distribution of vascular volume at a lobar level for TLC and FRC matched well (within a few percent) to each other and to corresponding lobar lung volumes.

Association of TPVV Measurements with Covariates

Pearson correlation coefficients were used to assess associations between TPVV and the following factors: total lung volume, age, BSA, BMI, height, and pack years. Since TPVV and total lung volume were strongly correlated, correlations between TPVV normalized to total lung volume and the other factors was also determined (Table 19). Age (Figure 33) demonstrated a weak inverse relationship to TPVV (r = -.020, p 0.2). Once total lung volume was accounted for, smoking history (assessed by pack years) is associated with a decrease in TPVV that reached near significance (p = 0.09) (Figure 34). Strong linear correlations exist between measures of body size and TPVV (Figure 35) and TPVV normalized to lung volume (Figure 36). Total lung volume, height and weight together account for 65% of the variability observed in TPVV measurements.

Association to Spirometry

Accounting for total lung volume, height and weight, partial correlations were determined for TPVV and the following spirometry parameters: FVC, FEV_1, FEV_1/FVC ratio. Results are summarized in Table 20. Strong direct correlations between TPVV and pre-bronchodilator spirometry measurements of FEV_1 (r = 0.52; p = 0.001), FVC (r = 0.46; p = 0.004) and FEV_1/FVC ratio (r = 0.42; p =0.009) existed. When divided based

on smoking status, a decreased association (to a non-significant level) existed for the nonsmoker subjects between TPVV and FVC (r = 0.36 versus 0.56 in smokers), FEV_1 (r = 0.32 versus 0.77 in smokers), FEV_1/FVC (r = 0.30 versus 0.56 in smokers) ratio, while smokers demonstrated a significant correlation for all 3 measurements.

Association to MDCT Perfusion Parameters

For the 28 subjects (9 nonsmokers, 19 smokers) with perfusion and TPVV measurements, mean PBF was 221 ± 64 ml/min/100 ml (range: 140 - 420 ml/min/100ml) and mean MTT was 4.3 ± 0.8 seconds (range: 2.0 - 6.3 seconds). Mean CV measurements were 0.50 ± 0.12 (range: 0.36 - 0.78) and 0.52 ± 0.10 (range: 0.33 - 0.76) for PBF and MTT respectively. In chapter 5, age and pack years were determined to be factors affecting MTT and PBF measurements and therefore, were added to the original model of total lung volume, height and weight for the determination of associations between TPVV and perfusion measurements. Partial correlations are summarized in Table 20. Mean MTT (r = 0.06, p = 0.8) and regional PBF (r = 0.2; p = 0.4) measurements didn't correlate well with TPVV measurements. CV of MTT and CV of PBF demonstrated weak inverse correlations with TPVV (r = -0.24 for both), but these correlations did not reach significance levels (p value: CV MTT: 0.26; CV PBF: 0.27).

TPVV Measurements in COPD Subjects

Clinical Significance and Rationale

The purpose of this study was to test for an association between pulmonary vascular volume, assessed by MDCT TPVV measurements, and COPD severity, spirometry, CT percentage of emphysema, and endothelial dysfunction as assessed by FMD of the brachial artery. TPVV measurements reflect a balance of alterations in vascular tone and presence of pathological lesions occurring in the pulmonary vasculature. If vasculature-related changes and endothelial dysfunction are prominent,

one would expect the presence of subclinical hypertension, and therefore an increase in TPVV measurements should result. If emphysematous destruction has destroyed the capillary-alveolar junction, there will be a decreased capillary volume and therefore decreasing in TPVV. We studied 93 subjects with spirometry, CT imaging and FMD measurements among a random sample of former smokers in an ongoing cohort study, The Emphysema and Cancer Action Project (EMCAP) study.

Methodology for the EMCAP Cohort

Study Design

The EMCAP study recruited 557 participants at one site of a lung cancer CT screening research program in 2001-2002 (16). Inclusion criteria were current and former smoking with 10 or more pack-years, age 60 years and older, willingness to undergo CT screening for lung cancer, and no cancer history other than nonmelanoma skin cancer. Our sample was restricted to former smokers because current cigarette smoking causes acute reductions in FMD (23, 207). Of 557 EMCAP participants, 313 (56%) denied current smoking at baseline and follow-up and were hence eligible for the FMD study. Sixty-one percent (119 subjects) of the 196 randomly invited sample subjects successfully participated in the FMD study. Written informed consent was obtained prior to entering the study from all subjects. The Columbia University Institutional Review Board approved all study activities. The University of Iowa Institutional Review Board approved all data analysis activities of this study.

An interviewer-administered questionnaire provided information on age, gender, race/ethnicity, educational attainment, and physician diagnoses of cardiovascular diseases. Blood pressure measured with mercury sphygmomanometers and cuffs of appropriate size. Height and weight were determined by the use of calibrated scales and body mass index (BMI) was calculated as weight (kg) divided by height squared (m^2). Current smoking status was verified by urinary cotinine levels determined by an enyzme-

linked immunosorbent assay (Orasure Technologies, Inc., Bethlehem, PA), with current smoking defined as urinary cotinine levels above 500 ng/ml.

Pulmonary Function Tests

Pre- and post-bronchodilator spirometry was performed according to American Thoracic Society (ATS) guidelines (1) using the EasyOne portable spirometer (ndd Medical Technologies, Chelmsford, MA), which had been previously validated against a dry seal, rolling-barrel spirometer (10). Assessment of spirometry quality followed ATS/European Respiratory Society (ERS) recommendations (122, 123). COPD and COPD severity were defined according to ATS/ERS COPD criteria using post-bronchodilator measures (24) described in Chapter 2. Single-breath DL_{CO} was measured with a Sensormedics Autobox 220 Series instrument (Viasys Healthcare, Yorba Linda, CA) following ATS/ERS guidelines (111) according to the method of Jones and Meade (88).. The participant exhaled to residual volume, then was switched to a gas mixture of 0.43% CO, 10% helium, 21% oxygen, and balance nitrogen. The subject then inhaled rapidly to TLC, breath-held for 10 seconds, then exhaled to residual volume. The average of all acceptable tests (minimum of two tests) was reported.

FMD Measurements

A non-invasive measure of endothelial function is FMD of the brachial artery. This test measures endothelium-dependent, NO-mediated vasodilation. FMD was measured in 2005–2006 using a standardized protocol adapted from a large multicenter study (17), consistent with published guidelines (28). Subjects fasted for 12 hours, avoided exercise for 6 hours, and rested in the supine position for 15 minutes (28). Regular medications were not withheld. Brachial artery diameter was measured 6 cm above the antecubital crease of the right arm using B-mode ultrasound with a 15-MHz linear array transducer (SONOS 5500; Philips, Andover, MA). A blood pressure cuff was inflated to at least 50 mm Hg above systolic blood pressure to occlude arterial flow to the

forearm for 5 minutes (28), then brachial artery diameter was re-measured during reactive hyperemia 1 minute after cuff deflation (53, 135). End-diastolic images were digitized by a frame grabber (model LG3; Scion Corporation, Frederick, MD). A single reader blinded to clinical status measured all brachial artery diameters off-line using analysis software for three consecutive cardiac cycles at rest and 1 minute post deflation for each participant. FMD was expressed as percentage change from rest (100 x [brachial artery diameter during reactive hyperemia – diameter at rest]/diameter at rest). Absolute intra-observer variability for FMD measurements was 1.3%.

MDCT Imaging Acquisition and Analysis

All participants underwent low-dose, non-contrast, full-lung CT scanning on a Siemens 16 MDCT scanner (120 kV, 169 mAs, 6:1 pitch, 5-mm and 1-mm slice thickness reconstructions, single breath-hold, contiguous slices from the thoracic inlet to the adrenal glands). The CT percentage of emphysema in the lungs (emphysema index) was assessed as the proportion of lung volume below a threshold attenuation of -910 HU compared with the total volume of the lung (131). Volumetric images were analyzed with PW 2.0 (VIDA Diagnostics, Coralville, IA) for the segmentation of lung, lobes and vessels. Lung and lobar volumes were determined. Manual editing of the lung segmentation was necessary to include the vasculature tree to the main branch pulmonary arteries. Vasculature segmentations were obtained in PW using a previously described algorithm (171). Vascular volumes were measured for the whole lung (TPVV), left and right lung, and the lobes using PASS software (55, 73).

Statistical Analysis

Mean and SDs of TPVV measurements were determined for the cohort on a whole lung, right and left lung and lobar level. Intra-observer variability measurements were determined from 13 subjects re-analyzed within 6 months (~10% cohort). Associations between TPVV measurements and spirometry-based measurements, and

TPVV and FMD measurements were determined using linear regression models accounting for confounders. All p-values were two-tailed with $P<0.05$ considered significant. Analysis were performed using SAS version 9.1 (SAS Institute, Cary, NC), S-plus 6.2 (Insightful Corp., Seattle, WA) or SPPS version 17.0 (SPSS, Inc; Chicago, IL).

EMCAP Results

Participant Characteristics

Out of the 119 subjects, 93 subjects had complete clinical data, pulmonary function testing, MDCT volumetric imaging, FMD measurements, and were cotinine-confirmed former smokers. Participants in the study sample were elderly, fairly evenly divided among gender (43% female, 57% male), 18% nonwhite, and had moderately heavy smoking histories (Table 21). Lung function in this sample of former smokers ranged from normal to severely impaired. Spirometry tests are summarized in Table 21. The majority of subjects (62) did not have COPD (defined as post-bronchodilator $FEV_1/FVC < 0.70$). The remaining 31 subjects were staged according to GOLD classifications with 7, 18, 3 and 3 subjects classified as mild (stage I), moderate (stage II), severe (stage III) and very severe (stage IV) respectively. Table 21 also shows the characteristics of the 62 subjects that did not have COPD. No significant differences exist between the overall sample and the subgroup with COPD except CT percentage of emphysema and pulmonary function measures.

TPVV Measurements

TPVV measurements were obtained in all 93 subjects. A 3-D rendering of the vasculature, airways and lobes is shown in Figure 37. The average TPVV measurement for the whole cohort was 168 ± 34 cm^3, with a range of values from 110 cm^3 to 276 cm^3. The absolute intra-observer variability for TPVV measurements was 4.0 ± 2.0 cm^3. The mean total lung volume was 5150 ± 1199 cm^3 with a range of values from 2685 cm^3 to

8315 cm^3. Total lung volume is directly correlated with TPVV measurements, with 83% of the variability in TPVV accounted for by total lung volume (Figure 38). The right lung (90.9 cm^3, 54%) demonstrated slightly higher vascular volume than the left lung (76.7 cm^3, 46%). Lobar vascular and lung volumes matched within 1% (Table 22). Therefore, once normalized to lung or lobar volume, the vascular volume was fairly homogenously distributed across the lung. For the 31 former smoking subjects with COPD, the upper and middle lobes (LUL: 0.32; RUL: 0.032; RML: 0.029) demonstrated a slight decrease in TPVV normalized to lung volume compared with the lower lobes (LLL: 0.033; RLL: 0.034) and the mean TPVV (0.032) (Table 23). This corresponds with CT percentage of emphysema measurements for the lobes which demonstrate increased values in the upper and middle lobes (LUL: 48%; RUL: 47%; RML: 50%) compared with the lower lobes (LLL: 41%; RLL: 43%).

Association with Spirometry and CT measures of COPD severity

Associations with TPVV, spirometry, and CT measures of emphysema were determined for two models (Table 24). In model 1, the only factor accounted for was the total lung volume. Model 2 included age, gender, height, weight, race/ethnicity and pack years in addition to total lung volume. CT percentage of emphysema demonstrated a strong significant inverse correlation with TPVV measurement (Both models: $p = 0.002$) for both models. Post-bronchodilator FEV_1 was significantly associated with TPVV for model 1 ($p = 0.04$) with a 1 SD increase in TPVV resulting in a 33 mL (95% CI: 2-64 ml) change in FEV_1. This association diminished in model 2 to a non-significant level ($p = 0.11$). Post-bronchodilator FVC and FEV_1/FVC ratios demonstrate trends of direct association that were non-significant for both models. DL_{CO} measurements demonstrated a direct association, but also were at near significance level with p-values of 0.08 and 0.15 for model 1 and 2 respectively.

Association with FMD Measurements

FMD measurements of this cohort have been analyzed for these subjects and are reported by Barr et al (9). It was determined that endothelial dysfunction, measured by FMD, was associated with lower post-bronchodilator FEV_1 and higher CT percentage of emphysema in formers smokers across a range of disease severity including individuals with normal lung function and anatomy to severe COPD/emphysema (9). In the subset of 93 subjects studied, the mean diameter of the brachial artery before cuff inflation was 3.8 ± 0.7 mm. The mean increase in brachial artery diameter during reactive hyperemia after cuff deflation was 0.13 ± 0.11 mm. The corresponding mean FMD, or percentage change in the brachial artery diameter, was 3.8 ± 3.2%.

FMD and TPVV measurements demonstrate an inverse association that did not reach significant levels in this population (Table 25). The mean difference in FMD per 1 SD of TPVV was -1.2% (95% CI: -2.8, 0.4, p-value: 0.13) for Model 1 and -1.1% (95% CI: -2.8, 0.6, p-value: 0.21) for Model 2. This translated to a non-significant mean difference change of -0.05 mm (95% CI: -0.10, 0.01; p-value: p = 0.10) and -0.04 mm (95% CI: -0.10, 0.02; p-value: 0.15) in absolute diameter for 1 SD change of TPVV. Partial correlation coefficients for FMD (% change) were -0.16 and -0.14 for percent change; and -0.17 and -0.16 for absolute change in Model 1 and 2, respectively. The baseline diameter measured with FMD was significantly different in Model 1 (p = 0.05) demonstrating a direct correlation. A larger brachial artery diameter correlated to an increased TPVV.

Discussion

TPVV measurements can be made from non-contrast volumetric CT images of the lungs and reflect the physiological state of the pulmonary vasculature by providing a pulmonary blood volume measurement. We present TPVV measurements from 2 cohorts. In the BRP cohort, we analyzed nonsmokers and smokers without COPD to

determine the range of normal values. In this population, there was no detectable difference in TPVV. Gender did appear to influence TPVV measurements. Age and pack years demonstrated non-significant declines in TPVV. Total lung volume, and measures of body size such as height, BMI, and BSA were significantly correlated with TPVV measurements. Total lung volume, height and weight were determined to be significant covariates, accounting for 65% of the variability of TPVV measurement. The total lung volume can be determined from the lung segmentation obtained during the analysis process needed to obtain TPVV measurements. If TPVV is used as an endpoint variable, it will be important to collect accurate height and weight measurements to correct for body sizes. These findings support our current knowledge that a larger lung volume and/or body size would have an increased vascular volume to accommodate the needs of the extra tissue.

In the BRP cohort, TPVV was directly significantly correlated with FEV_1, FVC, and FEV_1/FVC ratio in normal nonsmokers and smokers without clinical disease. In the EMCAP cohort, spirometry measures did not reach significance with a full model including age, gender, race/ethnicity, height, weight, and pack years and total lung volume, but levels were near significance. In the EMCAP study, the CT-based emphysema percentage measurements were strongly inversely associated with TPVV. An increased volume of emphysematous tissue on CT suggests more severe disease. Screening studies have demonstrated CT findings of emphysema in "normal" smoking recruited subjects with normal lung function measures, demonstrating the ability of CT to detect more mild cases of disease compared to the global spirometry based clinical diagnoses (65, 112, 130, 131). DL_{CO} measures were associated as near significance levels suggesting a weak direct association with this measure and TPVV. DL_{CO} quantify the diffusing capacity of the capillary, with decreasing levels correlating with decreased ability for gas exchange. One explanation for these associations and trends is the presence of parenchymal destruction, leading to a decreased pulmonary vascular volume.

Increasing disease severity such as decline in spirometry measures and increased CT percentage of emphysema indicate the presence of more pathological lesions in the lung. As CT percentage of emphysema measurements increase, more parenchymal damage is present in the lung, and some of this destruction will be of vasculature structures such as the capillary bed. An impaired gas exchange would results with these pathological processes, explaining the DL_{CO} results.

While MDCT-based perfusion CV measurements and TPVV did not demonstrate a significant correlation in the 28 subjects analyzed, the data demonstrated a trend for increased CV to inversely relate to TPVV. In chapter 5 we demonstrated that smokers with preclinical emphysema have increased CV. This trend of an increased CV correlating with a decreased TPVV agrees with the data suggesting that decreased TPVV is related to increased disease severity (decreased lung function, increased CT percentage of emphysema). In addition, this population includes nonsmokers and smokers with normal lung function, and smokers with preclinical emphysema. All of these individuals are clinical normal subjects and exhibit minimal disease if any at all. At this stage of disease, these subject may have a more localized or regional pattern of vasculature changes that is masked by the use of a global pulmonary vasculature volume measurement.

Endothelial dysfunction is known to occur early in COPD subjects (144) and an impaired FMD has been correlated with a decline in lung function measures and a higher CT percentage of emphysema (9, 126). The trends observed in the EMCAP study suggest that endothelial dysfunction is correlated with an increased TPVV. This correlation was not significant, but it is possible that vascular alterations are present in COPD subjects, but factors such as parenchymal destruction leading to destruction of the capillary bed are more prominent, and therefore masking the pulmonary vascular effects. We know that vascular alterations of the small vessels are one of the characteristic features of pulmonary hypertension in COPD. Many of the pathological lesions

characterized for smokers with minimal disease or mild COPD include intimal thickening of the pulmonary muscular arteries and endothelial dysfunction of the pulmonary arteries responsible for vascular tone (144, 165). Barr et al. also demonstrated with this EMCAP study data that FMD measurements are linearly related to lung function and CT lung density in smokers. The overall changes in a global TPVV measurement may not be sensitive enough to pick up subtle differences in the dynamic vascular tone. One major limitation of this measurement lies in the fact it is a global measurement and does not allow for arterial and venous volume separation. Pathological changes specific to the arterial bed may go undetected therefore, a study looking at specifically changes in the arterial side including dimensions would be valuable. Dilated arterial vessels, even in the event of a decreased TPVV, would suggest the presence of subclinical hypertension.

New CT-based techniques that discriminate vessels based on their association with airways or with the placement of seed points are currently being developed. An example of the vascular trees separated into arteries and veins with a fuzzy logic based algorithm is shown in Figure 39 (164). This algorithm holds much promise since it will not only be possible to distinguish the pulmonary artery and vein volume distribution, but also determine centerlines much like airway analysis. This would allow for vasculature pruning to a specified generation and therefore more accurate comparisons of vascular volumes. This will be especially important when tracking changes to ensure that changes are not from differences in vascular segmentations but reflect actual physiologic changes present in the individual. This is also important for the comparison of two lung inflation volume such as TLC and FRC, which visually demonstrated differences in performance of the algorithm. At FRC, the lung is denser and the contrast between vessels and air spaces is decreased. This will make it more difficult for the algorithm to capture vessels specifically at the higher generations where vessel diameters are small and partial volume effects are more prominent.

To summarize, studies from two cohorts have demonstrated that a decreased TPVV is associated with a decline in lung function (decreased FEV_1) and increase in CT percentage of emphysema, and demonstrates trends suggesting an inverse correlation between TPVV and CV of perfusion-based measurements, and TPVV and endothelial function assessed by FMD. These findings collectively suggest that as COPD severity increases, the pulmonary vascular volume is overall decreased; but also as endothelial dysfunction occurs, an increase in the TPVV measurements was observed, suggestive of the presence of vascular changes in COPD subjects. For further characterization of alterations to the vascular volume with disease, more sophisticated methods of CT assessment will need to be developed and applied to clinical data. By applying more specific CT-based measurements such as the separation of the pulmonary arterial volume, we will be able to further characterize important pathological alterations and etiology of a vascular phenotype in COPD subjects.

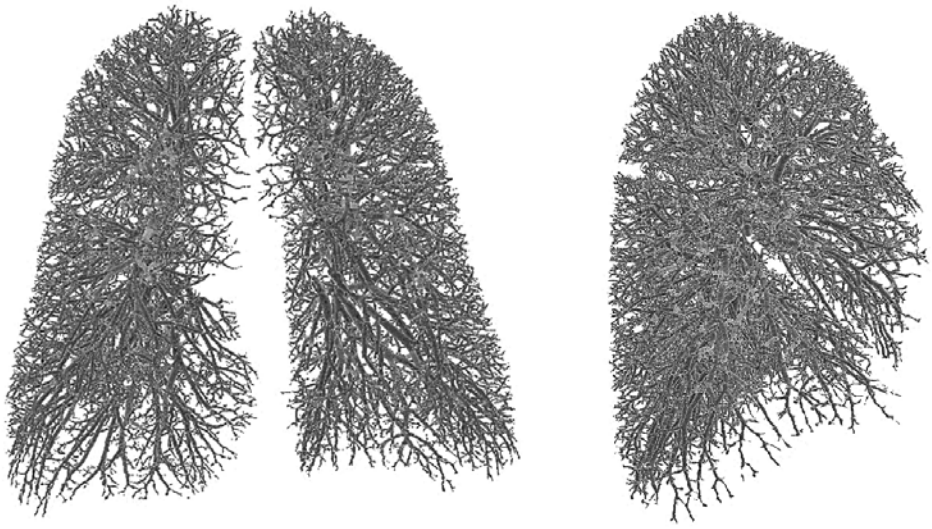

Figure 28. Vascular segmentations from a non-smoker subject in the BRP cohort at an AP (left) and lateral (right) viewpoint.

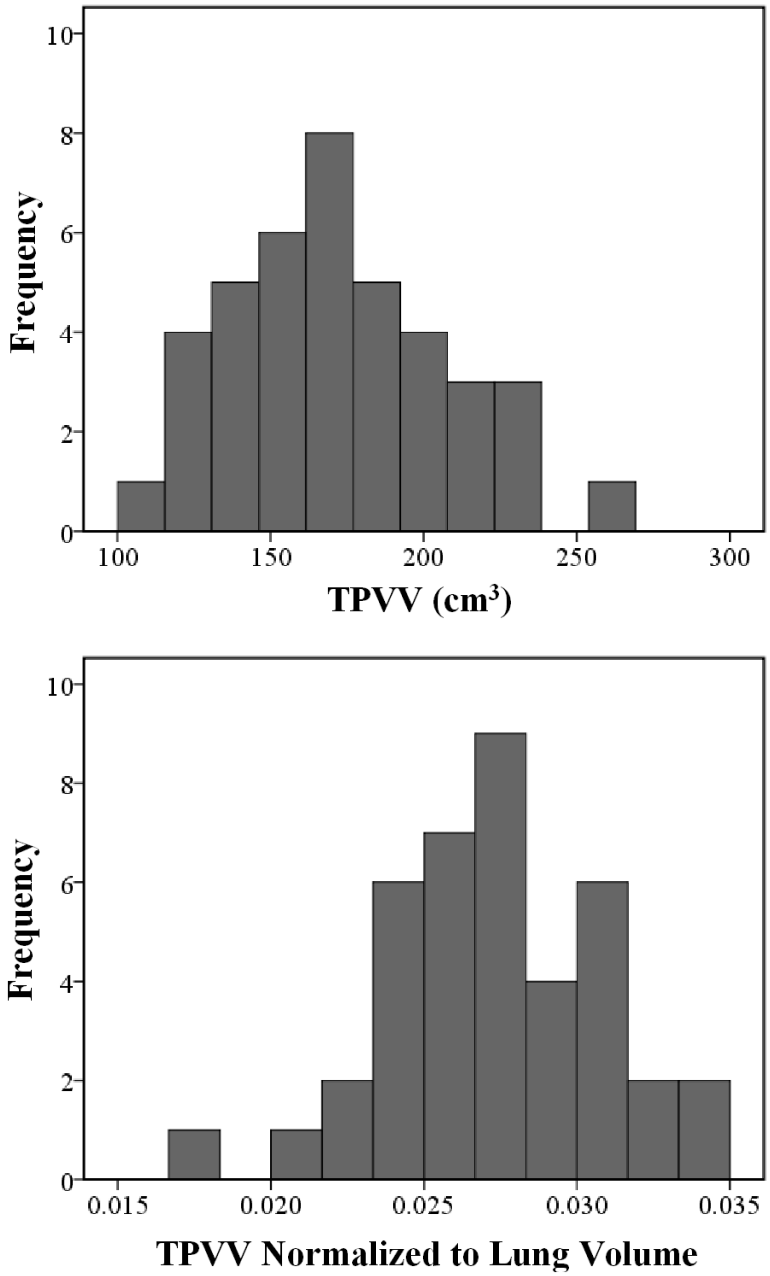

Figure 29. Histograms of TPVV and TPVV normalized to total lung volume (determined from quantitative image analysis of lung MDCT images). TPVV and TPVV normalized to lung volume measurements are normally distributed (Shapiro-Wilk statistic: TPVV: p = 0.44; TPVV normalized to lung volume: p = 0.74). TPVV measurements ranged from 114.6 cm^3 to 255.2 cm^3, with a mean TPVV value of 172.2 ± 35.5 cm^3 (95% CI: 160.9 - 183.6 cm^3). TPVV normalized to lung volume ranged from 0.0179 to 0.0339 with a mean value of 0.0272 ± 0.0035 (95% CI: 0.0261 - 0.0284).

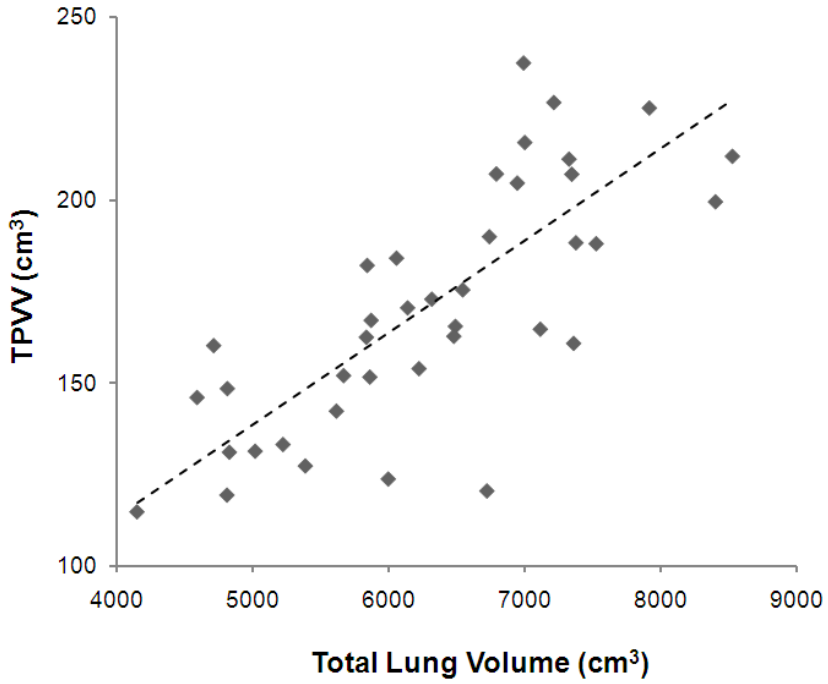

Figure 30. TPVV demonstrated a strong direct linear correlation (r = 0.76) with the total lung volume determined by quantitative image analysis. These measurements were taken at the TLC lung inflation volume.

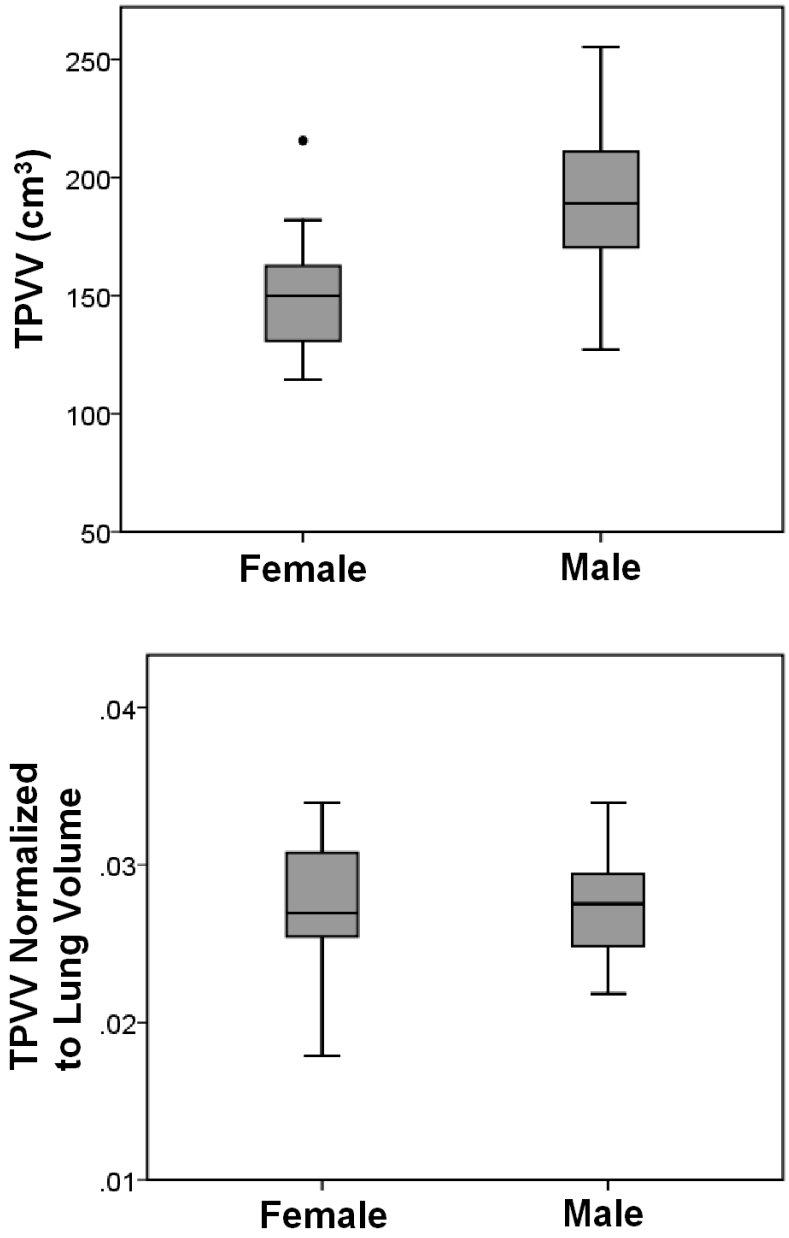

Figure 31. TPVV and TPVV normalized to lung volume divided by gender. TPVV measurements were larger in male subjects (top), but males also had larger total lung volumes. Once TPVV was normalized to total lung volume (bottom), there were no significant differences due to gender.

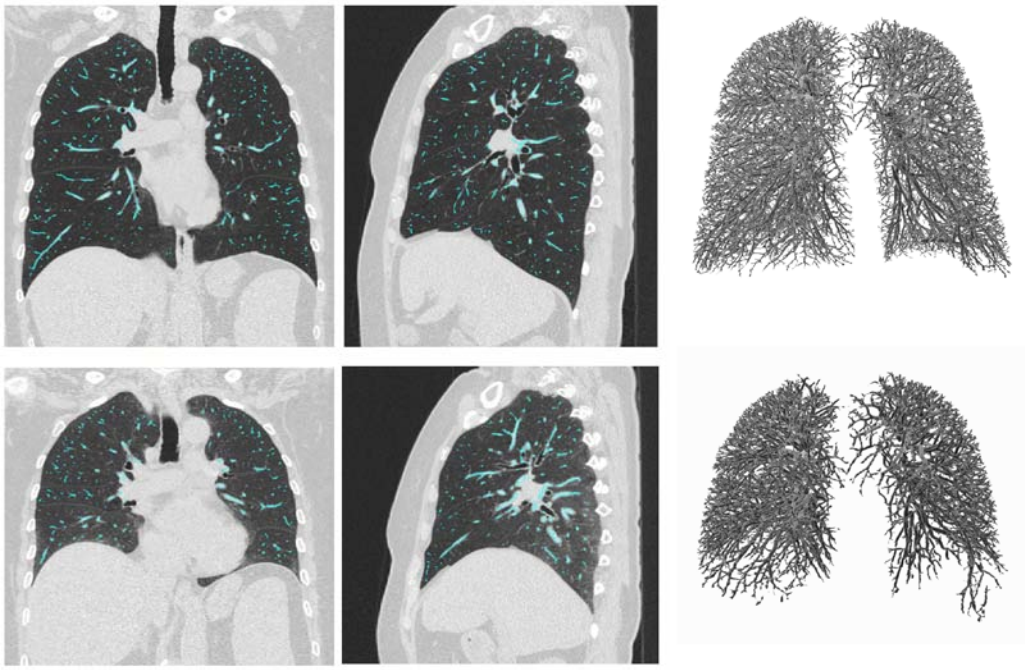

Figure 32. A coronal (left) and sagittal (middle) slice demonstrating vascular segmentation results from a subject at two lung inflation levels: TLC (top) and FRC (bottom). Corresponding pulmonary vasculature segmentations at a lung inflation of TLC (right upper) and FRC (right lower). While both segmentations appear to capture the vasculature out to the peripheral regions of the lung, the FRC vessel segmentation did not capture the higher generation as well as the TLC vessel segmentation (based on visual assessment). CT images shown with lung window leveling (1500/-500).

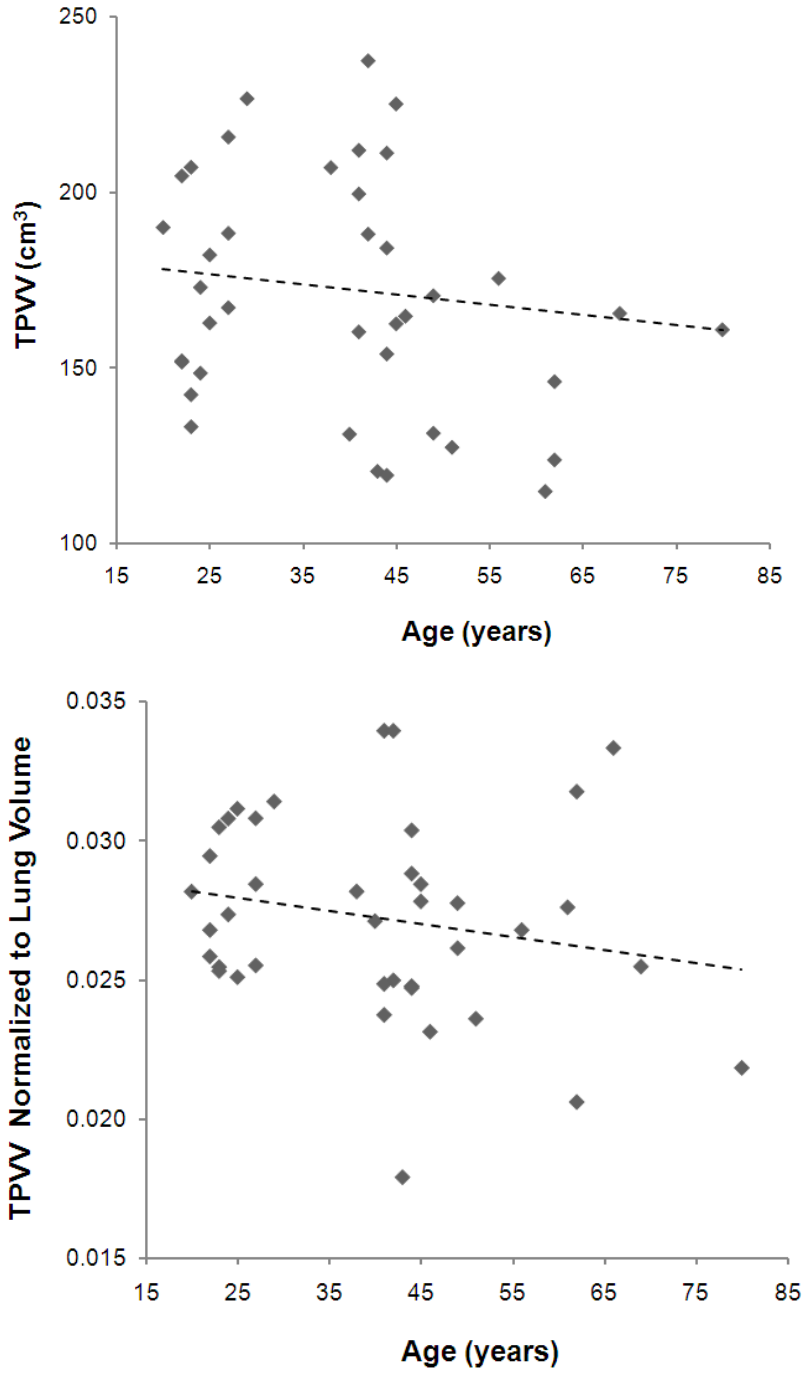

Figure 33. TPVV and TPVV normalized to lung volume measurements demonstrated a weak inverse correlation with the subject's age that was not significant for either TPVV ($r = -0.13$, $p = 0.44$) or TPVV normalized to total lung volume ($r = -0.21$, $p = 0.21$).

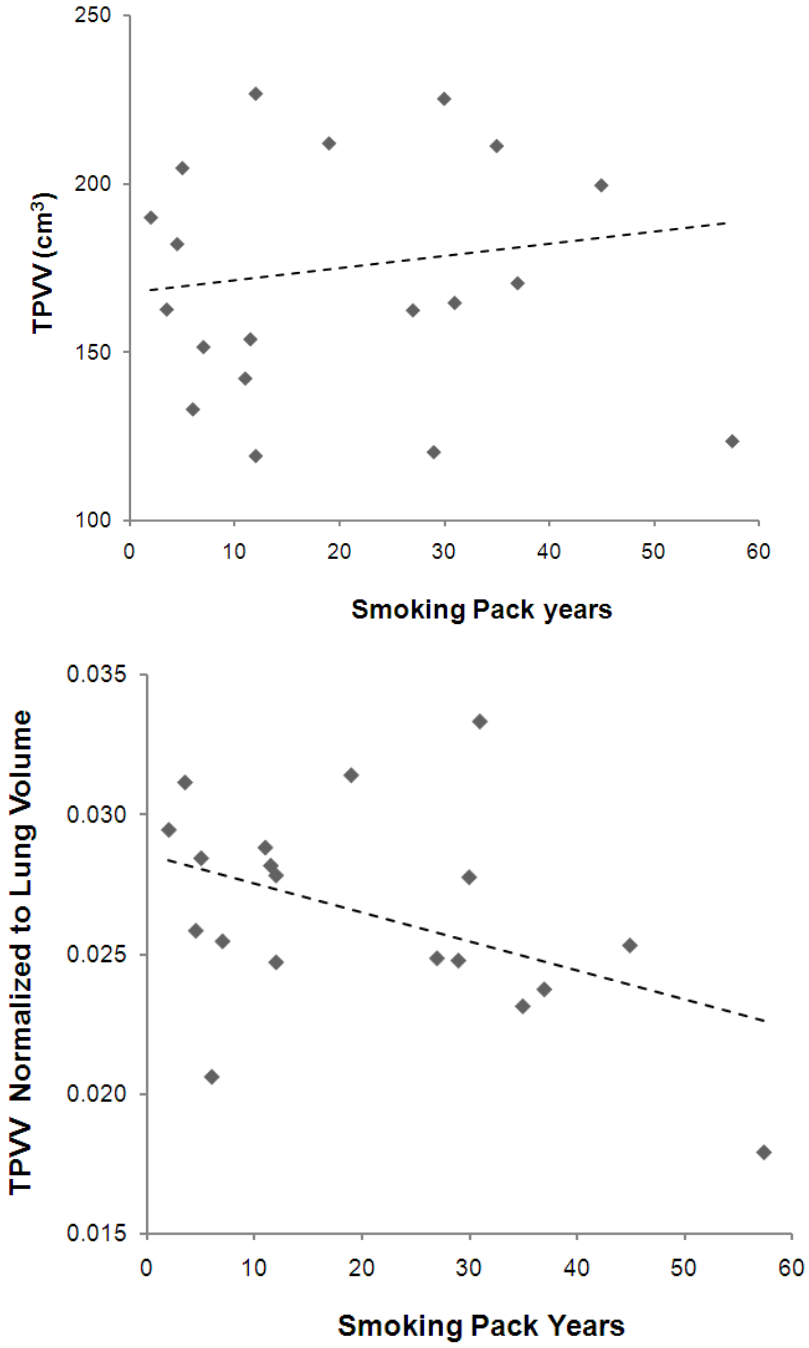

Figure 34. TPVV and TPVV normalized to lung volume measurements did not significantly correlate with pack years in the 20 smoking subjects. Pack years were determined from the number of packs smoked per day multiplied by the number of years smoking. After lung volume was accounted for in the smokers, pack years was inversely related to TPVV measurement, though this correlation was not significant ($r = -0.19$, $p = 0.42$).

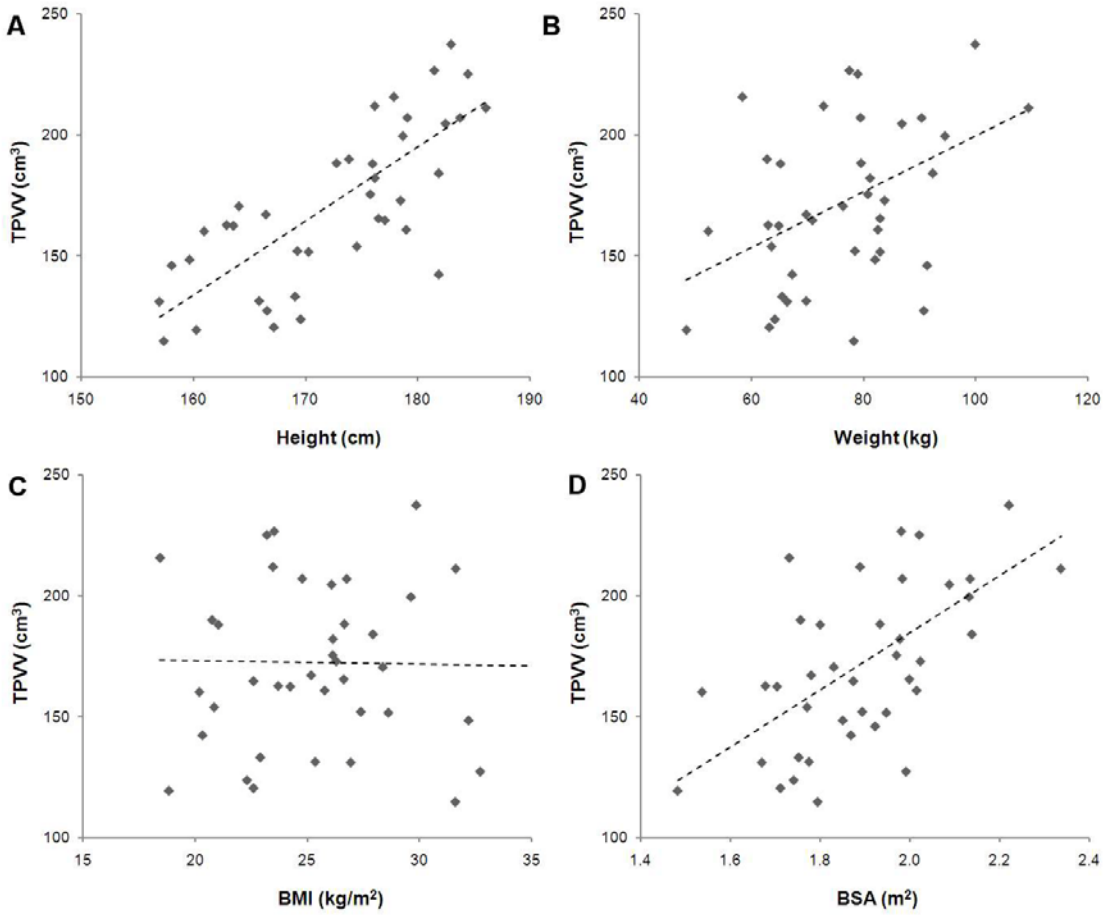

Figure 35. Linear regression plots for TPVV versus measures of body size including height (A), weight (B), BMI (C) and BSA (D) in the cohort of 40 subjects (20 smokers and 20 nonsmokers). TPVV was strongly correlated with height, weight, and BSA, with BSA measurements having the strongest correlation ($r = 0.60$, $p<0.01$). BMI and TPVV measurements did not demonstrate a correlation.

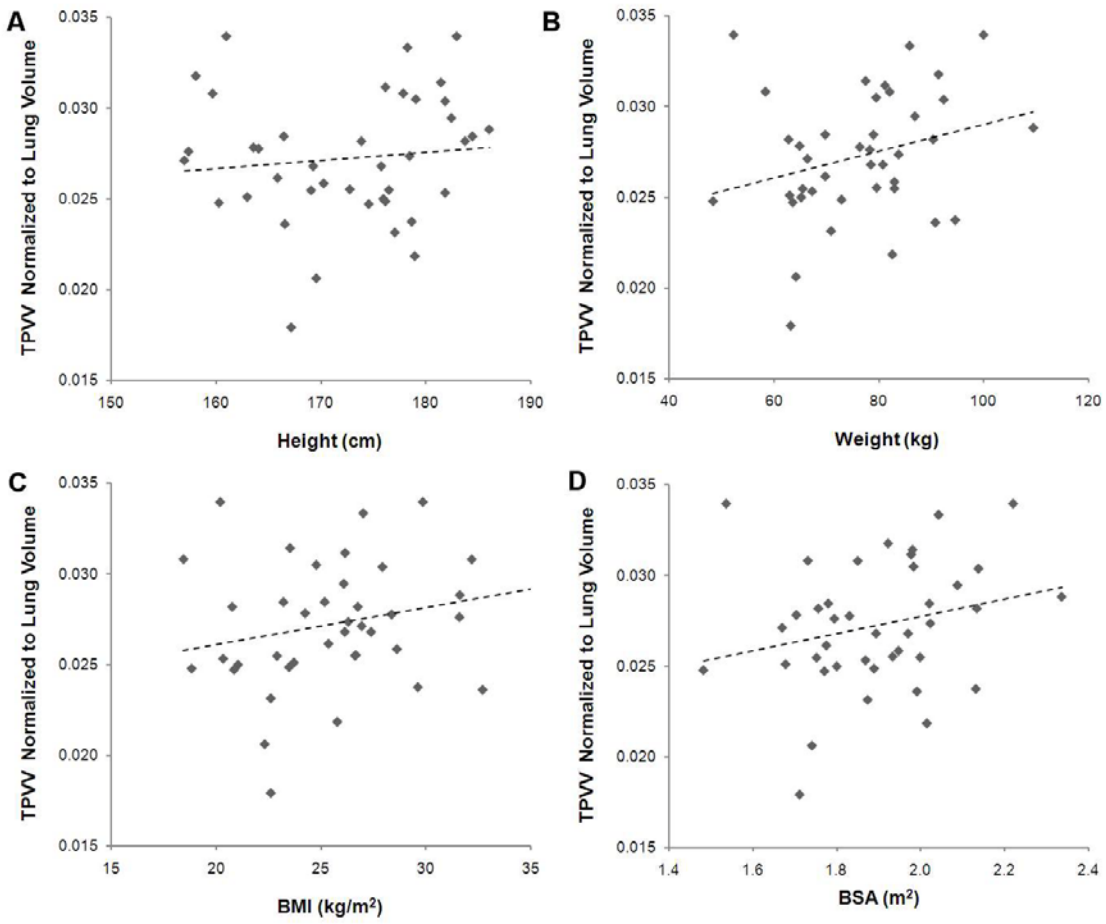

Figure 36. Linear regression plots for TPVV normalized to lung volume versus measures of body size including height (A), weight (B), BMI (C) and BSA (D) in the cohort of 40 subjects (20 smokers and 20 nonsmokers). BSA remains the variable with the strongest association to TPVV when normalized to lung volume. BSA demonstrates a modest, direct correlation ($r = 0.24$, $p = 0.13$) to TPVV measurements normalized to lung volume.

Figure 37. 3-D representation of the vascular, airway and lobar segmentations for a subject with COPD stage II. Airways are shown in dark blue with the 5 lobes color-coded.

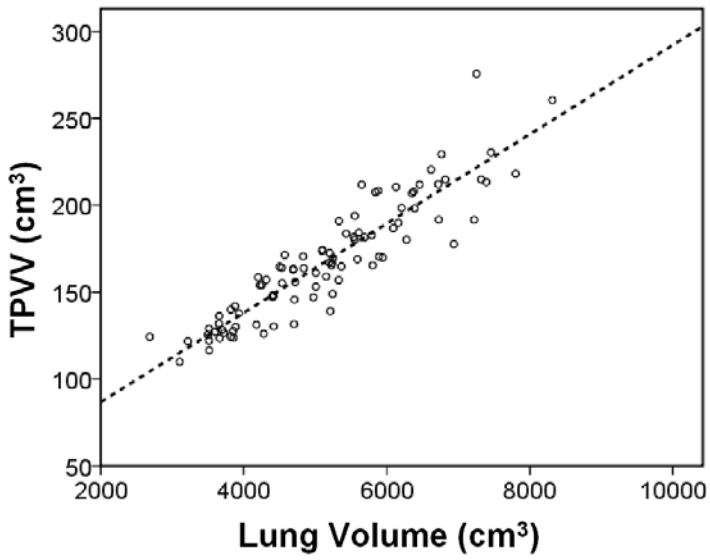

Figure 38. Simple linear regression demonstrates a strong linear association between total lung volume and TPVV measurements ($R^2 = 0.83$) for subjects in the EMCAP study.

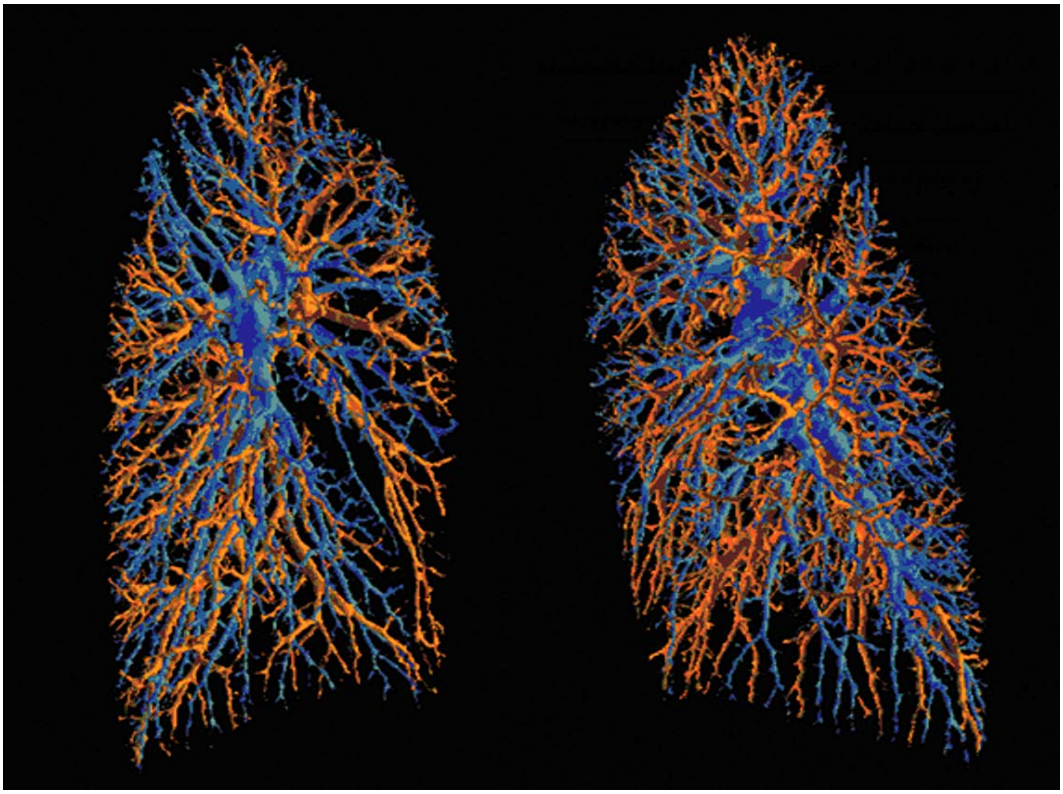

Figure 39. Surface color-coded 3-D rendition of the left and right lung vascular trees with arteries (blue) and veins (red) separated with a fuzzy logic based algorithm. Vasculature segmentations were obtained from a non-contrast MDCT volumetric scan of the lung breath-held at TLC.

Table 15. Demographic and hemodynamic data for nonsmokers and smokers in the BRP cohort.

Parameter	Nonsmokers	Smokers
No. of subjects	20	20
Age (y)	42 ± 17 [22, 80]	38 ± 14 [20, 66]
No. of females*	10 (50%)	8 (40%)
Ethnicity*,		
Caucasian	19 (95%)	15 (75%)
African American	1 (5%)	3 (15%)
Hispanic		1 (5%)
American Indian		1 (5%)
Weight (kg)	79 ± 12 [52, 100]	74 ± 14 [48, 110]
Height (cm)	171 ± 9 [157, 184]	174 ± 8 [163, 186]
Body Surface Area (m^2)	1.9 ± 0.2 [1.5, 2.2]	1.9 ± 0.2 [1.5, 2.3]
Body Mass Index (kg/m^2)	26.9 ± 4.3 [18.4, 36.6]	24.3 ± 3.4 [18.8, 31.6]
Heart rate (bpm)	67 ± 8 [48, 81]	74 ± 12 [52, 102]
Blood Pressure (mm Hg)		
Systolic	124 ± 10 [102, 138]	123 ± 15 [88, 154]
Diastolic	69 ± 10 [53,88]	73 ± 9 [55, 88]
Pack years	--	22 ± 17 [2, 58]
Pre-bronchodilator, FEV_1 %*	104.4 ± 11.5	100.2 ± 15.4
Pre-bronchodilator FVC, %*	108.3 ± 17.7	95.8 ± 20.8
Pre-bronchodilator FEV_1/FVC	0.81 ± 0.06	0.77 ± 0.07

Note: Data are mean ± standard deviation with range [low, high] in brackets, or percentages in parenthesis.

* Pre-bronchodilator spirometry results are reported as percent predicted.

Table 16. TPVV and lung volume measurements based on smoking status and gender.

		Nonsmokers			Smokers		
	All	All	Male	Female	All	Male	Female
N	40	20	10	10	20	12	8
Lung Volume	6339 ± 1079	6046 ± 1085	6773 ± 694	5318 ± 911	6633 ± 1015	7154 ± 893	5851 ± 614
TPVV	172.2 ± 35.5	168.9 ± 32.2	184.8 ± 29.6	153.1 ± 27.6	175.5 ± 39.1	196.2 ±33.3	144.4 ± 23.6
TPVV, Normalized to Lung Volume	0.0272 ± 0.0035	0.0281 ± 0.0032	0.0273 ± 0.0036	0.0289 ± 0.0028	0.0264 ± 0.0037	0.0274 ± 0.0031	0.0248 ± 0.0041

Note: TPVV and lung volume are reported as mean ± SD, with units of cm^3.

Table 17. Lobar distribution of vascular volume for nonsmokers and smokers at TLC lung inflation volume.

	All	Nonsmokers	Smokers
N	40	20	20
Left	80.6 ± 18.6 (47%)	78.0 ± 17.0 (46%)	83.2 ± 20.2 (47%)
LUL	37.3 ± 9.3 (22%)	35.6 ± 8.0 (21%)	39.0 ±10.4 (22%)
LLL	43.3 ± 10.5 (25%)	42.3 ± 10.4 (25%)	44.2 ± 10.9 (25%)
Right	91.6 ± 17.5 (53%)	91.0 ± 16.1 (54%)	92.3 ± 19.2 (53%)
RUL	31.4 ± 6.4 (18%)	31.5 ± 6.8 (19%)	31.4 ± 6.2 (18%)
RML	12.8 ± 3.6 (7%)	12.5 ± 3.0 (7%)	13.2 ± 4.1 (7%)
RLL	47.4 ± 10.2 (28%)	47.0 ± 9.3 (28%)	47.8 ± 11.3 (27%)

Note: TPVV and lung volume are reported as mean ± SD, with percent of total vascular (or lung) volume in parentheses.

Definition of Abbreviations: TLC: Total Lung Capacity; N: number of subjects; LUL: left upper lobe; LLL: left lower lobe; RUL: right upper lobe; RML: right middle lobe; RLL: right lower lobe.

Table 18. Lobar distribution of vascular volume for TLC and FRC lung volumes in 10 nonsmokers.

	TLC		FRC	
	TPVV	Lung Volume	TPVV	Lung Volume
Whole Lung	163.0 ± 30.0	6090 ± 1202	101.4 ± 26.4	3206 ± 855
Left	75.4 ± 15.2 (46%)	2860 ± 618 (47%)	45.1 ± 14.0 (44%)	1469 ± 435 (46%)
LUL	35.2 ± 7.7 (22%)	1407 ± 352 (23%)	24.7 ± 7.9 (24%)	853 ± 251 (26%)
LLL	40.3 ± 8.6 (25%)	1453 ± 287 (24%)	20.4 ± 6.8 (20%)	616 ± 205 (19%)
Right	87.6 ± 15.2 (54%)	3230 ± 594 (53%)	56.6 ± 13.4 (56%)	1737 ± 431 (54%)
RUL	30.1 ± 5.4 (19%)	1112 ± 219 (18%)	21.7 ± 5.9 (21%)	690 ± 183 (22%)
RML	11.4 ± 3.3 (7%)	495 ± 142 (8%)	9.8 ± 2.9 (10%)	345 ± 107 (11%)
RLL	46.1 ± 8.9 (28%)	1623 ± 305 (27%)	24.8 ± 5.8 (25%)	702 ± 178 (22%)

Note: TPVV and lung volume for TLC and FRC are reported mean ± SD, with percent of total vascular (or lung) volume in parentheses.

Definition of Abbreviations: TLC: Total Lung Capacity; FRC: Functional Residual Capacity; LUL: left upper lobe; LLL: left lower lobe; RUL: right upper lobe; RML: right middle lobe; RLL: right lower lobe.

Table 19. Pearson correlation coefficients for covariates.

	All		Non Smokers		Smokers	
	R	p-value	r	p-value	r	p-value
TPVV						
Lung Volume	0.76	<0.01	0.79	<0.01	0.77	<0.01
BSA	0.60	<0.01	0.46	0.04	0.72	<0.01
Height	0.73	<0.01	0.81	<0.01	0.67	<0.01
BMI	-0.02	0.92	-0.42	0.07	0.47	0.04
Weight	0.42	<0.01	0.16	0.51	0.66	<0.01
Age	-0.13	0.44	-0.34	0.14	0.12	0.63
Pack years	0.15	0.35	---	---	0.16	0.51
TPVV Normalized to Lung Volume						
BSA	0.24	0.13	-0.08	0.73	0.47	0.04
Height	0.11	0.51	-0.08	0.72	0.40	0.08
BMI	0.23	0.15	0.01	0.96	0.34	0.14
Weight	0.27	0.09	-0.03	0.89	0.45	0.05
Age	-0.20	0.21	-0.37	0.11	-0.13	0.58
Pack years	-0.27	0.09	---	---	-0.19	0.42

Table 20. Associations between TPVV, spirometry, and MDCT perfusion parameter measurements for all 40 subjects.

	r	p-value
Spirometry		
FVC	0.46	0.004
FEV_1	0.52	0.001
FEV_1/FVC	0.42	0.009
MDCT Perfusion Parameters		
PBF (ml/min/100ml)	0.19	0.38
MTT (seconds)	0.06	0.79
CV of PBF	-0.24	0.27
CV of MTT	-0.24	0.26

Note: Associations between TPVV measurements are reported as partial correlation coefficients which accounted for the variability due to covariates. For spirometry, the model included total lung volume, height, and weight. For MDCT perfusion parameters the model included total lung volume, height, weight, age, and pack years.

Definition of Abbreviations: FVC: forced vital capacity; FEV_1: forced expiratory volume in 1 second; PBF: pulmonary blood flow; MTT: mean transit time; CV: coefficient of variation.

Table 21. Characteristics of cotinine-confirmed former smokers with valid flow-mediated dilation measures, spirometry, and TPVV measurements in the EMCAP study.

	Former Smokers (n = 93)	Former Smokers without COPD* (n = 62)
Age, yr	70 ± 5	70 ± 5
Female, %	43	45
Ethnicity, %		
White	82	79
African American	6	8
Hispanic	9	8
Asian/Pacific Islander	3	5
Education, %		
Graduate degree	27	24
Four-year college	33	39
High school/some college	33	32
No high school degree	7	5
Cotinine level, ng/ ml	13 ± 41	15 ± 49
Pack-years	47 ± 26	43 ± 23
Height, cm	168 ± 9	167 ± 9
BMI, kg/m^2	28 ± 4	28 ± 4
Blood pressure, mm Hg		
Systolic	128 ± 15	128 ± 16
Diastolic	73 ± 9	73 ± 9
Pre-bronchodilator FVC, %	84.7 ± 18.5	88.2 ± 16.8
Pre-bronchodilator FEV_1, %	78.4 ± 20.4	85.8 ± 14.8
Pre-bronchodilator FEV_1/FVC ratio	0.69 ± 0.10	0.74 ± 0.06
Post-bronchodilator FVC, %	85.7 ± 17.1	87.6 ± 14.8
Post-bronchodilator FEV_1, %	81.9 ± 20.0	89.3 ± 14.0
Post-bronchodilator FEV_1/FVC ratio	0.72 ± 0.10	0.77 ± 0.04
Bronchodilator response, %	5.3 ± 8.1	4.6 ± 7.5
COPD,* %		
None	67	100
Mild	8	
Moderate	19	
Severe or Very Severe	6	
DL_{CO} , %	66.1 ± 13.4	68.3 ± 10.7
DL_{CO}/V_A, %	82.2 ± 14.6	83.4 ± 12.8
CT emphysema index, %	25.4 ± 10.3	23.7 ± 9.1

Note: Results are mean ± SD unless otherwise noted. Spirometry are reported as percent predicted.

* Defined as a post-bronchodilator response < 0.70.

Table 22. TPVV and lobar volumes for the 93 former smokers in the EMCAP study.

	TPVV (cm^3)	Lung Volume (cm^3)	TPVV Normalized to Lung Volume*
Whole Lung	167.6 ± 33.6	5150 ± 1199	0.033
Left	76.7 ± 16.8 (46%)	2388 ± 582 (46%)	0.032
LUL	38.9 ± 8.3 (23%)	1263 ± 314 (24%)	0.031
LLL	37.8 ± 10.8 (23%)	1125 ± 336 (22%)	0.034
Right	90.9 ± 18.1 (54%)	2762 ± 647 (54%)	0.033
RUL	35.2 ± 7.9 (21%)	1086 ± 254 (21%)	0.032
RML	13.4 ± 5.1 (8%)	446 ± 172 (9%)	0.030
RLL	42.4 ± 11.4 (25%)	1230 ± 362 (24%)	0.034

Note: Pulmonary vascular volume and lung volume are reported mean ± SD, with percent of total vascular (or lung) volume in parentheses.

* TPVV is normalized per corresponding lung or lobar volume.

Definition of Abbreviations: TPVV: total pulmonary vascular volume; LUL: left upper lobe; LLL: left lower lobe; RUL: right upper lobe; RML: right middle lobe; RLL: right lower lobe.

Table 23. TPVV, lobar volumes, and CT percentage of emphysema in the subset of 31 former smokers with COPD in the EMCAP study.

	TPVV (cm^3)	Lung Volume (cm^3)	TPVV Normalized to Lung/Lobar Volume	CT percentage of emphysema
Whole Lung	175.7 ± 39.3	5503 ± 1386	0.032	46 ± 9%
Left	79.7 ± 18.5	2526 ± 641	0.032	45 ± 9%
LUL	40.5 ± 9.9	1352 ± 364	0.030	48 ± 9%
LLL	39.2 ± 11.2	1174 ± 360	0.033	41 ± 10%
Right	95.9 ± 22.1	2978 ± 783	0.032	46 ± 9%
RUL	38.3 ± 8.4	1203 ± 254	0.032	47 ± 9%
RML	13.9 ± 7.4	476 ± 232	0.029	50 ± 12%
RLL	44.1 ± 12.8	1299 ± 432	0.034	43 ± 11%

Note: Pulmonary vascular volume and lung volume are reported mean ± SD, with percent of total vascular (or lung) volume in parentheses. TPVV is normalized per corresponding lung or lobar volume.

Definition of Abbreviations: TPVV: total pulmonary vascular volume; LUL: left upper lobe; LLL: left lower lobe; RUL: right upper lobe; RML: right middle lobe; RLL: right lower lobe.

Table 24. Mean differences in FVC, FEV_1, FEV_1/FVC ratio, DL_{CO}, and CT percentage of emphysema per 1 SD change in TPVV measurements in former smokers.

	Difference in Lung Measure per 1 SD Change in TPVV	P value	Partial r
Post-bronchodilator FVC, ml			
Model 1	31 (-2, 64)	0.06	0.19
Model 2	20 (-11, 51)	0.21	0.14
Post-bronchodilator FEV_1, ml			
Model 1	33 (2, 64)	0.04	0.22
Model 2	23 (-6, 52)	0.12	0.17
Post-bronchodilator FEV_1/FVC ratio, %			
Model 1	4.2 (-0.6, 9.1)	0.09	0.18
Model 2	3.4 (-0.5, 8.4)	0.17	0.15
DL_{CO}, ml/min/mm Hg			
Model 1	1.88 (-0.22, 3.98)	0.08	0.18
Model 2	1.39 (-0.50, 3.28)	0.13	0.17
CT percentage of emphysema, %			
Model 1	-4.7 (-7.6, -1.8)	0.002	-0.32
Model 2	-4.2 (-6.4, -2.0)	0.0003	-0.39

Note: Values in parenthesis denote the 95% confidence interval.

Model 1 is adjusted for total lung volume.
Model 2 is adjusted for total lung volume, age, height, weight, gender, race/ethnicity, and pack years.

Definition of Abbreviations: FVC: forced vital capacity; FEV_1: forced expiratory volume in 1 second; CT: computed tomography; TPVV: total pulmonary vascular volume.

Table 25. Mean differences in FMD parameters per 1 SD change in TPVV measurements in former smokers.

	Difference in Lung Measure per 1 SD Change in TPVV	P value	Partial r
FMD, diameter change %			
Model 1	-1.22 (-2.81, 0.36)	0.13	-0.16
Model 2	-1.08 (-2.78, 0.63)	0.21	-0.14
FMD, absolute diameter change, mm			
Model 1	-0.05 (-0.10, 0.01)	0.10	-0.17
Model 2	-0.04 (-0.10, 0.02)	0.15	-0.16
FMD, baseline diameter, mm			
Model 1	0.31 (0, 0.62)	0.05	0.21
Model 2	0.19 (-0.08, 0.47)	0.16	0.15

Note: Values in parenthesis denote the 95% confidence interval.

Model 1 is adjusted for total lung volume.
Model 2 is adjusted for total lung volume, age, height, weight, gender, race/ethnicity, and pack years.

Definition of Abbreviations: FMD: flow-mediated dilatation; TPVV: total pulmonary vascular volume.

CHAPTER 7: CONCLUSION

Since its introduction in the 1970s, CT has emerged as a powerful method for the non-invasive assessment of the lung. Technology has drastically improved with scanners capable of imaging the entire lung in a few seconds to provide high-resolution anatomical information and functional techniques to provide perfusion and ventilation measures. CT imaging is emerging as a means for phenotyping disease states of the lung. CT measures have included mainly airway and parenchymal density based measures (73, 151). Many multicenter trials currently in progress focusing on characterizing asthma (SARP), COPD (COPDgene), interstitial lung disease, or cancer lung screening programs all focus at phenotyping lung disease with these structural measures. Structural alterations are likely to be the end stage results to functional abnormalities occurring in the lung. This body of work focuses on function as a primary phenotype and then relates function to structural changes.

As a precursor to using perfusion imaging to phenotype lung disease, we validated the technique using traditional methods of fluorescent microspheres and also developed a new *ex* vivo model. In the swine experiments comparing FMS and MDCT PBF measurements, we demonstrated good correlation at a FMS piece size resolution of 1.8 cm^3 and regional volume level of 8-10 cm^3. In order to further validate the perfusion technique, and for further cross-modality imaging technique validation and physiological assessment of the lung, an *ex vivo* perfusion model was developed utilizing techniques and fluids from the lung transplantation field. This model will prove valuable for controlled lung experiments focusing on new imaging technique development or obtaining a better understanding of lung physiology and pathology.

MDCT-based pulmonary vascular measures were then applied to two human cohorts to test hypotheses focused on early vasculature changes in COPD. We demonstrated increased heterogeneity in regional MTT and PBF measurements in

smokers with preclinical emphysema compared with smokers with normal lung function and imaging studies and nonsmokers. This work characterizes a vascular phenotype of emphysema and supports the notion that inflammatory-based vascular responses to hypoxia (HPV) are occurring in smokers susceptible to COPD, but are successfully blocked in smokers without signs of emphysema. In parallel to our HPV hypothesis, studies have demonstrated the presence of endothelial dysfunction. We sough to explore the relationship between pulmonary vascular volume and endothelial function through a new CT-based measure of the pulmonary vascular volume, TPVV. This measure was determined from analysis of non-contrast TLC volumetric MDCT images of the lungs. We established normative values of TPVV in a group of nonsmokers and smokers in the BRP cohort. Total lung volume and measures of body size were found to be strongly associated with TPVV measures. Spirometry was directly correlated with TPVV measurements in the BRP cohort and EMCAP cohort (though with a full model, it did not reach significance). CT EI was strongly inversely correlated with TPVV. Endothelial function, assessed by FMD, in the EMCAP study demonstrated a non-significant, weak indirect correlation suggesting that endothelial dysfunction was correlated with an increased pulmonary blood volume. This work further characterized pathological vasculature-related changes in COPD subjects. It also helped identify new directions for better assessment. Vascular volumes may not be as sensitive to changes in the pulmonary arterial bed such as those occurring in diseases such as pulmonary hypertension. Techniques are now in development for the separation of arteries and veins from vasculature segmentations obtained from non-contrast MDCT lung images, much like the invasive pulmonary casts made by Ewald Weibel et al (199). Having a non-invasive method to separate the pulmonary arterial and venous volumes will be important as we further characterize and phenotype with imaging the vascular changes present in pulmonary disease (164).

As CT continues to play an important role in disease characterization, we will gain a better understanding of the pathogenesis and progression of disease for COPD subjects. New scanners allow for volumetric images of the lung in seconds and increased axial coverage allowing for larger lung volumes to be examined with functional technique requiring axial mode of scanning such as perfusion. Characterization of CT measures from a full spectrum of COPD, as assessed by airway diameter and wall thickness, and amount and distribution of emphysema should not be the only the key elements used for phenotyping COPD. Functional information will be able to complement structural, anatomical information to answer questions based on the physiology and pathological changes of the lung due to disease. As we gain more insight in lung disease, better treatments and new targets for pharmaceutical therapies which will improve the mortality and morbidity associated with COPD. In summary, functional CT vasculature measures including functional perfusion imaging and measures of the pulmonary vasculature volume have been used to characterize a new phenotype which may be of importance as imaging gains importance in the search for genotypes associated with COPD and other potentially genetic-based lung disease.

REFERENCES

1. Standardization of spirometry, 1994 update. American thoracic society. *American journal of respiratory and critical care medicine* 1995;152:1107-1136.

2. Adamson RH, Liu B, Fry GN, Rubin LL, Curry FE. Microvascular permeability and number of tight junctions are modulated by camp. *The American journal of physiology* 1998;274:H1885-1894.

3. Arcasoy SM, Kotloff RM. Lung transplantation. *The New England journal of medicine* 1999;340:1081-1091.

4. Aronson D, Roterman I, Yigla M, Kerner A, Avizohar O, Sella R, Bartha P, Levy Y, Markiewicz W. Inverse association between pulmonary function and c-reactive protein in apparently healthy subjects. *American journal of respiratory and critical care medicine* 2006;174:626-632.

5. Aykac D, Hoffman EA, McLennan G, Reinhardt JM. Segmentation and analysis of the human airway tree from three-dimensional x-ray ct images. *IEEE transactions on medical imaging* 2003;22:940-950.

6. Barbera JA, Peinado VI, Santos S. Pulmonary hypertension in chronic obstructive pulmonary disease. *Eur Respir J* 2003;21:892-905.

7. Barnes PJ. Chronic obstructive pulmonary disease. *The New England journal of medicine* 2000;343:269-280.

8. Barnes PJ, Chowdhury B, Kharitonov SA, Magnussen H, Page CP, Postma D, Saetta M. Pulmonary biomarkers in chronic obstructive pulmonary disease. *American journal of respiratory and critical care medicine* 2006;174:6-14.

9. Barr RG, Mesia-Vela S, Austin JH, Basner RC, Keller BM, Reeves AP, Shimbo D, Stevenson L. Impaired flow-mediated dilation is associated with low pulmonary function and emphysema in ex-smokers: The emphysema and cancer action project (emcap) study. *American journal of respiratory and critical care medicine* 2007;176:1200-1207.

10. Barr RG, Stemple KJ, Mesia-Vela S, Basner RC, Derk SJ, Henneberger PK, Milton DK, Taveras B. Reproducibility and validity of a handheld spirometer. *Respiratory care* 2008;53:433-441.

11. Beck KC. Regional trapping of microspheres in the lung compares well with regional blood flow. 1987. p. 883-889.

12. Behrenbeck T, Kinsey JH, Harris LD, Robb RA, Ritman EL. Three-dimensional spatial, density, and temporal resolution of the dynamic spatial reconstructor. *Journal of computer assisted tomography* 1982;6:1138-1147.

13. Bentley MD, Lerman LO, Hoffman EA, Fiksen-Olsen MJ, Ritman EL, Romero JC. Measurement of renal perfusion and blood flow with fast computed tomography. *Circ Res* 1994;74:945-951.

14. Biederer J, Heller M. Artificial thorax for mr imaging studies in porcine heart-lung preparations. *Radiology* 2003;226:250-255.

15. Biederer J, Plathow C, Schoebinger M, Tetzlaff R, Puderbach M, Bolte H, Zaporozhan J, Meinzer HP, Heller M, Kauczor HU. Reproducible simulation of respiratory motion in porcine lung explants. *Rofo* 2006;178:1067-1072.

16. Biederer J, Schoene A, Freitag S, Reuter M, Heller M. Simulated pulmonary nodules implanted in a dedicated porcine chest phantom: Sensitivity of mr imaging for detection. *Radiology* 2003;227:475-483.

17. Bild DE, Bluemke DA, Burke GL, Detrano R, Diez Roux AV, Folsom AR, Greenland P, Jacob DR, Jr., Kronmal R, Liu K, et al. Multi-ethnic study of atherosclerosis: Objectives and design. *American journal of epidemiology* 2002;156:871-881.

18. Block M, Liu YH, Harris LD, Robb RA, Ritman EL. Quantitative analysis of a vascular tree model with the dynamic spatial reconstructor. *Journal of computer assisted tomography* 1984;8:390-400.

19. Blomley MJ, Coulden R, Bufkin C, Lipton MJ, Dawson P. Contrast bolus dynamic computed tomography for the measurement of solid organ perfusion. *Investigative radiology* 1993;28 Suppl 5:S72-77; discussion S78.

20. Boroto K, Remy-Jardin M, Flohr T, Faivre JB, Pansini V, Tacelli N, Schmidt B, Gorgos A, Remy J. Thoracic applications of dual-source ct technology. *European journal of radiology* 2008;68:375-384.

21. Brandes H, Albes JM, Conzelmann A, Wehrmann M, Ziemer G. Comparison of pulsatile and nonpulsatile perfusion of the lung in an extracorporeal large animal model. *Eur Surg Res* 2002;34:321-329.

22. Burrows B, Kettel LJ, Niden AH, Rabinowitz M, Diener CF. Patterns of cardiovascular dysfunction in chronic obstructive lung disease. *The New England journal of medicine* 1972;286:912-918.

23. Celermajer DS, Sorensen KE, Georgakopoulos D, Bull C, Thomas O, Robinson J, Deanfield JE. Cigarette smoking is associated with dose-related and potentially reversible impairment of endothelium-dependent dilation in healthy young adults. *Circulation* 1993;88:2149-2155.

24. Celli BR, MacNee W. Standards for the diagnosis and treatment of patients with copd: A summary of the ats/ers position paper. *Eur Respir J* 2004;23:932-946.

25. Chon D, Beck KC, Larsen RL, Shikata H, Hoffman EA. Regional pulmonary blood flow in dogs by 4d-x-ray ct. *J Appl Physiol* 2006;101:1451-1465.

26. Christensen GE, Johnson HJ. Consistent image registration. *IEEE transactions on medical imaging* 2001;20:568-582.

27. Clough AV, Haworth ST, Roerig DL, Hoffman EA, Dawson CA. Influence of gravity on radiographic contrast material-based measurements of regional blood flow distribution. *Academic radiology* 2003;10:128-138.

28. Corretti MC, Anderson TJ, Benjamin EJ, Celermajer D, Charbonneau F, Creager MA, Deanfield J, Drexler H, Gerhard-Herman M, Herrington D, et al. Guidelines for the ultrasound assessment of endothelial-dependent flow-mediated vasodilation of the brachial artery: A report of the international brachial artery reactivity task force. *Journal of the American College of Cardiology* 2002;39:257-265.

29. Coxson HO. Quantitative computed tomography assessment of airway wall dimensions: Current status and potential applications for phenotyping chronic obstructive pulmonary disease. *Proceedings of the American Thoracic Society* 2008;5:940-945.

30. Coxson HO, Rogers RM. Quantitative computed tomography of chronic obstructive pulmonary disease. *Academic radiology* 2005;12:1457-1463.

31. Cypel M, Yeung JC, Hirayama S, Rubacha M, Fischer S, Anraku M, Sato M, Harwood S, Pierre A, Waddell TK, et al. Technique for prolonged normothermic ex vivo lung perfusion. *J Heart Lung Transplant* 2008;27:1319-1325.

32. Dahl M, Vestbo J, Lange P, Bojesen SE, Tybjaerg-Hansen A, Nordestgaard BG. C-reactive protein as a predictor of prognosis in chronic obstructive pulmonary disease. *American journal of respiratory and critical care medicine* 2007;175:250-255.

33. Dakin JH, Evans TW, Hansell DM, Hoffman EA. Regional pulmonary blood flow in humans and dogs by 4d computed tomography. *Academic radiology* 2008;15:844-852.

34. Date H, Lima O, Matsumura A, Tsuji H, d'Avignon DA, Cooper JD. In a canine model, lung preservation at 10 degrees c is superior to that at 4 degrees c. A comparison of two preservation temperatures on lung function and on adenosine triphosphate level measured by phosphorus 31-nuclear magnetic resonance. *The Journal of thoracic and cardiovascular surgery* 1992;103:773-780.

35. de Perrot M, Fischer S, Liu M, Imai Y, Martins S, Sakiyama S, Tabata T, Bai XH, Waddell TK, Davidson BL, et al. Impact of human interleukin-10 on vector-induced inflammation and early graft function in rat lung transplantation. *American journal of respiratory cell and molecular biology* 2003;28:616-625.

36. de Perrot M, Keshavjee S. Lung transplantation. Lung preservation. *Chest surgery clinics of North America* 2003;13:443-462.

37. Dock DS, Kraus WL, Mc GL, Hyland JW, Haynes FW, Dexter L. The pulmonary blood volume in man. *The Journal of clinical investigation* 1961;40:317-328.

38. Du Bois D, Du Bois EF. A formula to estimate the approximate surface area if height and weight be known. *Arch Intern Medicine* 1916;17:863-871.

39. Easley RB, Fuld MK, Fernandez-Bustamante A, Hoffman EA, Simon BA. Mechanism of hypoxemia in acute lung injury evaluated by multidetector-row ct. *Academic radiology* 2006;13:916-921.

40. Egan TM, Haithcock JA, Nicotra WA, Koukoulis G, Inokawa H, Sevala M, Molina PL, Funkhouser WK, Mattice BJ. Ex vivo evaluation of human lungs for transplant suitability. *Ann Thorac Surg* 2006;81:1205-1213.

41. Erasmus ME, Fernhout MH, Elstrodt JM, Rakhorst G. Normothermic ex vivo lung perfusion of non-heart-beating donor lungs in pigs: From pretransplant function analysis towards a 6-h machine preservation. *Transpl Int* 2006;19:589-593.

42. Fink C, Johnson TR, Michaely HJ, Morhard D, Becker C, Reiser M, Nikolaou K. Dual-energy ct angiography of the lung in patients with suspected pulmonary embolism: Initial results. *Rofo* 2008.

43. Frost-Arner L, Bergqvist D. Effect of isovolemic hemodilution with dextran and albumin on thrombus formation in artificial vessel grafts inserted into the abdominal aorta of the rabbit. *Microsurgery* 1995;16:357-361.

44. Gan WQ, Man SF, Senthilselvan A, Sin DD. Association between chronic obstructive pulmonary disease and systemic inflammation: A systematic review and a meta-analysis. *Thorax* 2004;59:574-580.

45. Gevenois PA, De Vuyst P, de Maertelaer V, Zanen J, Jacobovitz D, Cosio MG, Yernault JC. Comparison of computed density and microscopic morphometry in pulmonary emphysema. *American journal of respiratory and critical care medicine* 1996;154:187-192.

46. Glenny RW, Bernard S, Brinkley M. Validation of fluorescent-labeled microspheres for measurement of regional organ perfusion. 1993. p. 2585-2597.

47. Glenny RW, Bernard S, Robertson HT, Hlastala MP. Gravity is an important but secondary determinant of regional pulmonary blood flow in upright primates. *J Appl Physiol* 1999;86:623-632.

48. Glenny RW, Lamm WJ, Albert RK, Robertson HT. Gravity is a minor determinant of pulmonary blood flow distribution. *J Appl Physiol* 1991;71:620-629.

49. Glenny RW, McKinney S, Robertson HT. Spatial pattern of pulmonary blood flow distribution is stable over days. *J Appl Physiol* 1997;82:902-907.

50. Glenny RW, Polissar L, Robertson HT. Relative contribution of gravity to pulmonary perfusion heterogeneity. *J Appl Physiol* 1991;71:2449-2452.

51. Glenny RW, Robertson HT. Fractal properties of pulmonary blood flow: Characterization of spatial heterogeneity. *J Appl Physiol* 1990;69:532-545.

52. Glenny RW, Robertson HT. Fractal modeling of pulmonary blood flow heterogeneity. *J Appl Physiol* 1991;70:1024-1030.

53. Gokce N, Keaney JF, Jr., Hunter LM, Watkins MT, Nedeljkovic ZS, Menzoian JO, Vita JA. Predictive value of noninvasively determined endothelial dysfunction for long-term cardiovascular events in patients with peripheral vascular disease. *Journal of the American College of Cardiology* 2003;41:1769-1775.

54. Greenleaf JF, Ritman EL, Sass DJ, Wood EH. Spatial distribution of pulmonary blood flow in dogs in left decubitus position. *The American journal of physiology* 1974;227:230-244.

55. Guo J, Fuld MK, Alford SK, Reinhardt J, Hoffman EA. Pulmonary analysis software suite 9.0: Integrating quantitative measures of function with structural analyses. In: Brown M, Bruijne Md, Ginneken Bv, Kiraly A, Kuhnigk JM, Lorenz C, Mori K, Reinhardt J, editors. First International Workshop on Pulmonary Imaging; 2008. p. 283-292.

56. Gust R, Kozlowski J, Stephenson AH, Schuster DP. Synergistic hemodynamic effects of low-dose endotoxin and acute lung injury. *American journal of respiratory and critical care medicine* 1998;157:1919-1926.

57. Hakim TS, Lisbona R, Dean GW. Gravity-independent inequality in pulmonary blood flow in humans. *J Appl Physiol* 1987;63:1114-1121.

58. Han MK, McLaughlin VV, Criner GJ, Martinez FJ. Pulmonary diseases and the heart. *Circulation* 2007;116:2992-3005.

59. Handa T, Nagai S, Hirai T, Chin K, Kubo T, Oga T, Niimi A, Matsumoto H, Ito Y, Takahashi K, et al. Computed tomography analysis of airway dimensions and lung density in patients with sarcoidosis. *Respiration; international review of thoracic diseases* 2008.

60. Hardesty RL, Griffith BP. Autoperfusion of the heart and lungs for preservation during distant procurement. *The Journal of thoracic and cardiovascular surgery* 1987;93:11-18.

61. Hatabu H, Tadamura E, Levin DL, Chen Q, Li W, Kim D, Prasad PV, Edelman RR. Quantitative assessment of pulmonary perfusion with dynamic contrast-enhanced mri. *Magn Reson Med* 1999;42:1033-1038.

62. Haverich A. Experience with lung transplantation. *Ann Thorac Surg* 1999;67:305-312.

63. Hayama M, Date H, Oto T, Aoe M, Andou A, Shimizu N. Improved lung function by means of retrograde flush in canine lung transplantation with non-heart-beating donors. *The Journal of thoracic and cardiovascular surgery* 2003;125:901-906.

64. Hillier SC, Graham JA, Hanger CC, Godbey PS, Glenny RW, Wagner WW, Jr. Hypoxic vasoconstriction in pulmonary arterioles and venules. *J Appl Physiol* 1997;82:1084-1090.

65. Hisamitsu O, Nakashima R, Otsuka N, Mishima Y, Tomiguchi S, Narimatsu A, Nonami Y, Mihara S, Koyama W, Marubayashi T, et al. Emphysema detected by lung cancer screening with low-dose spiral ct: Prevalence, and correlation with smoking habits and pulmonary function in japanese male subjects. *Respirology (Carlton, Vic* 2006;11:205-210.

66. Hlastala MP, Chornuk MA, Self DA, Kallas HJ, Burns JW, Bernard S, Polissar NL, Glenny RW. Pulmonary blood flow redistribution by increased gravitational force. *J Appl Physiol* 1998;84:1278-1288.

67. Hlastala MP, Lamm WJ, Karp A, Polissar NL, Starr IR, Glenny RW. Spatial distribution of hypoxic pulmonary vasoconstriction in the supine pig. *J Appl Physiol* 2004;96:1589-1599.

68. Hoffman EA. Effect of body orientation on regional lung expansion: A computed tomographic approach. *J Appl Physiol* 1985;59:468-480.

69. Hoffman EA, Behrenbeck T, Chevalier PA, Wood EH. Estimation of regional pleural surface expansile forces in intact dogs. *J Appl Physiol* 1983;55:935-948.

70. Hoffman EA, Chon D. Computed tomography studies of lung ventilation and perfusion. *Proceedings of the American Thoracic Society* 2005;2:492-498, 506.

71. Hoffman EA, Hoford JD. Tool box-based cardiac volumes: Visualization and quantitation by computed tomography. *American journal of cardiac imaging* 1993;7:164-178.

72. Hoffman EA, Lai-Fook SJ, Wei J, Wood EH. Regional pleural surface expansile forces in intact dogs by wick catheters. *J Appl Physiol* 1983;55:1523-1529.

73. Hoffman EA, Reinhardt JM, Sonka M, Simon BA, Guo J, Saba O, Chon D, Samrah S, Shikata H, Tschirren J, et al. Characterization of the interstitial lung diseases via density-based and texture-based analysis of computed tomography images of lung structure and function. *Academic radiology* 2003;10:1104-1118.

74. Hoffman EA, Ritman EL. Effect of body orientation on regional lung expansion in dog and sloth. *J Appl Physiol* 1985;59:481-491.

75. Hoffman EA, Ritman EL. Heart-lung interaction: Effect on regional lung air content and total heart volume. *Annals of biomedical engineering* 1987;15:241-257.

76. Hoffman EA, Simon BA, McLennan G. State of the art. A structural and functional assessment of the lung via multidetector-row computed tomography: Phenotyping chronic obstructive pulmonary disease. *Proceedings of the American Thoracic Society* 2006;3:519-532.

77. Hoffman EA, Tajik JK, Kugelmass SD. Matching pulmonary structure and perfusion via combined dynamic multislice ct and thin-slice high-resolution ct. *Comput Med Imaging Graph* 1995;19:101-112.

78. Hogg JC, Holst P, Corry P, Ruff F, Housley E, Morris E. Effect of regional lung expansion and body position on pulmonary perfusion in dogs. *J Appl Physiol* 1971;31:97-101.

79. Hopkins SR, Henderson AC, Levin DL, Yamada K, Arai T, Buxton RB, Prisk GK. Vertical gradients in regional lung density and perfusion in the supine human lung: The slinky effect. *J Appl Physiol* 2007;103:240-248.

80. Hu S, Hoffman EA, Reinhardt JM. Automatic lung segmentation for accurate quantitation of volumetric x-ray ct images. *IEEE transactions on medical imaging* 2001;20:490-498.

81. Hughes JM, Glazier JB, Maloney JE, West JB. Effect of extra-alveolar vessels on distribution of blood flow in the dog lung. *J Appl Physiol* 1968;25:701-712.

82. Hughes JM, Glazier JB, Maloney JE, West JB. Effect of lung volume on the distribution of pulmonary blood flow in man. *Respiration physiology* 1968;4:58-72.

83. Hutton BF, Braun M. Software for image registration: Algorithms, accuracy, efficacy. *Seminars in nuclear medicine* 2003;33:180-192.

84. Ingemansson R, Budrikis A, Bolys R, Sjoberg T, Steen S. Effect of temperature in long-term preservation of vascular endothelial and smooth muscle function. *Ann Thorac Surg* 1996;61:1413-1417.

85. Inokawa H, Sevala M, Funkhouser WK, Egan TM. Ex-vivo perfusion and ventilation of rat lungs from non-heart-beating donors before transplant. *Ann Thorac Surg* 2006;82:1219-1225.

86. Jang YM, Oh YM, Seo JB, Kim N, Chae EJ, Lee YK, Lee SD. Quantitatively assessed dynamic contrast-enhanced magnetic resonance imaging in patients with chronic obstructive pulmonary disease: Correlation of perfusion parameters with pulmonary function test and quantitative computed tomography. *Investigative radiology* 2008;43:403-410.

87. Jatoi NA, Jerrard-Dunne P, Feely J, Mahmud A. Impact of smoking and smoking cessation on arterial stiffness and aortic wave reflection in hypertension. *Hypertension* 2007;49:981-985.

88. Jones RS, Meade F. A theoretical and experimental analysis of anomalies in the estimation of pulmonary diffusing capacity by the single breath method. *Quarterly journal of experimental physiology and cognate medical sciences* 1961;46:131-143.

89. Joppa P, Petrasova D, Stancak B, Tkacova R. Systemic inflammation in patients with copd and pulmonary hypertension. *Chest* 2006;130:326-333.

90. Kalender WA, Seissler W, Klotz E, Vock P. Spiral volumetric ct with single-breath-hold technique, continuous transport, and continuous scanner rotation. *Radiology* 1990;176:181-183.

91. Kanazawa H, Asai K, Hirata K, Yoshikawa J. Possible effects of vascular endothelial growth factor in the pathogenesis of chronic obstructive pulmonary disease. *The American journal of medicine* 2003;114:354-358.

92. Kanazawa H, Asai K, Nomura S. Vascular endothelial growth factor as a non-invasive marker of pulmonary vascular remodeling in patients with bronchitis-type of copd. *Respiratory research* 2007;8:22.

93. Kasahara Y, Tuder RM, Cool CD, Lynch DA, Flores SC, Voelkel NF. Endothelial cell death and decreased expression of vascular endothelial growth factor and vascular endothelial growth factor receptor 2 in emphysema. *American journal of respiratory and critical care medicine* 2001;163:737-744.

94. Kasahara Y, Tuder RM, Taraseviciene-Stewart L, Le Cras TD, Abman S, Hirth PK, Waltenberger J, Voelkel NF. Inhibition of vegf receptors causes lung cell apoptosis and emphysema. *The Journal of clinical investigation* 2000;106:1311-1319.

95. Kayano K, Toda K, Naka Y, Pinsky DJ. Identification of optimal conditions for lung graft storage with euro-collins solution by use of a rat orthotopic lung transplant model. *Circulation* 1999;100:II257-261.

96. Kelly RF, Murar J, Hong Z, Nelson DP, Hong F, Varghese A, Weir EK. Low potassium dextran lung preservation solution reduces reactive oxygen species production. *Ann Thorac Surg* 2003;75:1705-1710.

97. Kimblad PO, Massa G, Sjoberg T, Steen S. Endothelium-dependent relaxation in pulmonary arteries after lung preservation and transplantation. *Ann Thorac Surg* 1993;56:1329-1333; discussion 1333-1324.

98. Kimblad PO, Sjoberg T, Massa G, Solem JO, Steen S. High potassium contents in organ preservation solutions cause strong pulmonary vasocontraction. *Ann Thorac Surg* 1991;52:523-528.

99. King Gregory G, Muller Nestor L, Pare Peter D. Evaluation of airways in obstructive pulmonary disease using high-resolution computed tomography. 1999. p. 992-1004.

100. Krayer S, Rehder K, Beck KC, Cameron PD, Didier EP, Hoffman EA. Quantification of thoracic volumes by three-dimensional imaging. *Journal of applied physiology: respiratory, environmental and exercise physiology* 1987;62:591-598.

101. Kruuv J, Glofcheski D, Cheng KH, Campbell SD, Al-Qysi HM, Nolan WT, Lepock JR. Factors influencing survival and growth of mammalian cells exposed to hypothermia. I. Effects of temperature and membrane lipid perturbers. *Journal of cellular physiology* 1983;115:179-185.

102. Lamm WJ, Starr IR, Neradilek B, Polissar NL, Glenny RW, Hlastala MP. Hypoxic pulmonary vasoconstriction is heterogeneously distributed in the prone dog. *Respiratory physiology & neurobiology* 2004;144:281-294.

103. Lee YK, Oh YM, Lee JH, Kim EK, Lee JH, Kim N, Seo JB, Lee SD. Quantitative assessment of emphysema, air trapping, and airway thickening on computed tomography. *Lung* 2008;186:157-165.

104. Leibow AA. Pulmonary emphysema with special reference to vascular change. *Am Rev Respir Dis* 1959;80:67-93.

105. Levitzky M. Pulmonary physiology. 7th Edition ed: McGraw-Hill Companies, Inc.; 2007. p. Capillary Picture.

106. Ley-Zaporozhan J, Ley S, Eberhardt R, Weinheimer O, Fink C, Puderbach M, Eichinger M, Herth F, Kauczor HU. Assessment of the relationship between lung parenchymal destruction and impaired pulmonary perfusion on a lobar level in patients with emphysema. *European journal of radiology* 2007;63:76-83.

107. Ley S, Mereles D, Risse F, Grünig E, Ley-Zaporozhan J, Tecer Z, Puderbach M, Fink C, Kauczor H-U. Quantitative 3d pulmonary mr-perfusion in patients with pulmonary arterial hypertension: Correlation with invasive pressure measurements. *European journal of radiology* 2007;61:251-255.

108. Li H, Srinivasan SR, Berenson GS. Comparison of the measures of pulsatile arterial function between asymptomatic younger adult smokers and former smokers: The bogalusa heart study. *American journal of hypertension* 2006;19:897-901.

109. Liu YH, Hoffman EA, Hagler DJ, Seward JB, Julsrud PR, Mair DD, Ritman EL. Accuracy of pulmonary vascular dimensions estimated with the dynamic spatial reconstructor. *American journal of physiologic imaging* 1986;1:201-207.

110. Liu YH, Hoffman EA, Ritman EL. Measurement of three-dimensional anatomy and function of pulmonary arteries with high-speed x-ray computed tomography. *Investigative radiology* 1987;22:28-36.

111. Macintyre N, Crapo RO, Viegi G, Johnson DC, van der Grinten CP, Brusasco V, Burgos F, Casaburi R, Coates A, Enright P, et al. Standardisation of the single-breath determination of carbon monoxide uptake in the lung. *Eur Respir J* 2005;26:720-735.

112. Madani A, Keyzer C, Gevenois PA. Quantitative computed tomography assessment of lung structure and function in pulmonary emphysema. *Eur Respir J* 2001;18:720-730.

113. Mahler DA, Weinberg DH, Wells CK, Feinstein AR. The measurement of dyspnea. Contents, interobserver agreement, and physiologic correlates of two new clinical indexes. 1984. p. 751-758.

114. Mahmud A, Feely J. Effect of smoking on arterial stiffness and pulse pressure amplification. *Hypertension* 2003;41:183-187.

115. Maina JN, West JB. Thin and strong! The bioengineering dilemma in the structural and functional design of the blood-gas barrier. *Physiological reviews* 2005;85:811-844.

116. Man SF, Connett JE, Anthonisen NR, Wise RA, Tashkin DP, Sin DD. C-reactive protein and mortality in mild to moderate chronic obstructive pulmonary disease. *Thorax* 2006;61:849-853.

117. Mannino DM, Buist AS. Global burden of copd: Risk factors, prevalence, and future trends. *Lancet* 2007;370:765-773.

118. Martins S, de Perrot M, Imai Y, Yamane M, Quadri S, Segall L, Dutly A, Sakiyama S, Chaparro A, Davidson BL, et al. Transbronchial adminstration of adenoviral-mediated interleukin-10 gene to the donor improves function in a pig lung transplant model. *Gene Therapy* 2004;11:1786-1796.

119. McAllister DA, Maclay JD, Mills NL, Mair G, Miller J, Anderson D, Newby DE, Murchison JT, Macnee W. Arterial stiffness is independently associated with emphysema severity in patients with chronic obstructive pulmonary disease. *American journal of respiratory and critical care medicine* 2007;176:1208-1214.

120. McCormack DG, Paterson NA. Loss of hypoxic pulmonary vasoconstriction in chronic pneumonia is not mediated by nitric oxide. *The American journal of physiology* 1993;265:H1523-1528.

121. Menger MD. Microcirculatory disturbances secondary to ischemia-reperfusion. *Transplantation proceedings* 1995;27:2863-2865.

122. Miller MR, Crapo R, Hankinson J, Brusasco V, Burgos F, Casaburi R, Coates A, Enright P, van der Grinten CP, Gustafsson P, et al. General considerations for lung function testing. *Eur Respir J* 2005;26:153-161.

123. Miller MR, Hankinson J, Brusasco V, Burgos F, Casaburi R, Coates A, Crapo R, Enright P, van der Grinten CP, Gustafsson P, et al. Standardisation of spirometry. *Eur Respir J* 2005;26:319-338.

124. Mills NL, Miller JJ, Anand A, Robinson SD, Frazer GA, Anderson D, Breen L, Wilkinson IB, McEniery CM, Donaldson K, et al. Increased arterial stiffness in patients with chronic obstructive pulmonary disease: A mechanism for increased cardiovascular risk. *Thorax* 2008;63:306-311.

125. Milnor WR, Jose AD, McGaff CJ. Pulmonary vascular volume, resistance, and compliance in man. *Circulation* 1960;22:130-137.

126. Moro L, Pedone C, Scarlata S, Malafarina V, Fimognari F, Antonelli-Incalzi R. Endothelial dysfunction in chronic obstructive pulmonary disease. *Angiology* 2008;59:357-364.

127. Moudgil R, Michelakis ED, Archer SL. Hypoxic pulmonary vasoconstriction. *J Appl Physiol* 2005;98:390-403.

128. Muhlfeld C, Muller K, Pallesen LP, Sandhaus T, Madershahian N, Richter J, Wahlers T, Wittwer T, Ochs M. Impact of preservation solution on the extent of blood-air barrier damage and edema formation in experimental lung transplantation. *Anat Rec (Hoboken)* 2007;290:491-500.

129. Muller C, Bittmann I, Hatz R, Kellner B, Schelling G, Furst H, Reichart B, Schildberg F. Improvement of lung preservation - from experiment to clinical practice. *Eur Surg Res* 2002;34:77-82.

130. Muller NL. Ct diagnosis of emphysema. It may be accurate, but is it relevant? *Chest* 1993;103:329-330.

131. Muller NL, Staples CA, Miller RR, Abboud RT. "Density mask". An objective method to quantitate emphysema using computed tomography. *Chest* 1988;94:782-787.

132. Musch G, Layfield JD, Harris RS, Melo MF, Winkler T, Callahan RJ, Fischman AJ, Venegas JG. Topographical distribution of pulmonary perfusion and ventilation, assessed by pet in supine and prone humans. *J Appl Physiol* 2002;93:1841-1851.

133. Nakano Y, Muller NL, King GG, Niimi A, Kalloger SE, Mishima M, Pare PD. Quantitative assessment of airway remodeling using high-resolution ct. *Chest* 2002;122:271S-275S.

134. Nath DS, Walter AR, Johnson AC, Radosevich DM, Prekker ME, Herrington CS, Dahlberg PS, Kelly RF. Does perfadex affect outcomes in clinical lung transplantation? *J Heart Lung Transplant* 2005;24:2243-2248.

135. Neunteufl T, Heher S, Katzenschlager R, Wolfl G, Kostner K, Maurer G, Weidinger F. Late prognostic value of flow-mediated dilation in the brachial artery of patients with chest pain. *The American journal of cardiology* 2000;86:207-210.

136. Niimi A, Matsumoto H, Amitani R, Nakano Y, Mishima M, Minakuchi M, Nishimura K, Itoh H, Izumi T. Airway wall thickness in asthma assessed by computed tomography. Relation to clinical indices. *American journal of respiratory and critical care medicine* 2000;162:1518-1523.

137. O'Rourke MF, Gallagher DE. Pulse wave analysis. *J Hypertens Suppl* 1996;14:S147-157.

138. Ohno Y, Hatabu H, Murase K, Higashino T, Kawamitsu H, Watanabe H, Takenaka D, Fujii M, Sugimura K. Quantitative assessment of regional pulmonary perfusion in the entire lung using three-dimensional ultrafast dynamic contrast-enhanced magnetic resonance imaging: Preliminary experience in 40 subjects. *J Magn Reson Imaging* 2004;20:353-365.

139. Ohno Y, Murase K, Higashino T, Nogami M, Koyama H, Takenaka D, Kawamitu H, Matsumoto S, Hatabu H, Sugimura K. Assessment of bolus injection protocol with appropriate concentration for quantitative assessment of pulmonary perfusion by dynamic contrast-enhanced mr imaging. *J Magn Reson Imaging* 2007;25:55-65.

140. Oto T, Griffiths AP, Rosenfeldt F, Levvey BJ, Williams TJ, Snell GI. Early outcomes comparing perfadex, euro-collins, and papworth solutions in lung transplantation. *Ann Thorac Surg* 2006;82:1842-1848.

141. Park W, Hoffman EA, Sonka M. Segmentation of intrathoracic airway trees: A fuzzy logic approach. *IEEE transactions on medical imaging* 1998;17:489-497.

142. Pauwels RA, Buist AS, Calverley PM, Jenkins CR, Hurd SS. Global strategy for the diagnosis, management, and prevention of chronic obstructive pulmonary disease. Nhlbi/who global initiative for chronic obstructive lung disease (gold) workshop summary. *American journal of respiratory and critical care medicine* 2001;163:1256-1276.

143. Peinado VI, Barbera JA, Abate P, Ramirez J, Roca J, Santos S, Rodriguez-Roisin R. Inflammatory reaction in pulmonary muscular arteries of patients with mild chronic obstructive pulmonary disease. *American journal of respiratory and critical care medicine* 1999;159:1605-1611.

144. Peinado VI, Barbera JA, Ramirez J, Gomez FP, Roca J, Jover L, Gimferrer JM, Rodriguez-Roisin R. Endothelial dysfunction in pulmonary arteries of patients with mild copd. *The American journal of physiology* 1998;274:L908-913.

145. Pinsky DJ, Yan SF, Lawson C, Naka Y, Chen JX, Connolly ES, Jr., Stern DM. Hypoxia and modification of the endothelium: Implications for regulation of vascular homeostatic properties. *Seminars in cell biology* 1995;6:283-294.

146. Prisk GK, Yamada K, Henderson AC, Arai TJ, Levin DL, Buxton RB, Hopkins SR. Pulmonary perfusion in the prone and supine postures in the normal human lung. *J Appl Physiol* 2007;103:883-894.

147. Puderbach M, Risse F, Biederer J, Ley-Zaporozhan J, Ley S, Szabo G, Semmler W, Kauczor HU. In vivo gd-dtpa concentration for mr lung perfusion measurements: Assessment with computed tomography in a porcine model. *European radiology* 2008;18:2102-2107.

148. Rabe KF, Hurd S, Anzueto A, Barnes PJ, Buist SA, Calverley P, Fukuchi Y, Jenkins C, Rodriguez-Roisin R, van Weel C, et al. Global strategy for the diagnosis, management, and prevention of chronic obstructive pulmonary disease: Gold executive summary. *American journal of respiratory and critical care medicine* 2007;176:532-555.

149. Rabinowitz M, Rapaport E. Determination of circulating pulmonary blood volume in dogs by an arteriovenous dye equilibration method. *Circulation research* 1954;2:525-536.

150. Reed JH, Jr., Wood EH. Effect of body position on vertical distribution of pulmonary blood flow. *J Appl Physiol* 1970;28:303-311.

151. Reilly J. Using computed tomographic scanning to advance understanding of chronic obstructive pulmonary disease. *Proceedings of the American Thoracic Society* 2006;3:450-455.

152. Reinhardt JM, Christensen GE, Hoffman EA, Ding K, Cao K. Registration-derived estimates of local lung expansion as surrogates for regional ventilation. *Inf Process Med Imaging* 2007;20:763-774.

153. Reinhardt JM, D'Souza ND, Hoffman EA. Accurate measurement of intrathoracic airways. *IEEE transactions on medical imaging* 1997;16:820-827.

154. Reinhardt JM, Ding K, Cao K, Christensen GE, Hoffman EA, Bodas SV. Registration-based estimates of local lung tissue expansion compared to xenon ct measures of specific ventilation. *Medical image analysis* 2008;12:752-763.

155. Remy-Jardin M, Edme JL, Boulenguez C, Remy J, Mastora I, Sobaszek A. Longitudinal follow-up study of smoker's lung with thin-section ct in correlation with pulmonary function tests. *Radiology* 2002;222:261-270.

156. Ritman EL, Harris LD, Kinsey JH, Robb RA. Computed tomographic imaging of the heart: The dynamic spatial reconstructor. *Radiologic clinics of North America* 1980;18:547-555.

157. Ritman EL, Kinsey JH, Robb RA, Gilbert BK, Harris LD, Wood EH. Three-dimensional imaging of heart, lungs, and circulation. *Science (New York, NY* 1980;210:273-280.

158. Robb RA. The dynamic spatial reconstructor: An x-ray video-fluoroscopic ct scanner for dynamic volume imaging of moving organs. *IEEE transactions on medical imaging* 1982;1:22-33.

159. Robb RA, Lent AH, Gilbert BK, Chu A. The dynamic spatial reconstructor: A computed tomography system for high-speed simultaneous scanning of multiple cross sections of the heart. *Journal of medical systems* 1980;4:253-288.

160. Robertson HT, Altemeier WA, Glenny RW. Physiological implications of the fractal distribution of ventilation and perfusion in the lung. *Annals of biomedical engineering* 2000;28:1028-1031.

161. Robertson HT, Hlastala MP. Microsphere maps of regional blood flow and regional ventilation. *J Appl Physiol* 2007;102:1265-1272.

162. Rosenkranz S. Pulmonary hypertension: Current diagnosis and treatment. *Clin Res Cardiol* 2007;96:527-541.

163. Sabit R, Bolton CE, Edwards PH, Pettit RJ, Evans WD, McEniery CM, Wilkinson IB, Cockcroft JR, Shale DJ. Arterial stiffness and osteoporosis in chronic obstructive pulmonary disease. *American journal of respiratory and critical care medicine* 2007;175:1259-1265.

164. Saha PK, Gao Z, Alford SK, Sonka M, Hoffman EA. A novel multi-scale topo-morphometric approach for separating arteries and veins via pulmonary ct imaging. *Proc SPIE* 2009;7259-35.

165. Santos S, Peinado VI, Ramirez J, Melgosa T, Roca J, Rodriguez-Roisin R, Barbera JA. Characterization of pulmonary vascular remodelling in smokers and patients with mild copd. *Eur Respir J* 2002;19:632-638.

166. Santos S, Peinado VI, Ramirez J, Morales-Blanhir J, Bastos R, Roca J, Rodriguez-Roisin R, Barbera JA. Enhanced expression of vascular endothelial growth factor in pulmonary arteries of smokers and patients with moderate chronic obstructive pulmonary disease. *American journal of respiratory and critical care medicine* 2003;167:1250-1256.

167. Schimmel C, Frazer D, Glenny RW. Extending fluorescent microsphere methods for regional organ blood flow to 13 simultaneous colors. *American journal of physiology* 2001;280:H2496-2506.

168. Schuster DP. The opportunities and challenges of developing imaging biomarkers to study lung function and disease. *American journal of respiratory and critical care medicine* 2007;176:224-230.

169. Schuster DP, Kaplan JD, Gauvain K, Welch MJ, Markham J. Measurement of regional pulmonary blood flow with pet. *J Nucl Med* 1995;36:371-377.

170. Schuster DP, Marklin GF. The effect of regional lung injury or alveolar hypoxia on pulmonary blood flow and lung water measured by positron emission tomography. *The American review of respiratory disease* 1986;133:1037-1042.

171. Shikata H, Hoffman EA, Sonka M. Automated segmentation of pulmonary vascular tree from 3d ct images. In: Amir AA, Armando M, editors: SPIE; 2004. p. 107-116.

172. Simon BA. Non-invasive imaging of regional lung function using x-ray computed tomography. *Journal of clinical monitoring and computing* 2000;16:433-442.

173. Simon BA. Regional ventilation and lung mechanics using x-ray ct. *Academic radiology* 2005;12:1414-1422.

174. Simon BA, Christensen GE, Low DA, Reinhardt JM. Computed tomography studies of lung mechanics. *Proceedings of the American Thoracic Society* 2005;2:517-521, 506-517.

175. Sin DD, Man SF. Chronic obstructive pulmonary disease as a risk factor for cardiovascular morbidity and mortality. *Proceedings of the American Thoracic Society* 2005;2:8-11.

176. Sin DD, Man SF. Chronic obstructive pulmonary disease: A novel risk factor for cardiovascular disease. *Canadian journal of physiology and pharmacology* 2005;83:8-13.

177. Smith HC. The dynamic spatial reconstructor: Noninvasive vivisection of the heart, lungs, and circulation. *Journal of cardiography* 1981;11:1049-1060.

178. Solberg S, Larsen T, Jorgensen L, Sorlie D. Cold induced endothelial cell detachment in human saphenous vein grafts. *The Journal of cardiovascular surgery* 1987;28:571-575.

179. Sonka M, Park W, Hoffman EA. Rule-based detection of intrathoracic airway trees. *IEEE transactions on medical imaging* 1996;15:314-326.

180. Starr IR, Lamm WJ, Neradilek B, Polissar N, Glenny RW, Hlastala MP. Regional hypoxic pulmonary vasoconstriction in prone pigs. *J Appl Physiol* 2005;99:363-370.

181. Steen S. Preservation of the endothelium in cardiovascular surgery-some practical suggestions--a review. *Scand Cardiovasc J* 2001;35:297-301.

182. Steen S, Ingemansson R, Budrikis A, Bolys R, Roscher R, Sjoberg T. Successful transplantation of lungs topically cooled in the non-heart-beating donor for 6 hours. *Ann Thorac Surg* 1997;63:345-351.

183. Steen S, Ingemansson R, Eriksson L, Pierre L, Algotsson L, Wierup P, Liao Q, Eyjolfsson A, Gustafsson R, Sjoberg T. First human transplantation of a nonacceptable donor lung after reconditioning ex vivo. *Ann Thorac Surg* 2007;83:2191-2195.

184. Steen S, Kimblad PO, Sjoberg T, Lindberg L, Ingemansson R, Massa G. Safe lung preservation for twenty-four hours with perfadex. *Ann Thorac Surg* 1994;57:450-457.

185. Steen S, Liao Q, Wierup P, Bolys R, Pierre L, Sjoberg T. Transplantation of lungs from non-heart-beating donors after functional assessment ex vivo. *Ann Thorac Surg* 2003;76:244-252.

186. Stolz D, Christ-Crain M, Morgenthaler NG, Leuppi J, Miedinger D, Bingisser R, Muller C, Struck J, Muller B, Tamm M. Copeptin, c-reactive protein, and procalcitonin as prognostic biomarkers in acute exacerbation of copd. *Chest* 2007;131:1058-1067.

187. Sundaresan S, Trachiotis GD, Aoe M, Patterson GA, Cooper JD. Donor lung procurement: Assessment and operative technique. *Ann Thorac Surg* 1993;56:1409-1413.

188. Szilasi M, Dolinay T, Nemes Z, Strausz J. Pathology of chronic obstructive pulmonary disease. *Pathol Oncol Res* 2006;12:52-60.

189. Thabut G, Dauriat G, Stern JB, Logeart D, Levy A, Marrash-Chahla R, Mal H. Pulmonary hemodynamics in advanced copd candidates for lung volume reduction surgery or lung transplantation. *Chest* 2005;127:1531-1536.

190. Thieme SF, Becker CR, Hacker M, Nikolaou K, Reiser MF, Johnson TRC. Dual energy ct for the assessment of lung perfusion--correlation to scintigraphy. *European journal of radiology*;In Press, Corrected Proof.

191. Tkacova R, Kluchova Z, Joppa P, Petrasova D, Molcanyiova A. Systemic inflammation and systemic oxidative stress in patients with acute exacerbations of copd. *Respiratory medicine* 2007;101:1670-1676.

192. Trulock EP, Christie JD, Edwards LB, Boucek MM, Aurora P, Taylor DO, Dobbels F, Rahmel AO, Keck BM, Hertz MI. Registry of the international society for heart and lung transplantation: Twenty-fourth official adult lung and heart-lung transplantation report-2007. *J Heart Lung Transplant* 2007;26:782-795.

193. Tschirren J, Hoffman EA, McLennan G, Sonka M. Intrathoracic airway trees: Segmentation and airway morphology analysis from low-dose ct scans. *IEEE transactions on medical imaging* 2005;24:1529-1539.

194. Tschirren J, Hoffman EA, McLennan G, Sonka M. Segmentation and quantitative analysis of intrathoracic airway trees from computed tomography images. *Proceedings of the American Thoracic Society* 2005;2:484-487, 503-484.

195. Tuder RM, Zhen L, Cho CY, Taraseviciene-Stewart L, Kasahara Y, Salvemini D, Voelkel NF, Flores SC. Oxidative stress and apoptosis interact and cause emphysema due to vascular endothelial growth factor receptor blockade. *American journal of respiratory cell and molecular biology* 2003;29:88-97.

196. Van De Wauwer C, Neyrinck AP, Geudens N, Rega FR, Verleden GM, Verbeken E, Lerut TE, Van Raemdonck DE. Retrograde flush following topical cooling is superior to preserve the non-heart-beating donor lung. *Eur J Cardiothorac Surg* 2007;31:1125-1132; discussion 1132-1123.

197. Wang LS, Yoshikawa K, Miyoshi S, Nakamoto K, Hsieh CM, Yamazaki F, Guerreiro Cardoso PF, Schaefers HJ, Brito J, Keshavjee SH, et al. The effect of ischemic time and temperature on lung preservation in a simple ex vivo rabbit model used for functional assessment. *The Journal of thoracic and cardiovascular surgery* 1989;98:333-342.

198. Wei Q, Hu Y, Gelfand G, Macgregor J. Segmentation of lung lobes in high-resolution isotropic ct images. *IEEE transactions on bio-medical engineering* 2009.

199. Weibel ER. What makes a good lung? *Swiss Med Wkly* 2009;139:375-386.

200. West JB. Distribution of mechanical stress in the lung, a possible factor in localisation of pulmonary disease. *Lancet* 1971;1:839-841.

201. West JB. Respiratory physiology: The essentials. Baltimore: Lippincott Williams & Wilkins; 2000.

202. West JB. Thoughts on the pulmonary blood-gas barrier. *American journal of physiology* 2003;285:L501-513.

203. West JB, Dollery CT. Distribution of blood flow and ventilation-perfusion ratio in the lung, measured with radioactive carbon dioxide. *J Appl Physiol* 1960;15:405-410.

204. West JB, Dollery CT, Hugh-Jones P. The use of radioactive carbon dioxide to measure regional blood flow in the lungs of patients with pulmonary disease. *The Journal of clinical investigation* 1961;40:1-12.

205. West JB, Matthews FL. Stresses, strains, and surface pressures in the lung caused by its weight. *J Appl Physiol* 1972;32:332-345.

206. Wierup P, Haraldsson A, Nilsson F, Pierre L, Schersten H, Silverborn M, Sjoberg T, Westfeldt U, Steen S. Ex vivo evaluation of nonacceptable donor lungs. *Ann Thorac Surg* 2006;81:460-466.

207. Wiesmann F, Petersen SE, Leeson PM, Francis JM, Robson MD, Wang Q, Choudhury R, Channon KM, Neubauer S. Global impairment of brachial, carotid, and aortic vascular function in young smokers: Direct quantification by high-resolution magnetic resonance imaging. *Journal of the American College of Cardiology* 2004;44:2056-2064.

208. Wilkes DS, Egan TM, Reynolds HY. Lung transplantation: Opportunities for research and clinical advancement. *American journal of respiratory and critical care medicine* 2005;172:944-955.

209. Wilkinson IB, Hall IR, MacCallum H, Mackenzie IS, McEniery CM, van der Arend BJ, Shu YE, MacKay LS, Webb DJ, Cockcroft JR. Pulse-wave analysis: Clinical evaluation of a noninvasive, widely applicable method for assessing endothelial function. *Arteriosclerosis, thrombosis, and vascular biology* 2002;22:147-152.

210. Wittwer T, Franke U, Fehrenbach A, Meyer D, Sandhaus T, Pfeifer F, Dreyer N, Mueller T, Schubert H, Richter J, et al. Impact of retrograde graft preservation in perfadex-based experimental lung transplantation. *The Journal of surgical research* 2004;117:239-248.

211. Wittwer T, Franke UF, Fehrenbach A, Ochs M, Sandhaus T, Schuette A, Richter S, Dreyer N, Knudsen L, Muller T, et al. Experimental lung transplantation: Impact of preservation solution and route of delivery. *J Heart Lung Transplant* 2005;24:1081-1090.

212. Wolfkiel CJ, Ferguson JL, Chomka EV, Law WR, Labin IN, Tenzer ML, Booker M, Brundage BH. Measurement of myocardial blood flow by ultrafast computed tomography. *Circulation* 1987;76:1262-1273.

213. Wolfkiel CJ, Rich S. Analysis of regional pulmonary enhancement in dogs by ultrafast computed tomography. *Investigative radiology* 1992;27:211-216.

214. Won C, Chon D, Tajik J, Tran BQ, Robinswood GB, Beck KC, Hoffman EA. Ct-based assessment of regional pulmonary microvascular blood flow parameters. *J Appl Physiol* 2003;94:2483-2493.

215. Wright JL, Churg A. Advances in the pathology of copd. *Histopathology* 2006;49:1-9.

216. Wright JL, Tai H, Churg A. Cigarette smoke induces persisting increases of vasoactive mediators in pulmonary arteries. *American journal of respiratory cell and molecular biology* 2004;31:501-509.

217. Wright JL, Tai H, Churg A. Vasoactive mediators and pulmonary hypertension after cigarette smoke exposure in the guinea pig. *Journal of applied physiology: respiratory, environmental and exercise physiology* 2006;100:672-678.

218. Wu X, Latson L, Wang T, Driscoll D, Ensing G, Ritman E. Regional pulmonary perfusion estimated by high-speed volume scanning ct. *Am J Physiol Imaging* 1988;3:73-80.

219. Wu X, Latson LA, Driscoll DJ, Ensing GJ, Ritman EL. Dynamic three-dimensional anatomy of pulmonary arteries in pigs with aorto-to-pulmonary artery shunts. *American journal of physiologic imaging* 1987;2:169-175.

220. Yamada M, Kubo H, Ishizawa K, Kobayashi S, Shinkawa M, Sasaki H. Increased circulating endothelial progenitor cells in patients with bacterial pneumonia: Evidence that bone marrow derived cells contribute to lung repair. 2005. p. 410-413.

221. Yamada M, Kubo H, Kobayashi S, Ishizawa K, Numasaki M, Ueda S, Suzuki T, Sasaki H. Bone marrow-derived progenitor cells are important for lung repair after lipopolysaccharide-induced lung injury. 2004. p. 1266-1272.

222. Yamane M, Liu M, Kaneda H, Uhlig S, Waddell TK, Keshavjee S. Reperfusion-induced gene expression profiles in rat lung transplantation. *Am J Transplant* 2005;5:2160-2169.

223. Zerhouni EA, Naidich DP, Stitik FP, Khouri NF, Siegelman SS. Computed tomography of the pulmonary parenchyma. Part 2: Interstitial disease. *Journal of thoracic imaging* 1985;1:54-64.

224. Zhang L, Hoffman EA, Reinhardt JM. Atlas-driven lung lobe segmentation in volumetric x-ray ct images. *IEEE transactions on medical imaging* 2006;25:1-16.

225. Zierler KL. Equations for measuring blood flow by external monitoring of radioisotopes. *Circ Res* 1965;16:309-321.

226. Zwirewich CV, Terriff B, Muller NL. High-spatial-frequency (bone) algorithm improves quality of standard ct of the thorax. *Am J Roentgenol* 1989;153:1169-1173.